

2005

## Photonic band gap enhanced second-harmonic generation in a planar lithium niobate waveguide

Cong Deng  
*University of Dayton*

Follow this and additional works at: [https://ecommons.udayton.edu/graduate\\_theses](https://ecommons.udayton.edu/graduate_theses)

---

### Recommended Citation

Deng, Cong, "Photonic band gap enhanced second-harmonic generation in a planar lithium niobate waveguide" (2005). *Graduate Theses and Dissertations*. 2286.  
[https://ecommons.udayton.edu/graduate\\_theses/2286](https://ecommons.udayton.edu/graduate_theses/2286)

This Dissertation is brought to you for free and open access by the Theses and Dissertations at eCommons. It has been accepted for inclusion in Graduate Theses and Dissertations by an authorized administrator of eCommons. For more information, please contact [mschlange1@udayton.edu](mailto:mschlange1@udayton.edu), [ecommons@udayton.edu](mailto:ecommons@udayton.edu).

**Photonic Band Gap Enhanced Second-harmonic  
Generation in a Planar Lithium Niobate Waveguide**

Dissertation

Submitted to

School of Engineering

UNIVERSITY OF DAYTON

In Partial Fulfillment of the Requirements for

The Degree of

Doctor of Philosophy in Electro-Optics

By

**Cong Deng**

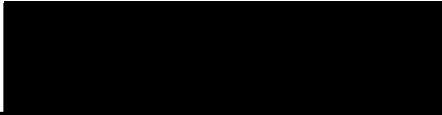
UNIVERSITY OF DAYTON

Dayton, Ohio

August, 2005


**Photonic Band Gap Enhanced Second-harmonic Generation in a  
Planar Lithium Niobate Waveguide**

**APPROVED BY:**



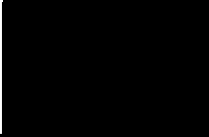
---

Joseph W. Haus, Ph.D.  
Professor and Director,  
Electro-Optics Graduate Program  
Committee Chairman



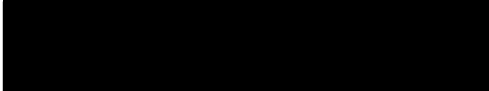
---

Andrew Sarangan, Ph.D.  
Assistant Professor,  
Electro-Optics Graduate Program  
Committee Member



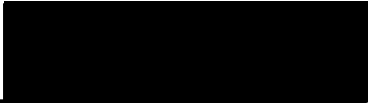
---

Partha Banerjee, Ph. D.  
Professor and Chair,  
Department of Electrical  
and Computer Engineering  
Committee Member



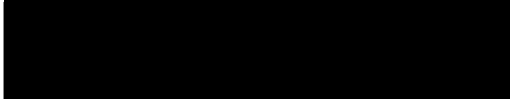
---

Peter E. Powers, Ph. D.  
Associate Professor of  
Department of Physics  
and Electro-Optics  
Committee Member



---

Donald L. Moon, Ph. D.  
Associate Dean,  
Graduate Engineering Program &  
Research  
School of Engineering



---

Joseph Saliba, Ph. D., P.E.  
Dean, School of Engineering

## ABSTRACT

Enhanced second harmonic generation (SHG) conversion efficiency was theoretically predicted in waveguide geometry with coupling to a one-dimensional grating photonic band gap (PBG). We report the first experimental results of band-edge enhanced Cerenkov SHG in a waveguide geometry. Cerenkov SHG is radiated into the substrate below the waveguide. The results are compared against a theoretical model that we designed to explore the critical design parameters of the system.

In our experiment, the samples were made with lithium niobate as the nonlinear material. By applying the proton exchange technique we fabricated a waveguide near the surface. The effective indices of waveguide modes were determined by using three techniques: prism-coupling, diffraction, and Cerenkov radiation. The WKB method was used to analyze the results. A comparison between the results derived from different methods was made to check the consistency of the methods. Ultraviolet laser lithography was used with photoresist to make PBG gratings on the sample. The photoresist gratings were used to scatter guided light in the waveguide, but initial etching experiments using an inductively coupled plasma (ICP) etcher on the photoresist gratings were also made. The photoresist and etched gratings were further characterized by using atomic force microscopy (AFM) and scanning electron microscopy (SEM) imaging.

An experimental setup was designed and constructed to investigate the Cerenkov second-harmonic generation (CSHG) in the substrate under band-edge resonance conditions in the waveguides. Guided SHG inside planar waveguides was also experimentally investigated. In this experiment, the second mode in the waveguide was tuned to a band-edge resonance to confine and enhance the guided electromagnetic field and enhance the nonlinear optical efficiency. In this dissertation, eight samples were investigated in detail and the highest conversion efficiency of CSHG with PBG was enhanced around 50 times above the CSHG signal without a PBG. A numerical model was successfully built to explain the experimental result. It's also found that the SHG inside the waveguides is not as strong as CSHG in the substrate.

**Index Terms:** second harmonic generation (SHG), Cerenkov second harmonic generation (CSHG), photonic band gap (PBG), lithium niobate, optical waveguide, proton exchange, and conversion efficiency.

## **ACKNOWLEDGEMENTS**

First of all, I would like to thank my advisor Dr. Joseph W. Haus who is most responsible for instructing me through my five-year studies. He is very knowledgeable, careful, accessible and patient in helping me with all the details in my research. His passion for science and technology has deeply influenced me. I do feel very lucky to have had him as my instructor. I would also like to express my deep gratitude to DAGSI fellowship, NSF grant and Electro-optics graduate program for funding my research.

Moreover, I like to extend my thanks to Dr. Andrew Sarangan, Dr. Partha Banerjee, and Dr. Peter E. Powers for serving on my advisory committee. They have made a lot effort in helping me from the proposal work to final defense in spite of their busy schedule. I would like to express my special thanks to Dr. John S. Loomis for carefully instructing me four very useful courses. It has been a wonderful thing to have the opportunity to learn a lot from those professors. In addition, I would like to express my special thank to Dr. Andrew Sarangan who has instructed me in my experiment. Without his help, it would have been impossible for me to complete my experiment. I also would like to thank Dr. Andre B. Fedotov, from International Laser Center, Faculty of Physics, Moscow State University, Moscow, Russia, for working with me to build the initial setup in my experiment. I like to thank the Air Force Research Laboratory (AFRL) at Wright Patterson Air Force Base for helping me with the ICP

etching. I wish to thank Dr. C. Sibilio, and Dr. D. Pezzetta, INFM at Dipartimento di Energetica, Università di Roma "La Sapienza", Rome, Italy, for giving me many valuable suggestions during the development of the project. I thank Dr. V. V. Yakovlev, University of Wisconsin – Milwaukee, for helping us in the initial experiment with a Cr: forsterite laser in his lab. I am also very grateful to my classmate Aziz Mahfoud, Joe Binford, Jang-Pyo Kim and many others who had helped and supported me through helpful discussions.

I deeply owe my family very much, especially my kind mother who has been giving me continuous support during the passing five years. I feel very glad that my son Zhe Deng just came here to enjoy the last stage piece of my research.

Many thanks to all who made this work possible!

Cong Deng

August, 2005

Dayton, Ohio

## TABLE OF CONTENTS

<b>APPROVAL PAGE.....</b>	<b>II</b>
<b>ABSTRACT.....</b>	<b>III</b>
<b>ACKNOWLEDGEMENTS.....</b>	<b>V</b>
<b>TABLE OF CONTENTS.....</b>	<b>VII</b>
<b>LIST OF FIGURES.....</b>	<b>X</b>
<b>CHAPTER 1 INTRODUCTION AND BACKGROUND.....</b>	<b>1</b>
<b>CHAPTER 2 INTRODUCTION TO THE THEORY.....</b>	<b>5</b>
<i>2.1 NONLINEAR OPTICS AND SECOND HARMONIC</i>	
<i>GENERATION.....</i>	<i>5</i>
<i>2.2 PHOTONIC BAND GAP AND ITS EFFECT ON</i>	
<i>ENHANCEMENT .....</i>	<i>10</i>
<b>CHAPTER 3 FABRICATION OF PHOTONIC BAND GAP (PBG)</b>	
<b>ON A LITHIUM NIOBATE WAVEGUIDE.....</b>	<b>15</b>
<i>3.1 INTRODUCTION.....</i>	<i>15</i>
<i>3.2 SAMPLE DESIGN.....</i>	<i>16</i>
<i>3.3 PROPERTIES OF LITHIUM NIOBATE .....</i>	<i>20</i>
<i>3.4 FABRICATION OF WAVEGUIDE.....</i>	<i>21</i>



3.5 GRATING FABRICATION.....	25
3.5.1 LASER LITHOGRAPHY TECHNIQUE.....	25
3.5.2 ETCHING LITHIUM NIOBATE.....	28
3.6 MEASUREMENT OF WAVEGUIDE	
EFFECTIVE INDEXES .....	32
3.6.1. CERENKOV RADIATION METHOD.....	33
3.6.2. PRISM COUPLING METHOD.....	35
3.6.3 DETERMINE WAVEGUIDE DEPTH USING	
WKB METHOD.....	37
3.7 METHOD OF GETTING RIGHT PBG PITCH	
ON THE WAVEGUIDE SURFACE .....	43
<b>CHAPTER 4 NUMERICAL MODELING .....</b>	<b>49</b>
4.1 INTRODUCTION.....	49
4.2 CALCULATION OF MODE PROFILES.....	51
4.3 CALCULATION OF COUPLING CONSTANT.....	54
4.4. CALCULATION OF CSHG EFFICIENCY.....	58
4.5 INTENSITY OF PUMP IN WAVEGUIDE	
WITH PBG ENHANCEMENT.....	65
4.6 CHAPTER SUMMARY.....	67
<b>CHAPTER 5 SHG EXPERIMENT AND RESULTS.....</b>	<b>69</b>
5.1 SETUP.....	69
5.2 SAMPLE IMAGES OF CSHG.....	73

5.3 SPECTRAL FEATURES IN CSHG .....	77
5.4. SHG INSIDE WAVEGUIDE.....	82
<b>CHAPTER 6 CONCLUSION AND</b>	
<b>FUTURE DIRCTIONS.....</b>	<b>85</b>
6.1 CONCLUSION.....	85
6.2 FUTURE DIRECTION.....	87
<b>REFERENCE.....</b>	<b>89</b>
<b>APPENDIX A MATLAB PROGRAMS.....</b>	<b>93</b>
<b>APPENDIX B PHOTOS OF SAMPLES IN EXPERIMENT.....</b>	<b>101</b>

## LIST OF FIGURES

Figure 2.1 - Energy-level diagram describing second-harmonic generation.....	7
Figure 2.2 - Transmission spectrum of a PBG for the fundamental wave. Here, $\omega$ is the normalized frequency. The low- frequency band edge is indicated by an arrow. ....	11
Figure 2.3 - Forward and backward propagating field intensities as a function of position when the fundamental field is tuned at the first transmission maximum at the low-frequency band edge as shown in Figure 2.2. The normalized frequency $\omega = 0.999731$ , and the Transmission is 1. The frequency shift is $\Delta\omega = 2.6900 \times 10^{-4}$ .....	12
Figure 2.4 - Field profile for the second transmission maximum near the low- frequency band edge, where the normalized frequency $\omega = 0.99968$ . The frequency shift is $\Delta\omega = 3.2000 \times 10^{-4}$ .....	12
Figure 2.5 - Field profile for the normalized angular frequency $\omega = 0.9997$ , which corresponds to the middle of the first and second transmission maximum at the Low-frequency band edge as shown in Figure 2.2. The frequency shift is $\Delta\omega = 3 \times 10^{-4}$ .....	13
Figure 3.1 - Principle of experimental sample in a three dimensional view for PBG enhanced SHG.....	17

Figure 3.2 – Sample with a size of $1\text{cm} \times 1\text{cm}$ putted on the top of a stage.....	17
Figure 3.3 – 2-D schematic diagram illustrating the principle of Cerenkov radiation in the sample in the side view of sample No.1.....	18
Figure 3.4 - The dispersion of the extra-ordinary index.....	20
Figure 3.5 - Proton exchange setup.....	23
Figure 3.6 - The real setup for making proton exchange $\text{LiNbO}_3$ waveguide.....	23
Figure 3.7 - Setup of Exposure System for holographic grating by photoresist on lithium niobate.....	27
Figure 3.8 – Rotating stage with a UV mirror and a sample holder surface.....	27
Figure 3.9 – Photoresist profile on lithium niobate. The picture is imaged using an atomic force microscope (AFM).....	28
Figure 3.10 - AFM of lithium niobate with ion milling.....	29
Figure 3.11 - AFM result. ICP etching on the +z surface of $\text{LiNbO}_3$ . The pitch is 710 nm and the Depth is 203 nm. Surface is non- uniform.....	30
Figure 3.12 - SEM of LN etched using ICP.....	31
Figure 3.13 - Tapping Mode AFM of lithium niobate etched using ICP.....	31
Figure 3.14 - Tapping Mode AFM of lithium niobate with ICP. The depth is 228 nm.....	32
Figure 3.15 a - Photos showing sample No.1 is pumped by the YAG and the CSHG output shown in a darkened room, viewed the Y direction in Fig. 2.3.....	34
Figure 3.15 b - Real photo of sample No.1, Pump and CSHG can be seen. The first grating can also be seen on the surface of sample.....	34
Figure 3.16 - Schematic of waveguide mode prism coupling measurement.....	36
Figure 3.17 - Experimental setup for prism coupling.....	36

Figure 3.18 - Result of prism coupling. An intensity drop is found at angle of $8.35^\circ$ , which is the position of 0.39 in the change of angle in this plot.....	37
Figure 3.19 - The profile of the refractive index in the waveguide of sample No.2.....	40
Figure 3.20 - The profile of refractive index in the waveguide No.3.....	41
Figure 3.21 - Quadratic fit of the refractive indices for sample No.2.....	42
Figure 3.22 - Quadratic fit of the refractive indices for sample No. 3.....	42
Figure 3.23 - Method changing the grating pitch seen by the pump beam by rotating sample, viewed in -X direction in Figure 3.1.....	44
Figure 3.24 - The coupling method for finding modes as well as effective indexes in the waveguide.....	45
Figure 3.25 - Setup of diffractive method. The pitch was calibrated by both AFM and SEM.....	46
Figure 3.26 - Pump vertically incidents on the second order Bragg grating, resulting two diffractive beams B and C in the waveguide.....	48
Figure 4.1 - The profile of the first TM modes of pump in waveguide in sample No.1. The area between the dash lines is waveguide. The air is in the right side.....	52
Figure 4.2 - The profile of the second TM modes of pump in waveguide in sample No.1. The area between the dash lines is waveguide. The air is in the right side.....	52
Figure 4.3 - Simplified model of sample.....	59
Figure 4.4 - The transmission and relative efficiency with detuning in nm units for direct comparison in the experiment.....	63

Figure 4.5 - The transmission spectra, on right side of band, with detuning in nm units for direct comparison with experiment. b. The relative efficiency with detuning in nm units for direct comparison with experiment.....	64
Figure 4.6 - The relative field of pump inside the waveguide at different positions. When $\Delta\lambda = 0.12278$ nm; relative intensity is $\eta = 48.0836$ , $T=1$ . the solid line shows the intensity inside the waveguide with grating the dot line shows the intensity inside the waveguide without grating for sample No.1.....	66
Figure 4.7 - The relative field of pump inside the waveguide at different positions. When $\Delta\lambda = 0.13861$ nm for sample No.1.....	66
Figure 4.8 - the relative field of pump inside the waveguide at different positions when $\Delta\lambda = 0.1307$ nm. For sample No.1.....	67
Figure 5.1 - Schematic of the CSHG experiment.....	69
Figure 5.2 – Real setup of the CSHG experiment 1-spectrometer 2-dimensional stages 3-focucal lens 4-dump 5-Nd:YAG laser 6-power detector 7-half plate 8-mirroirs 9-fiber 10-3 dimensional stage with rotation and tilt 11-IR scope.....	70
Figure 5.3 - The sample 3 is pumped by the a YAG and the CSHG output is shown in a lighted room, viewed -Z direction in Figure 2.3.....	74
Figure 5.4 - photos showing sample 3 is pumped by the YAG and the CSHG output shown in a darkened room, viewed the -Z direction in Figure 2.3.....	76
Figure 5.5 - CSHG output of sample No.1 on a screen vertical to the direction of beams, viewed in the -Y direction.....	76
Figure 5.6 - The spectrum of pump, showing the bandwidth of 0.4 nm.....	77
Figure 5.7 a - The CSH emission spectra for sample No.1.....	78

Figure 5.7 b - Log (I) for sample No.1. The Bandwidth is around 0.2 nm.....	79
Figure 5.8 - The CSHG emission spectra for sample No.4.....	80
Figure 5.9 - The SH emission spectra for sample No.5.....	81
Figure 5.10 - The SH emission spectra for sample No.6.....	81
Figure 5.11- Spectra of the second harmonic for sample No. 7 produced by 150-pulses of Nd: YAG. Laser radiation in the area where the refractive index is periodically perturbed due to the diffraction grating (squares) and in the region with a homogeneous cladding index (circles).....	83
Figure 5.12 - Spectra of the second harmonic for sample No.8 produced by unamplified 30-fs pulses of Cr: forsterite laser radiation in the area where the refractive index is periodically perturbed due to the diffraction grating and in the homogenous region of the cladding index. The spectrum of the second- harmonic signal produced in BBO crystal is shown for comparison. The inset shows the spectrum of the pump pulse.....	84
Figure B.1 - SHG experiment of sample No.1 with room lights on.....	101
Figure B.2 - SHG experiment of sample No.1 in dark.....	101
Figure B.3 - SHG experiment of sample No.1 with room lights on.....	102
Figure B.4 - SHG experiment of sample No.1 in dark.....	102
Figure B.5 - SHG experiment of sample No.1 in dark. CSHG can be seen on the screen.....	103
Figure B.6 - SHG experiment of sample No.1 in dark. CSHG can be seen on the screen.....	103
Figure B.7 - SHG experiment of sample No.1 in dark. CSHG can be seen on the screen.....	104
Figure B.8 - SHG experiment sample No.1 in dark.....	104

Table1. The typical data of sample No.1 used for the numerical modeling.....	50
--	----



## Chapter 1

### Introduction and Background

Sources of coherent light in the short wavelength spectral regions are required in many different applications such as color printing, high-definition projection displays, medicine for fluorescence assays of biological systems, medical sources for photo-excitation therapies, lithography with ultraviolet sources, higher-density optical data storage and optical tomography <sup>[1][2]</sup>.

Present blue-green sources are based mostly on gas lasers or resonantly frequency doubled solid-state lasers, which are inefficient, complex, and/or operate over a limited wavelength range. GaN based blue lasers are now becoming available, but they are still costly and have limited power output. Second-harmonic generation (SHG) in nonlinear optical waveguides, either using conversion from a guided mode at the fundamental frequency into an SH guided mode (guided-guided type of SHG) or through conversion of a fundamental guided mode into an SH radiation mode (so-called Cerenkov-type SHG) generation, offers a simple and inexpensive means of direct and efficient generation of short-wavelength, intense light. It does so by frequency doubling of light using low-cost laser diodes and compact diode-pumped solid state lasers currently available around wavelengths of 1  $\mu\text{m}$ . By using nonlinear optical waveguides, high conversion efficiencies can be obtained even for moderate input powers because of the high optical power density and long interaction lengths provided by guided-wave structures. Lithium niobate ( $\text{LiNbO}_3$ ) is an excellent optical material, most commonly

used as a substrate for applications in integrated electrooptic and nonlinear optical devices. In single-mode channel  $\text{LiNbO}_3$  guides, which provide tight optical confinement, even modest CW power of 2 mW coupled into a guided mode will result in a power density on the order of  $10^6 \text{ W/cm}^2$ . During the last few years, the quasi-phase matching (QPM) technique <sup>[3]</sup>, in which the ferroelectric domains of the material are periodically inverted to compensate for dispersion, has received special attention for SHG of blue <sup>[4]</sup> and green <sup>[5]</sup> light in nonlinear  $\text{LiNbO}_3$  waveguides.

Another useful concept is the addition of a resonant cavity that can be used to increase the SHG efficiency. The addition of a photonic band gap (PBG) grating over the waveguide is equivalent to a distributed cavity system. A Bragg grating is an example of a linear periodic media, i.e. a medium that has a spatially periodic refractive index. The transmission through such a linear periodic medium is characterized by the appearance of stop bands when the Bragg condition is satisfied <sup>[6][7]</sup>. For an incident wave with wavelength of  $\lambda$ , and a grating of period  $\Lambda$  the Bragg condition is given by  $\Lambda = m\lambda/2n$  where  $m$  is an integer and  $n$  is the effective index. A number of publications theoretically determined that the SHG conversion efficiency could be enhanced by several orders of magnitude by using this kind of PBG <sup>[6][7][8][9]</sup>.

Multi-layer PBGs, such as  $\text{Ga}_{0.7}\text{Al}_{0.3}\text{As}/\text{AlAs}$ , have already shown good agreement between theory and experiments. Experiments showed that the SHG conversion efficiency can be improved up to 60 times higher for the TM-TM configuration <sup>[10][11][12]</sup>. Although a grating-style PBG is also predicted to increase the SHG conversion efficiency in the waveguide <sup>[6][7]</sup>, no experiment that matches the theoretical calculations has been reported until now. The recent publications showed that a grating band-gap structure in planar nonlinear waveguides for SHG could be made using e-beam lithography and reactive ion etching. Atomic force microscopy was

applied to analyze the etching result <sup>[13]</sup>; however, no SHG experiments were performed with the reported samples.

It has been reported that there is a giant efficiency in a GaN photonic crystal <sup>[14]</sup>, but in this paper there is an especially weak signal without the PBG and the comparison between different situations because more nonlinear material was used in PBG case than that without PBG. This makes the comparison difficult. Also, G. Blau <sup>[15]</sup> has reported a PBG enhancement in a polymer waveguide. But it has not been mentioned how the great enhancement was and they did not use the same band edge resonance effect. Both of above papers only reported the enhancement for the case of SHG reflection, which means only a small amount of nonlinear material is used, in other word their design uses very limited path lengths in the nonlinear materials.

My goal is to experimentally explore the SHG conversion efficiency in waveguide geometry with grating PBG enhanced and to compare the results with detailed theoretical calculations. Finally, it's found that the SHG enhancement inside the waveguide is weak, and the SHG under the Cerenkov phase matching condition (CSHG) was very strong. We first report that the PBG can 50 times enhance CSHG. The dissertation work required several elements:

- Fabricate better-controlled proton exchange LiNbO<sub>3</sub> waveguides.
- Improve the method of characterizing the profile of refractive index by two methods: Cerenkov radiation and prism coupling methods. This ensured better comparison between theories and experiments.
- Optimize the UV laser lithography and the ICP processing on LiNbO<sub>3</sub> to control the input coupling efficiency and obtain stronger coupling of the forward- and backward-propagating pump modes. Find the optimal design to get higher SHG conversion efficiency.

- Modeling of the samples based on our characterization experiments. Do experiments on SHG to determine the efficiency. Finally obtain results so that direct comparison with theoretical computations can be made.

## Chapter 2

### Introduction to the Theory

#### *2.1 Nonlinear Optics and Second Harmonic Generation*

Nonlinear optics is a relatively new phenomenon that is an extension of conventional optics. It was rendered observable only after the invention of the laser. Typically, only laser light is strong enough to affect the nonlinear optical properties of a material system. After the high intensity light beam, say with an electric field amplitude of 100 KV/m or more, propagates through a nonlinear material, the response of system will be changed to produce a nonlinear effect. For instance, the first nonlinear optics experiment to generate second-harmonic light was successfully reported by Franken et al, in 1961, soon after the first working laser was made by Maiman in 1960. They found that the intensity of light generated at the second-harmonic frequency increases as the square of intensity of the applied laser light <sup>[16]</sup>.

The field strength of a laser can be generally represented as an electrical field:

$$E(t) = E(\omega)e^{-i\omega t} + c.c. \quad (2.1)$$

Then the wave equation in a nonlinear optical media can be described as:

$$\nabla^2 E - \frac{1}{c^2} \frac{\partial^2 E}{\partial t^2} = \frac{4\pi}{c^2} \frac{\partial^2 P}{\partial t^2} \quad (2.2)$$

Where  $c$  is the speed of light in vacuum, and  $P$  is the polarization, which includes linear and nonlinear terms. This equation is different from the expression for

linear material because there is a part of  $\partial^2 P / \partial t^2$  in it. In nonlinear material, it will be nonzero, then the charges in material will be accelerated, and therefore generate electromagnetic radiation according to Larmor's theorem from electromagnetism.

Generally the polarization  $P$  can be expressed as a power series in  $E$ :

$$\begin{aligned} P(t) &= \chi^{(1)} E(t) + \chi^{(2)} E^2(t) + \chi^{(3)} E^3(t) + \dots \\ &\equiv P^{(1)}(t) + P^{(2)}(t) + P^{(3)}(t) + \dots \end{aligned} \quad (2.3)$$

Where  $\chi^{(1)}$  is the linear susceptibility of the medium; dispersion is not included here. The quantities  $\chi^{(2)}$  and  $\chi^{(3)}$  are the nonlinear susceptibilities in second and third order and they describe the nonlinear-optical properties of the medium.

When the light in low intensity is incident on the material, there is a small amplitude of electric field  $E$ , the relationship between  $E$  and  $P$  is, therefore, a linear one

$$P(t) = \chi^{(1)} E(t). \quad (2.4)$$

If light is incident onto a crystal for which the second-order susceptibility  $\chi^{(2)}$  is nonzero, a nonlinear response is created. The nonlinear polarization that is created in such a crystal is given by

$$P^{(2)}(t) = 2\chi^{(2)} E E^* + (\chi^{(2)} E^2 e^{-2i\omega t} + c.c.), \quad (2.5)$$

where the complex field amplitudes from Equation 2.1 are used. It's noted that the second term in Equation 2.5 includes a frequency of  $2\omega$ . According to Equation 2.2, this second-order polarization term is a source that generates radiation, which in this case produces the second harmonic. Under proper experimental conditions, the process of second-harmonic generation can be so efficient that nearly all of the power in the

incident radiation at frequency  $\omega$  is converted to radiation at the second-harmonic frequency  $2\omega$ .

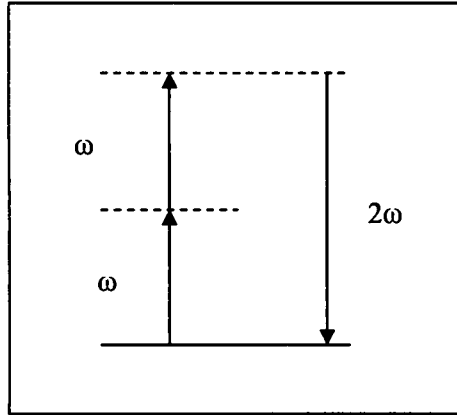


Figure 2.1 - Energy-level diagram describing second-harmonic generation.

The SHG process can also be depicted as shown in the Figure 2.1; It shows the interaction in terms of the exchange of photons between various frequency components of the field. In a single quantum-mechanical process, two photons of frequency  $\omega$  are destroyed and a photon of frequency  $2\omega$  is simultaneously created. The polarization can be simplified from Equation 2.5 and be expressed as:

$$P(2\omega) = \chi^{(2)} E^2(\omega) \quad (2.6)$$

The second-harmonic intensity in the non-depleted pump approximation is related to the pump intensity as

$$I(2\omega) = CI^2(\omega) \quad (2.7)$$

where  $C$  is a constant for certain material and conditions in our experiments. The intensity of second harmonic generation is proportional to the square of the pump intensity. Thus increasing the pump intensity produces a higher power of second harmonic generation.

Three main methods can be used to achieve a higher pump power. One is to use a mode locked laser to produce a train of short pulses that contain a very high power in each pulse. Another is use a waveguide to confine the pump in a very narrow space. The third is use a resonator to store higher pump power in the material. In our sample design the PBG acts like a resonator design to store the light inside the material. In our experiment, by combining above three methods at the same time, a huge intensity of pump can be produce around the waveguide. According the Equation 2.7, the SHG enhancement can be very high when we optimize the pump intensity. In this dissertation, we are primarily interested in the effect of PBG in the enhancement of SHG.

One of the primary issues for increasing SHG efficiency is the application of phase matching conditions. To keep the phases of the waves locked together, the indices should be equal for the pump and second-harmonic frequencies. There are several different methods reducing the dispersion of material so that we can achieve the phase matching condition

$$n(\omega) = n(2\omega). \quad (2.8)$$

Two generally used methods of phase matching are angle-tuning and temperature-tuning. Another method is the so called quasi- phase matching condition, which was first used by A. Armstrong<sup>[3]</sup>. Recently, it's also well known that the PBG grating can modify the indices of both pump and SHG at the same time, meaning that Equation 2.8 can be effectively reached by carefully making a PBG in the waveguide and therefore the enhancement can be improved<sup>[6-10]</sup>.

In our experiment the so called Cerenkov radiation SHG, which is in an automatic phase matching condition, is observed in the PBG enhanced structure. This method is unique in the nonlinear optical waveguide. The condition for the appearance



of a Cerenkov second harmonic radiation is satisfied when the effective index of the fundamental mode is less than the substrate index of the harmonic. The phase-matching condition becomes

$$n_{eff}(\omega) = n_s(2\omega) \cos(\alpha) \quad (2.9)$$

where  $n_{eff}$  is the effective index of the fundamental mode at  $\omega$ ,  $n_s(2\omega)$  is the substrate index at the second harmonic, and  $\alpha$  is called the Cerenkov radiation angle; i.e. the angle at which propagates into the substrate. The details of Cerenkov SHG will be discussed in section 3.6.1.

## 2.2 Photonic Band Gap and Its Effect on Enhancement

There are two different grating aided cavities depending on the wavelength that is resonant with the cavity. If the fundamental wavelength is resonant, its intensity is larger than that in a uniform medium and more light may be converted to the second harmonic. If the second harmonic is resonant with the cavity, the stored second-harmonic light increases the power extracted from the nonlinear polarization. The first case was exploited in our experiments and according to our calculations this gives the greatest conversion efficiency.

It's known, for both multi-layer and grating structure PBGs, the linear mode-coupled equations are the same as following:

$$\frac{\partial A_f}{\partial z} + \frac{1}{v_g} \frac{\partial A_f}{\partial t} = i \frac{\pi}{d} \kappa A_b e^{-2id\delta/\pi} - \frac{\pi}{d} \frac{\alpha}{2} A_f; \quad (2.10 \text{ a})$$

$$-\frac{\partial A_b}{\partial z} + \frac{1}{v_g} \frac{\partial A_b}{\partial t} = i \frac{\pi}{d} \kappa A_f e^{-2id\delta/\pi} - \frac{\pi}{d} \frac{\alpha}{2} A_b \quad (2.10 \text{ b})$$

where subscript “f” and “b” respectively mean forward and backward fields in the waveguide.  $A_f$  and  $A_b$  are field amplitudes of the forward and backward fields respectively.  $v_g$  is the group velocity at the fundamental frequency;  $\alpha$  is the normalized absorption.  $\kappa$  is the normalized grating coupling coefficient;  $d$  is the grating period;  $z$  is the position on the grating and  $t$  is the time variable. If we define the scaled center frequency of the first band as  $\omega_0$ , and  $n'(\omega) = \frac{dn(\omega)}{d\omega}$ , then

$$\delta = (\omega - \omega_0) \left( \frac{1}{\omega_0} + \frac{n'(\omega_0)}{n(\omega_0)} \right) \quad (2.11)$$

Thus,  $\delta$  is proportional to the detuning from the center of the first stop band  $(\omega - \omega_0)$  multiplied by a function of  $\omega_0$ . Small value of  $\delta$  means therefore that the analysis is confined to regions close to the center of the first band gap.

Further, the length and field amplitudes are scaled such that  $z \rightarrow z' = (\pi/d)z$ , and  $a_f = A_f e^{i\pi\tilde{x}/d}$  and  $a_b = A_b e^{i\pi\tilde{x}/d}$  respectively. The scaled equations for the fundamental field amplitudes are now

$$\frac{\partial a_f}{\partial z'} + \frac{d}{\pi v_g} \frac{\partial a_f}{\partial t} = -\frac{\alpha}{2} a_f + i\delta a_f + i\kappa a_b; \quad (2.12 a)$$

$$-\frac{\partial a_b}{\partial z'} + \frac{d}{\pi v_g} \frac{\partial a_b}{\partial t} = -\frac{\alpha}{2} a_b + i\delta a_b + i\kappa a_f. \quad (2.12 b)$$

The equations are valid over the entire grating. And they are solved with the boundary conditions:

$$a_f(0, t) = a(t) \quad (2.13 a)$$

$$a_b(L, t) = 0 \quad (2.13 b)$$

Following figures are plotted by using the analytic solutions of Equations 2.12 under the boundary conditions of Equation 2.13 <sup>[6][7]</sup>.

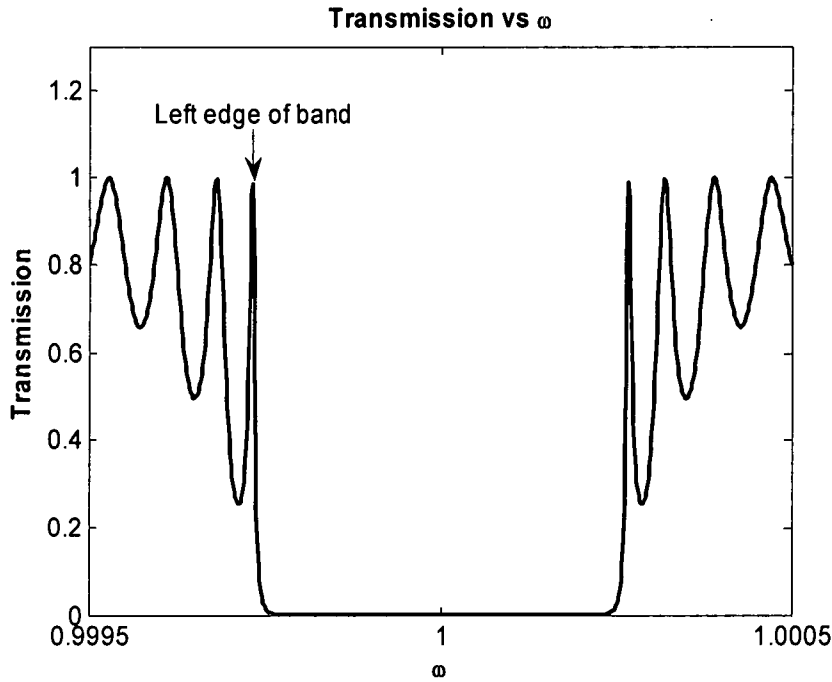


Figure 2.2 - Transmission spectrum of a PBG for the fundamental wave. Here,  $\omega$  is the normalized frequency. An arrow indicates the low- frequency band edge.

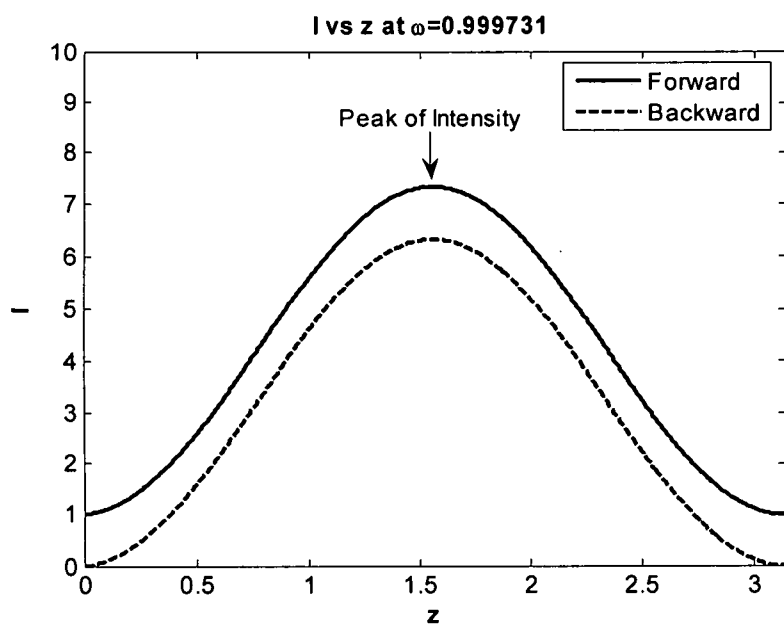


Figure 2.3 - Forward and backward propagating field intensities as a function of position when the fundamental field is tuned at the first transmission maximum at the low-frequency band edge as shown in Figure 2.2. The normalized frequency  $\omega = 0.999731$ , and the Transmission is 1. The frequency shift is  $\Delta\omega = 2.6900 \times 10^{-4}$ .

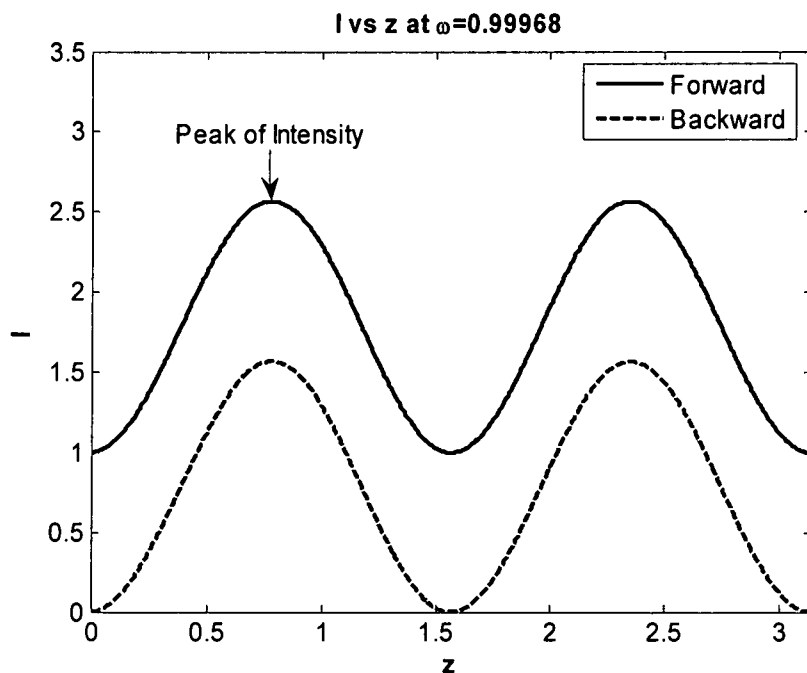


Figure 2.4 - Field profile for the second transmission maximum near the low-frequency band edge, where the normalized frequency  $\omega = 0.99968$ . The frequency shift is  $\Delta\omega = 3.2000 \times 10^{-4}$ .

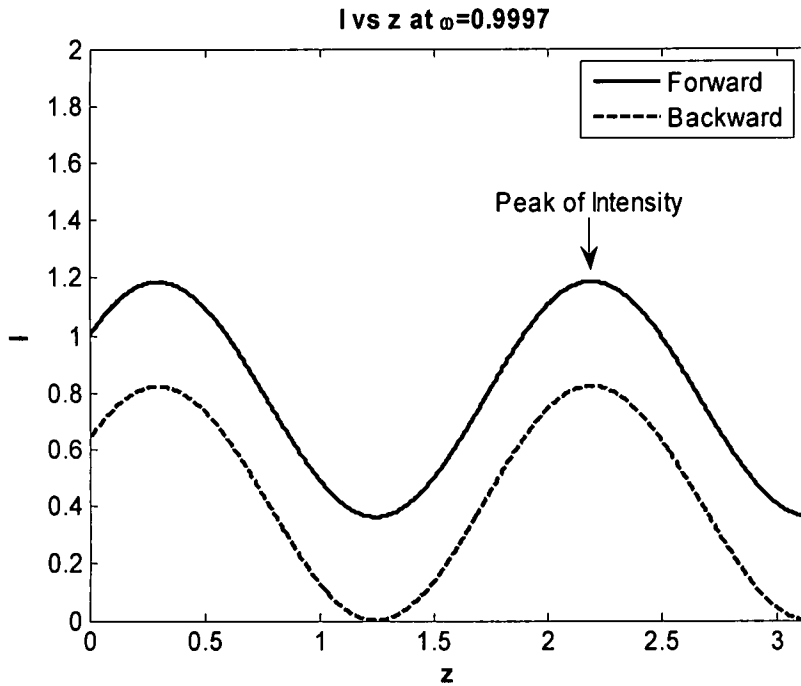


Figure 2.5 - Field profile for the normalized angular frequency  $\omega=0.9997$ , which corresponds to the middle of the first and second transmission maximum at the Low-frequency band edge as shown in Figure 2.2. The frequency shift is  $\Delta\omega = 3 \times 10^{-4}$ .

The normalized frequency at band-edge is also shown in Figure 2.2. The intensities are normalized with respect to the input forward intensity. Figure 2.3 shows a transmission spectrum of a one-dimensional PBG. In this Figure, the forward and backward intensities are more than seven times that of the input forward intensity at the middle point of material if we tune the frequency to the first transmission maximum at the low-frequency band edge. It clearly shows the effect of enhanced density of mode on the longitudinal field's profile of the fundamental field tuned at the band-edge transmission resonance.

For different conditions, the peak intensities in the waveguide, as shown in Figure 2.4 and 2.5, are much smaller than those in Figure 2.3. The frequency,  $\omega$ , in Figure 2.4 is tuned to the second transmission maximum, and  $\omega$  in Figure 2.5 is tuned to a frequency between the first and second transmission maxima. They are expressed

as shifts of normalized frequency from the center of the band gap. Figure 2.5 shows that the intensities in the material are not enhanced at all between the transmission resonance frequencies, showing the lack of penetration of light into the PBG. In our experiment, we will try to optimize the intensity enhancement by finding the frequency for the first transmission maximum, i.e. the  $\omega$  indicated in Figure 2.2 to get the intensity distribution result in Fig. 2.3. It's also noted that phase matching is another concurrent consideration, which affects the SHG efficiency.

## **Chapter 3**

### **Fabrication of Photonic Band Gap (PBG) Structures on Lithium Niobate Waveguides**

#### *3.1 Introduction*

A PBG can be experimentally applied for the purpose of enhancing SHG. However the fabrication of a PBG is always the key problem because of the high precision requirement for the grating pitch. In our experiments a lithium niobate waveguide was made by a method called proton exchange. The PBG was made by using a UV laser lithography method in our lab. Either the photoresist can be used to couple light to the grating or the grating can be subsequently impressed into the waveguide by dry etching technology. A new Cerenkov radiation method devised during this project and other diffraction methods were initially used to analyze the accuracy and tolerance of PBG.

The interest in using a guided-wave configuration for nonlinear interactions was recognized in early in the development of nonlinear optics. Many groups investigated the theory of a PBG for SHG enhancement in the waveguide, and the enhancement was predicted to be several orders of magnitude [6, 7, 8, 9, and 12], however no experiment reporting this enhancement was previously reported. The main problem for the fabrication of a PBG in this configuration is the fabrication accuracy of the PBG's pitch

in the lithographic process. One paper mentions an accuracy of 0.0027nm for a fixed-wavelength source with the PBG transmission at 3 GHz wide or 0.024 nm at the operating wavelength of 1.55  $\mu\text{m}$ , the tolerance of corresponding pitch  $\Delta\Lambda$  is less than 0.0027 nm. Some have pointed out that the tolerance should be in the order 7 ppm (parts in  $10^6$ ) to ensure the tuning of the fundamental wavelength to the band edge resonance<sup>[12]</sup>. It's difficult to reach those accuracies when the processing also includes etching steps in the process. A new method is developed to achieve a high accuracy of the PBG pitch in our experiment.

In a recent paper, an e-beam was used to make a 350 nm grating, but its accuracy related with the effective refractive index is not considered. So it's not a practical technique for production of our gratings. Also, the e-beam is too slow and expensive for general use.

In our experiment, a UV laser lithographic method was used to make a photoresist mask. The grating period was determined by using Cerenkov radiation method that will be introduced later. And then the result will be checked by several grating diffraction methods. Finally, the enhancement of SHG in the Cerenkov configuration was explored.

### *3.2 Sample Design*

The orientation of crystal is shown in a 3-dimensional coordinate system (X,Y,Z) shown in Figure 3.1. It's very important to note that the definition of the coordinate system is totally different from that in the crystals. For example, the designated +Z (or +C) crystallographic direction of the crystal is actually the +X direction defined in Figure 3.1.



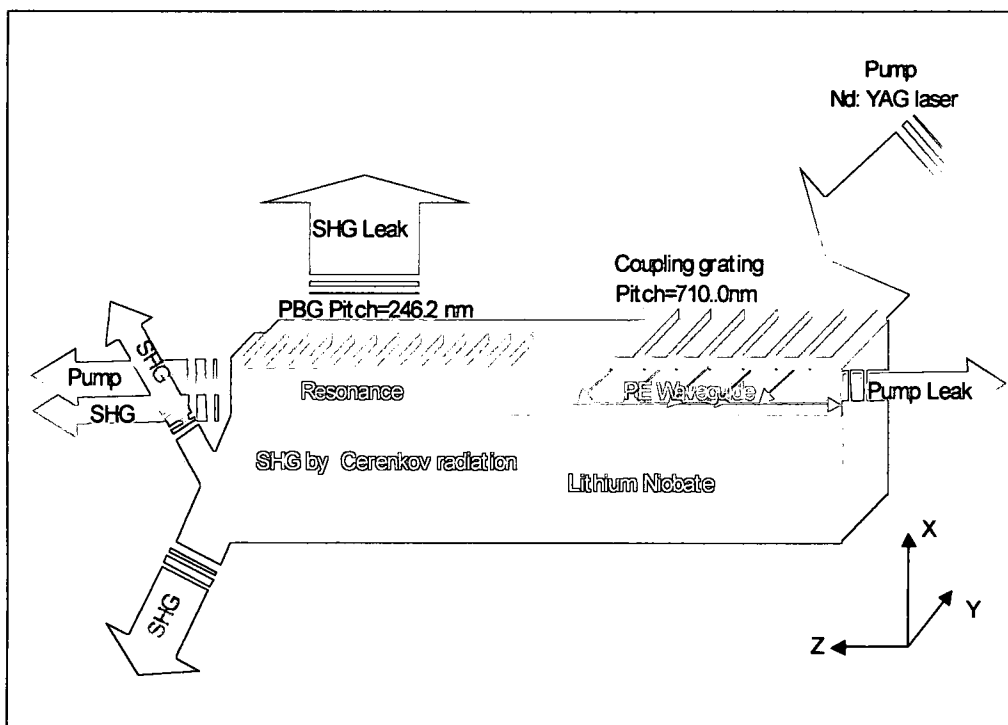


Figure 3.1 - Principle of experimental sample in a three dimensional view for PBG enhanced SHG.

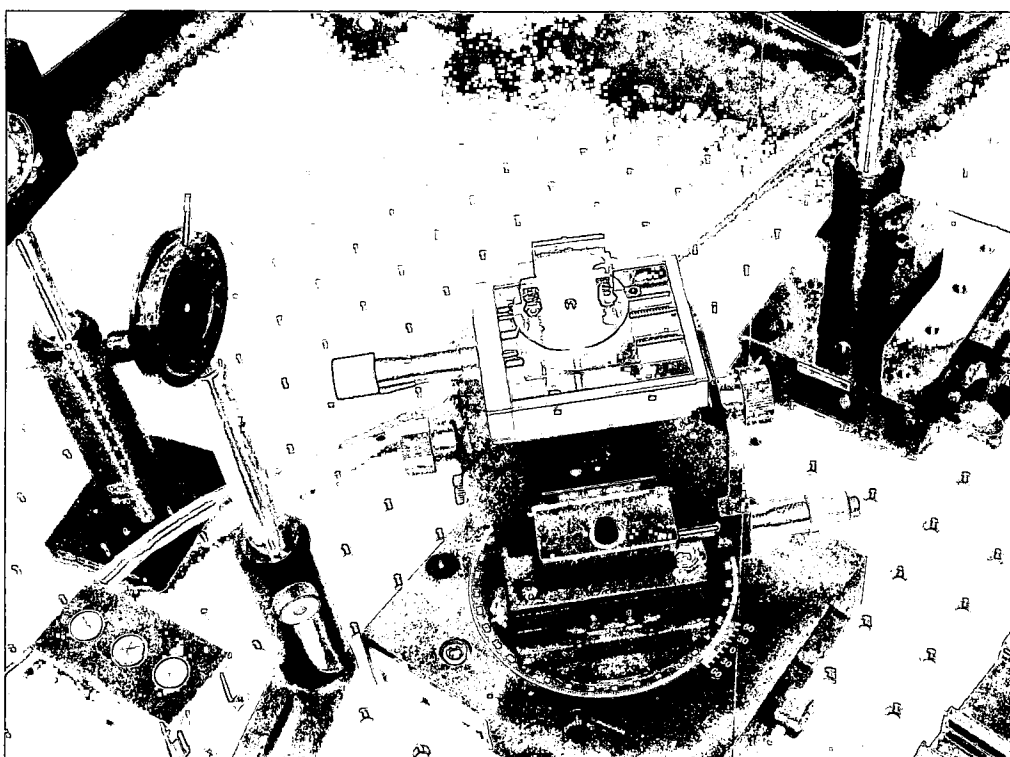


Figure 3.2 – Sample with a size of  $1\text{cm} \times 1\text{cm}$  placed on top of a stage.

In the experiment, the waveguide is made on the +Z surface of crystal. In Figure 3.1, the planar waveguide produced by proton exchange and a photoresist film is spin coated on the surface. Two different gratings are written on the sample. The grating that couples the pump into the waveguide has a pitch of 710 nm; it couples the pump wave into the waveguide (right side) at a around 45° angle in Figure 3.1. The actual photo of sample can be seen in Figure 3.2.

The PBG grating is chosen for the resonant enhancement of SHG using the band-edge resonance effect (half of left side), which is 246.2 nm for sample No. 1. On left side of the sample (parallel to Y-Z plane), the other half of the sample also has a homogeneous cladding index. The so-called Cerenkov phase-matching condition, in which a radiating second-harmonic field is phase matched to the fundamental field in the waveguide, is met. Therefore, two Cerenkov SHG signals are emitted with the same

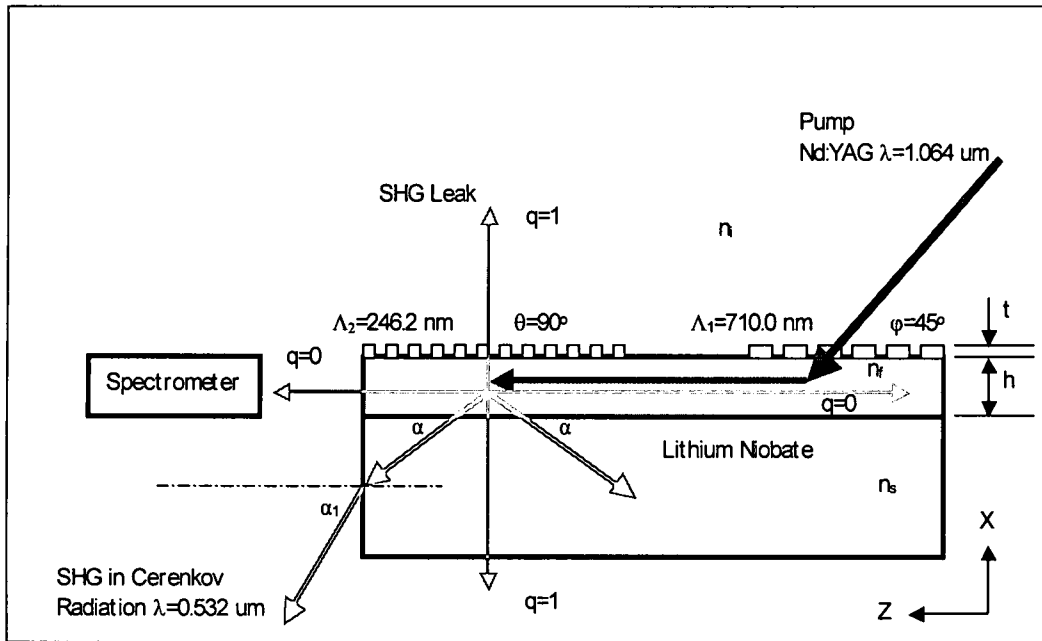


Figure 3.3 – 2-D schematic diagram illustrating the principle of Cerenkov radiation in the sample in the side view of sample No.1.

angle  $\alpha$ . A weaker SHG is emitted from the left edge of sample in X direction. A SHG was also weakly diffracted out vertically (X direction) from the PBG grating surface.

A side view in X-Z plane is shown in Figure 3.3 to explain the principle. For sample No.1, the thickness of grating is chosen to be  $t=100$  nm and the thickness of waveguide is  $h=1.5$   $\mu\text{m}$ . The  $n_i$ ,  $n_f$  and  $n_s$  are the refractive indices of air, waveguide and substrate respectively. A Nd: YAG laser (or other lasers in our later research) with wavelength of  $1.064\mu\text{m}$  is coupled into the PE waveguide with incident angle  $\varphi=45^\circ$ . Output wavelength is half of  $1.064$   $\mu\text{m}$ , equal to  $0.532$   $\mu\text{m}$ . The Bragg scattering angles for the pump and SHG light can be described by the following formulas:

$$k_0 n_0 \sin(\theta) = \beta - q\kappa \quad (3.1)$$

$$\text{and } k_0 = 2\pi / \lambda, \kappa = 2\pi / \Lambda, \quad (3.2)$$

Let's discuss the SHG at  $\lambda=0.532$   $\mu\text{m}$  by using Equations 3.1 and 3.2. Now  $n_0$  is the refractive index of either air or waveguide.  $\beta$  is the propagation coefficient of the guided mode in the waveguide. The  $q$  is the order of diffraction. The grating period  $\Lambda=246.2$  nm. If  $q$  is either 0 or 1, the diffraction angles  $\theta$  are calculated to be  $0$  or  $90^\circ$  respectively. Those four diffractive rays have been observed in our experiments. Cerenkov SHG radiation is emitted at an angle  $\alpha$ , and then refracted out from the edge of sample at the angle of  $\alpha_1$ , this is also shown in Figure 3.2 and 3.3, which will be carefully discussed later in this paper. The refractive angle  $\alpha_1$  on the left edge of sample in Figure 3.2 can be accurately measured and used to calculate the effective refractive index of modes inside the waveguide.

### 3.3 Properties of Lithium Niobate

The LiNbO<sub>3</sub> used in our experiment was made in the congruent melt process. Therefore, the index dispersion of our LiNbO<sub>3</sub> samples for the ordinary and extra-ordinary waves are given by <sup>[17]</sup>:

$$n_o^2 = 4.9048 + \frac{0.117680}{\lambda^2 - 0.047500} - 0.027169 \times \lambda^2, \quad (3.3)$$

$$n_e^2 = 4.5820 + \frac{0.099169}{\lambda^2 - 0.044432} - 0.021950 \times \lambda^2, \quad (3.4)$$

where  $n_o$  is the ordinary refractive index, and  $n_e$  is the extra-ordinary refractive index. Only TM modes are excited inside the waveguide for both pump and SHG light in our experiment because the proton exchange only increases the index for waves polarized in the TM direction of sample,

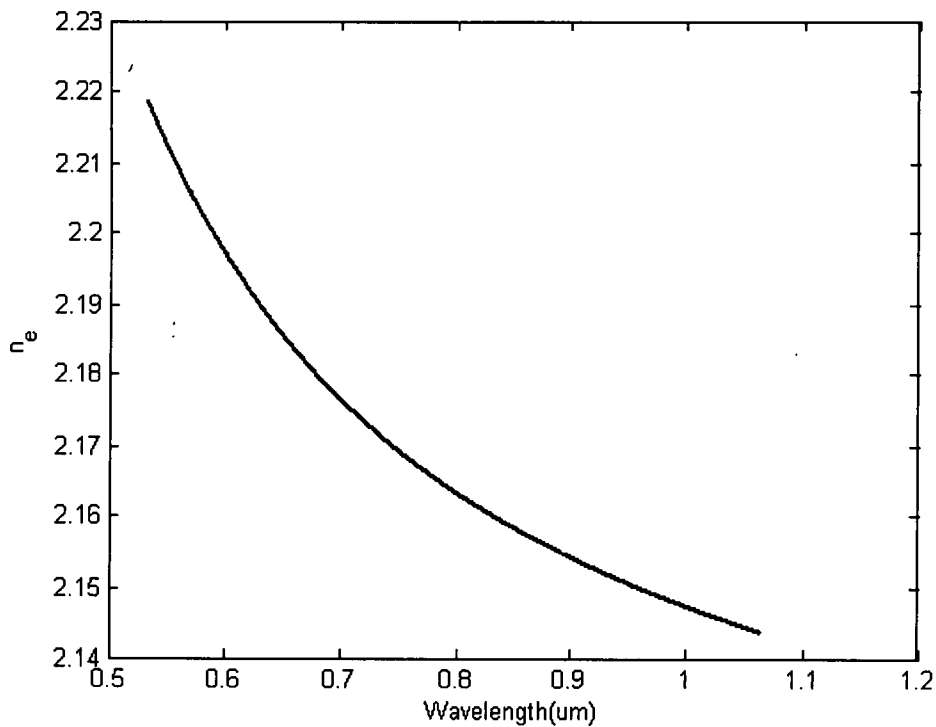


Figure 3.4 - The dispersion of the extra-ordinary index.

which is an electric field polarization in the plane of X-Z. Thus only the extra-ordinary index need be considered in this waveguide. By using Equation 3.4, the value of indexes are calculated to be

$$n_e=2.14 \text{ at } \lambda=1.064 \text{ } \mu\text{m} ;$$

$$n_e=2.21 \text{ at } \lambda=0.532 \text{ } \mu\text{m} .$$

The extra-ordinary index plot according to Equation 3.4 is shown as Figure 3.4. Most physical properties of lithium niobate crystals are described using an orthonormal coordinate system (X, Y, Z) where the Z-axis coincides with the hexagonal symmetry axis C, and the X-axis is taken parallel to one of the equivalent hexagonal “a” axes <sup>[17]</sup>. The orientation of +Z (also called +C) direction is important for etching processing. +Z and -Z surfaces were used to make waveguides in our experiments. It should be noted again that this coordinate is different from the one used in this theses to define the direction propagation inside the waveguide.

For pump of  $\lambda=1.064 \text{ } \mu\text{m}$ , the nonlinear coefficients are reported to be <sup>[17]</sup>:

$$d_{22} \cong 2.1 \text{ pm/V}$$

$$d_{31} \cong -4.35 \text{ pm/V} ,$$

$$d_{33} \cong -27.2 \text{ pm/V}$$

The orientation of our sample shown in Figure 3.1 and 3.2 is designed to couple light to the strongest nonlinear coefficient  $d_{33} \cong -27.2 \text{ pm/V}$ . Only  $d_{33}$  will be used in our experiment. We note, however, that  $d_{33}$  could be weakened by the processing conditions. Several items reported affect the nonlinear coefficient such as the proton exchange, annealing and the processing temperatures in the experiment.

### 3.4 Waveguide Fabrication

A suitable waveguide for a frequency conversion device in  $\text{LiNbO}_3$  should preserve the nonlinear susceptibility of the crystal, have low loss, be resistant to

photorefractive damage, and be compatible with the inverted domain structure. Two techniques are mainly used to fabricate waveguides in  $\text{LiNbO}_3$ . The first approach, introduced by Schmidt and Kaminow in 1974, consists of localized titanium ion diffusion. The second, proposed by Jackel in 1982, is based on proton exchange (PE) between  $\text{Li}^+$  ions of the crystal and  $\text{H}^+$  obtained from an acid.

However, the well-studied titanium diffused  $\text{LiNbO}_3$  waveguides are not generally suitable for SHG nonlinear optics for several reasons. The  $\text{Ti}:\text{LiNbO}_3$  waveguides fabrication is performed at elevated temperatures ( $\approx 950 \rightarrow 1100^\circ\text{C}$ ), which could modify the domain structure of the crystal. Also,  $\text{Ti}:\text{LiNbO}_3$  waveguides display photorefractive damage at near-infrared power levels exceeding tens of milliwatts, making them impractical for nonlinear optical applications. As an alternative, the proton exchange (PE) process and annealed proton exchange (APE) in  $\text{LiNbO}_3$  provide excellent waveguides for these purposes. PE waveguides have a step index profile with a large extraordinary refractive index change ( $\Delta n \sim 0.1 \sim 0.14$ ), which is around 0.1 in our experiment, and are fabricated at temperatures below  $350^\circ\text{C}$ , and furthermore the best PE and APE  $\text{LiNbO}_3$  waveguides were reported to have low propagation losses, and the resistance to photorefractive damage orders of magnitude greater than those of  $\text{Ti}:\text{LiNbO}_3$  <sup>[18][19]</sup>.

$\text{Ti}:\text{LiNbO}_3$  waveguide may be used in the case of Cerenkov SHG because, in this case, the nonlinearity in the substrate is not changed and it's more important than the nonlinearity in the waveguide. However, the index change is much smaller in this case and these waveguides can have a photorefractive effect.

A proton exchange (PE) setup is shown in Figure 3.5 and 3.6. PE and Annealing PE (APE), using benzoic acid as the proton source, have become popular techniques to form waveguides in LN. Particularly the good power handling capability and the

possibility to get high confinement have made this waveguide formation method the choice for nonlinear integrated optics, which will be discussed

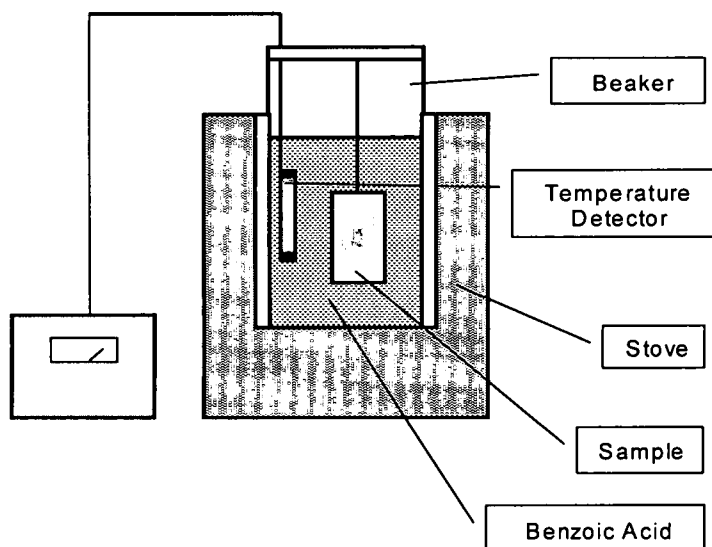


Figure 3.5 - Proton exchange setup

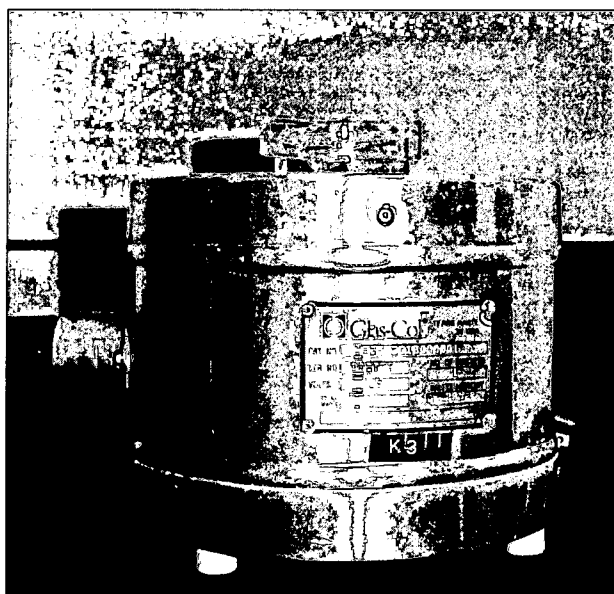


Figure 3.6 - The real setup for making exchange  $\text{LiNbO}_3$  waveguide.

in the following section. In the PE process the  $\text{LiNbO}_3$  sample is immersed in an acid, often a benzoic acid melt, at around  $215^\circ\text{C}$  for exchange time of 2 hours. The temperature was measured by a thermocouple that was connected to a calibrated multimeter. During the ion exchange reaction  $\text{Li}^+$ -ions diffuse out of the crystal surface, and  $\text{H}^+$ -ions diffuse into the crystal to replace the  $\text{Li}^+$ . The ion exchange results in approximately step-like proton concentration and refractive index profiles, which will be discussed in greater detail later. Effective waveguide could not be made if the temperature is lower than  $190^\circ\text{C}$  in our experiment. Finally, different waveguide depths were found by using different processing times. The waveguide depth can be calculated by using the WKB method; this will be examined in section 4.5.3. The range of waveguide depths is between  $0.4\text{ }\mu\text{m}$  and  $2.0\text{ }\mu\text{m}$ . Finally, a depth close to  $1.5\text{ }\mu\text{m}$  was found for our experiment (based on measurements described later) because the second mode in this waveguide results in a higher SHG efficiency than the first mode, which will be discussed in the section of modeling. It will also be shown later that the efficiency in a thinner waveguide with only one mode is also lower than that of the second modes in a thicker waveguide with two modes.

Most people mentioned that the PE processing might reduce the nonlinear coefficient  $d_{33}$  in the waveguide of  $\text{LiNbO}_3$  <sup>[20 - 22]</sup>, thus reduce the efficiency of SHG in the waveguide. This is consistent with our findings that it is much easier to produce CSHG radiation than SHG in the waveguide. Annealing is a technology to overcome this deficiency. Some reports claim only 50% of  $d_{33}$  could be recovered. But annealing can reduce the refractive index of waveguide from our experiment. Other reports claim that after heated in BA for more than half hour the  $d_{33}$  couldn't be recovered. I tested the results by making more samples with different PE times and anneal times.



Another processing chemical, pyrophosphoric acid, was also used in place of benzoic acid for proton exchange; it was widely reported to produce higher index increases, about 0.14 <sup>[23][24]</sup>. Therefore, in our experiment, the pyrophosphoric acid was also used during the proton exchange processing, but serious damage on the sample's surface was found, which means the waveguide was lossy due to additional scattering. We decided against further use of pyrophosphoric acid in our lab. However, this process could be modified and improved to achieve better waveguide characteristics in the future work. Benzoic acid vapor can be considered to improve the index profile <sup>[25]</sup>. Reverse proton exchange may be used to improve the confinement of fundamental mode in the waveguide <sup>[25 - 27]</sup>.

Annealing was tried in our experiment to help recover the  $d_{33}$  nonlinearity of  $\text{LiNbO}_3$ , but the result was not as good as we expected. After the samples were annealed at 350 °C for hours (from 1 to 24 hours), the nonlinearity could not be recovered, also the refractive index difference in the waveguide was reduced, which reduces the mode confinement in the waveguide.

### *3.5 Grating Fabrication*

#### *3.5.1 Laser Lithography Technique*

An Argon Ion laser with SHG in the wavelength of 244nm is used in our setup, shown in Figure 3.7. By changing the angle of interference,  $\theta$ , between the two beams we can alter the grating period. The pitch of the grating can be calculated from the formula:

$$\Lambda = \frac{\lambda}{2 \sin(\theta)}, \quad (3.5)$$

where

$$\theta = a \sin\left(\frac{\lambda}{2\Lambda}\right). \quad (3.6)$$

For example, the angles in Figure 3.5 on the rotating stage for two pitches of 246.2 nm and 710.0 nm for sample 3 are 30.30 ° and 9.86 ° respectively using Equation 3.6. So we have a wide range of angles that can be used in the experiments.

The laser is focused by the first lens. A spatial filter with a pinhole of diameter 15 µm is situated at the focal point of the lens, forming a clean diffractive beam, which is collimated by the second lens. The beam is expanded to cover the mirror and sample surfaces as shown in Figure 3.8. The light reflects off the mirror to form a second beam that interferes with the direct light. The two beams combine to the surface of sample forming a diffractive intensity grating pattern on the photoresist. The sample is exposed for 2 minutes with a laser whose power is around 45 mW before the pinhole. The photoresist is subsequently developed for 5 seconds.

In our experiment, we adjust the time so that the sample is over-exposed. This means that after development the substrate surface is exposed on the sample. In other words, there is no photoresist over part of the grating. This kind of grating can result in a strong coupling efficiency, and a strong resonance at the band edge of the PBG.

Figure 3.9 shows a picture of a photoresist grating on LiNbO<sub>3</sub> by using an atomic force microscopy (AFM). Our experiments give us very good control of the grating period and photoresist coverage by using different exposure times and photoresist development time. We found that the grating is uniform and smooth.

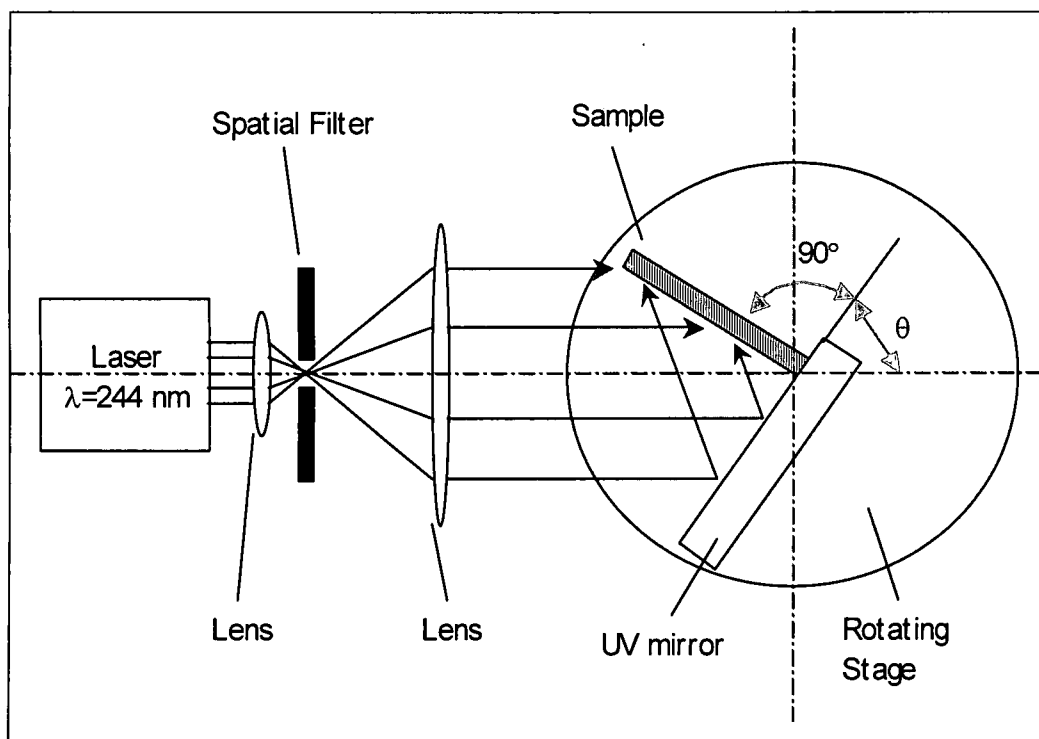


Figure 3.7 - Setup of Exposure System for holographic grating by photoresist on lithium niobate.

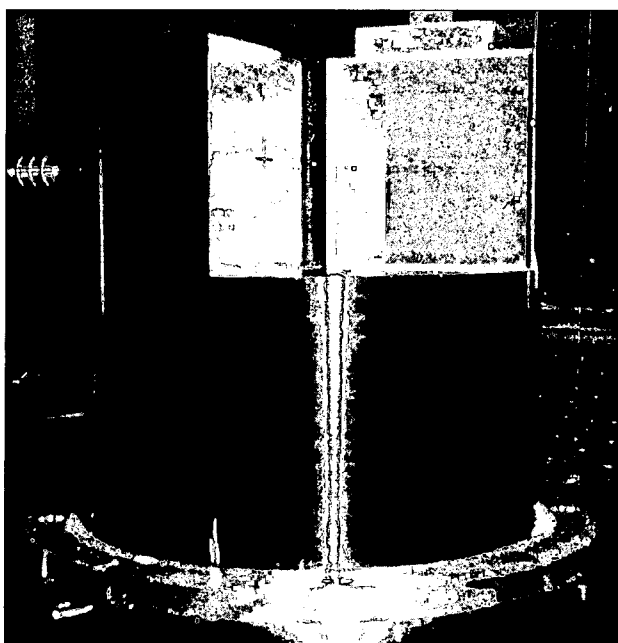


Figure 3.8 – Rotating stage with a UV mirror and a sample holder surface.

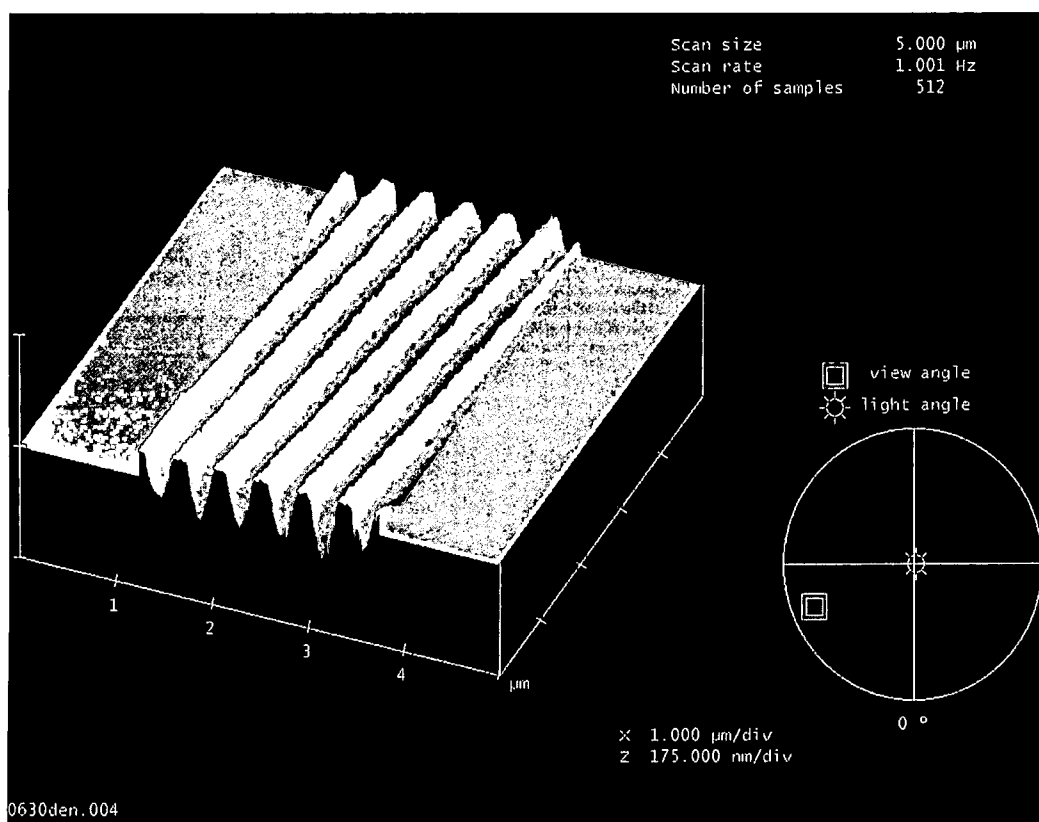


Figure 3.9 – Photoresist profile on lithium niobate. The picture is imaged using an atomic force microscope (AFM).

### 3.5.2 Etching Lithium Niobate

Etching is one of the most important parts of my experiment, which directly affects the SHG result. Generally, there are two main etching methods: wet and dry (or plasma) etching. Wet etching is mainly processed in mixed solution of hydrogen fluoride (HF) and  $\text{HNO}_3$ . Reaction Ion Etching (RIE) with Freon-14 ( $\text{CF}_4$ ) was previously reported as a dry etch method for lithium niobate <sup>[28]</sup>.

HF and  $\text{HNO}_3$  are conventional etch solutions for lithium niobate. Previous experimental results show that the etch rate is very slow and the revealed surfaces after the etch process are nonuniform. Therefore, wet etching in  $\text{LiNbO}_3$  is seldom used except for the observation of domain inversion happened in Z-Cut substrates. Other

methods include: inductively coupled plasma (ICP) etching, ion milling or reactive ion etching by an ion beam. In our experiments dry etching always resulted in rough wall sides, which we attribute to the thinness of the photoresist. These results in a lossy grating on  $\text{LiNbO}_3$  <sup>[29]</sup>. The positive Z crystallographic face can be etched by a mixture of HF and  $\text{HNO}_3$  acids if the substrate is previously proton exchanged <sup>[30][31]</sup>. Also laser assisted etching was previously reported <sup>[32][33]</sup>.

The etched samples were characterized using an atomic force microscope (AFM) measurement technique. Since there is a photoelectronic effect on the lithium niobate sample surface, the sample was charged when irradiated by the light used to calibrate the tip position. And therefore the force between the tip and the surface of material was changed, which makes the measurement impossible. To solve this problem, a 100 nm carbon coating was applied on the lithium niobate surface so that electronic charges were

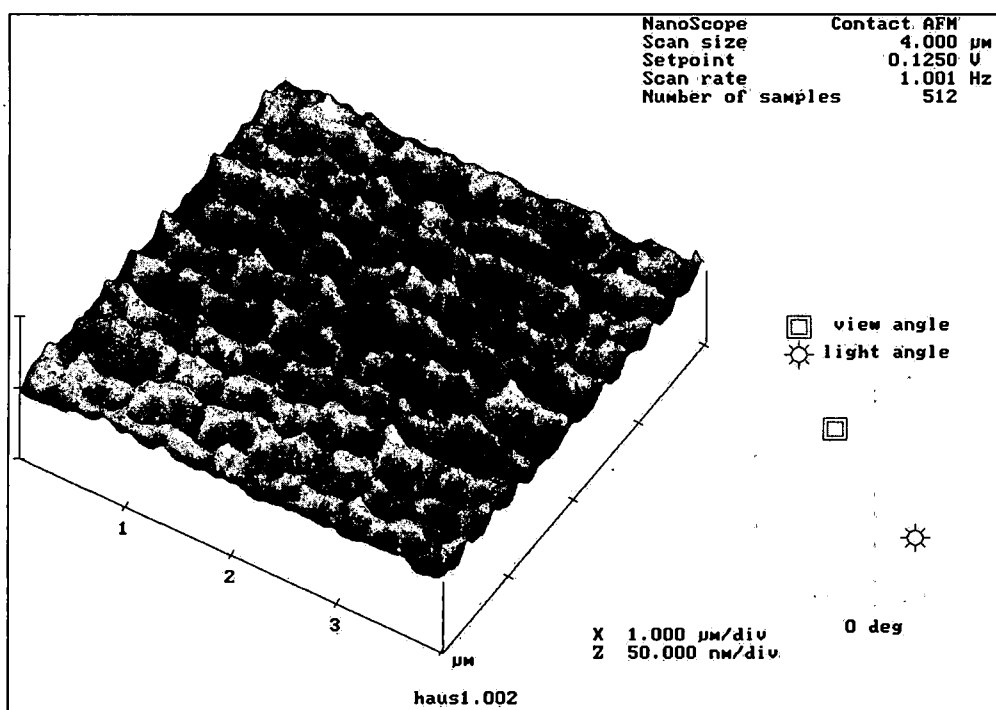


Figure 3.10 - AFM of lithium niobate with ion milling.

conducted into the grounded stage so that there is no electrostatic force contributing to the AFM measurements. The accurate topology of the samples can be measured by coating the material, as shown in the Figures 3.10 – 3.14.

No good quality gratings were obtained using wet etching in our experiment. The result after ion milling was not good either, as shown in Figure 3.10. The grating can barely be seen from this picture. Another dry etching method, the inductively coupled plasma (ICP) etching with Freon gas gave promising results. We believe this can be developed into a suitable grating technique for lithium niobate. Figures 3.11 - 3.14 display the results of ICP etching; we use both AFM and SEM measurement techniques to image the samples. The focus of future research will be on ICP etching.

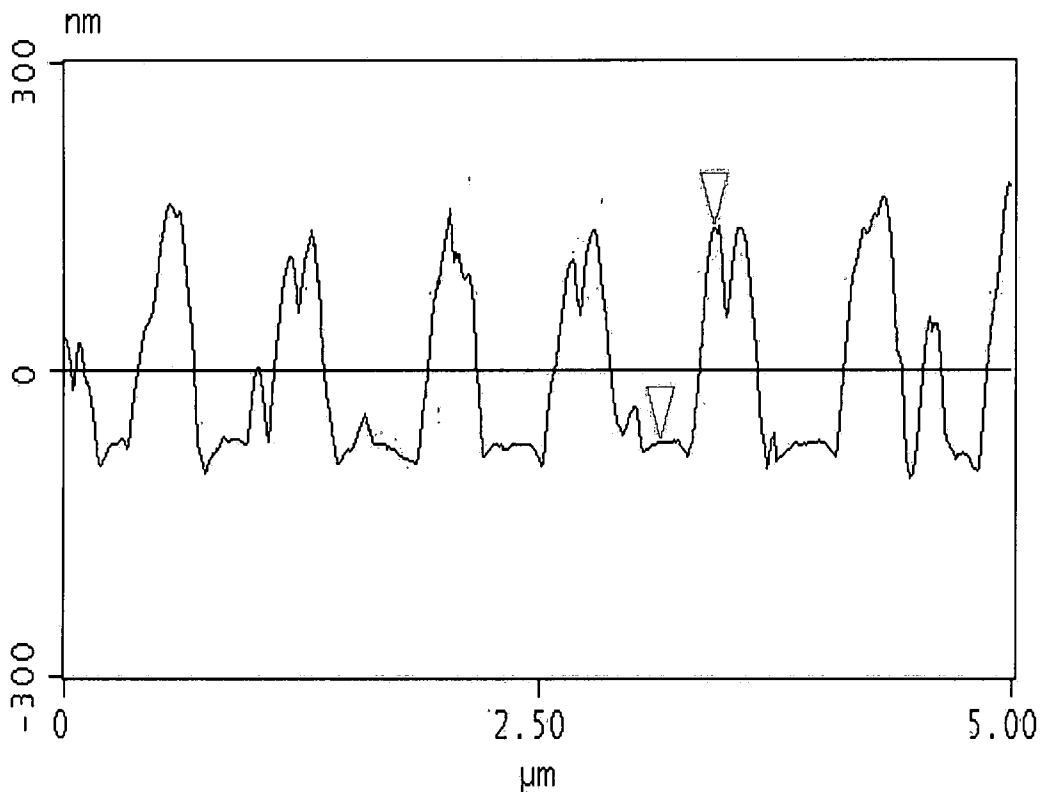


Figure 3.11 - AFM result. ICP etching on the +z surface of  $\text{LiNbO}_3$ . The pitch is 710nm and the Depth is 203 nm. Surface is non- uniform.

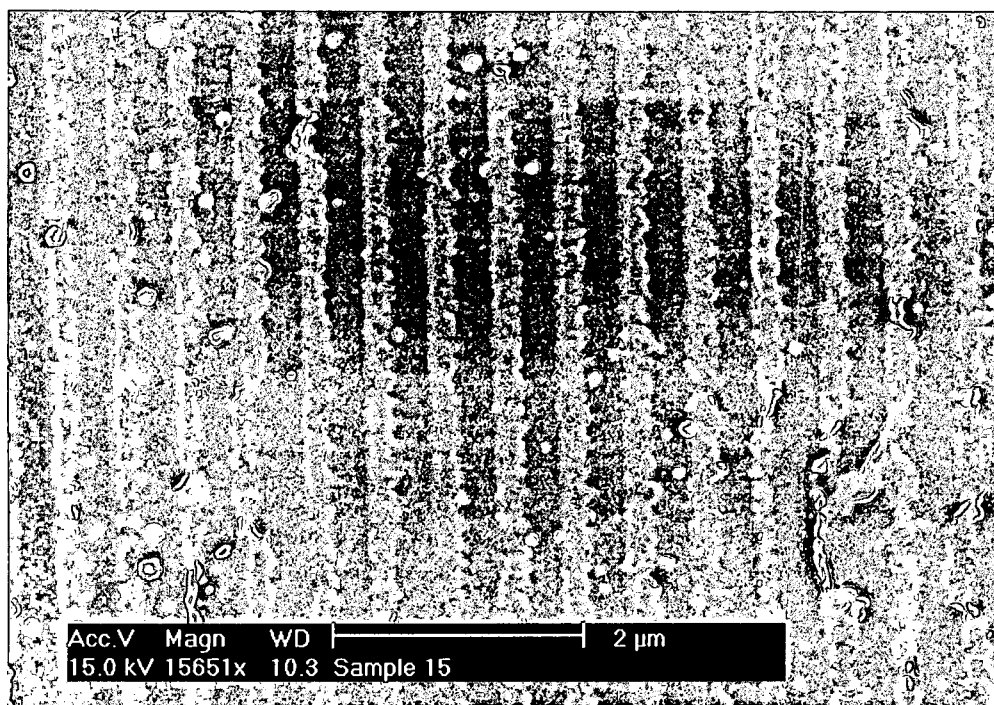


Figure 3.12 - SEM of LN etched using ICP.

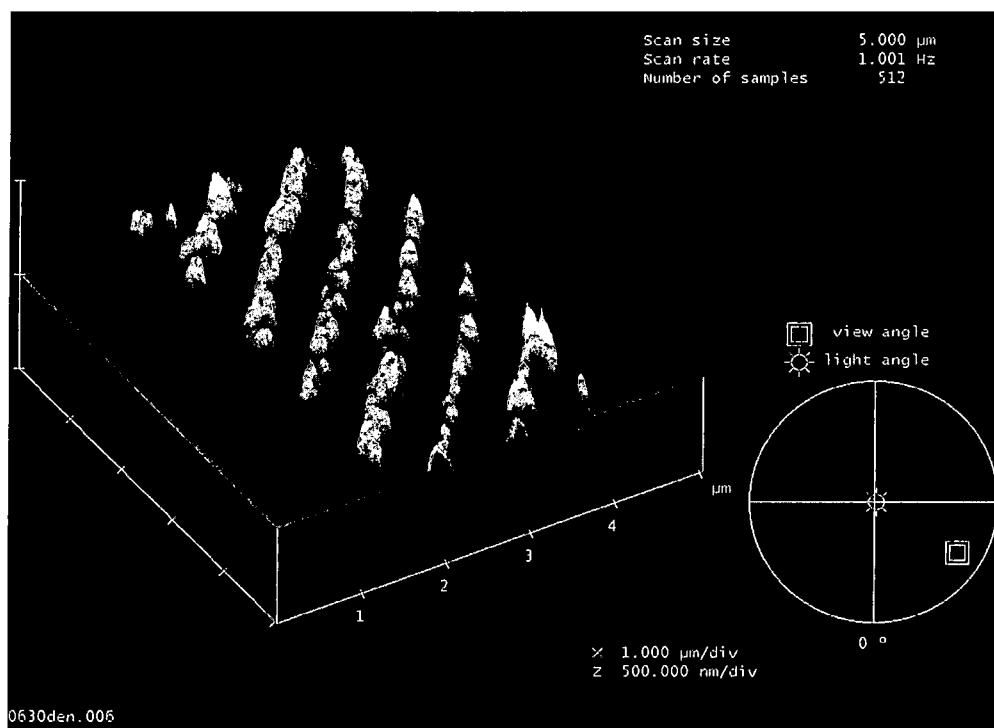


Figure 3.13 - Tapping Mode AFM of lithium niobate etched using ICP.

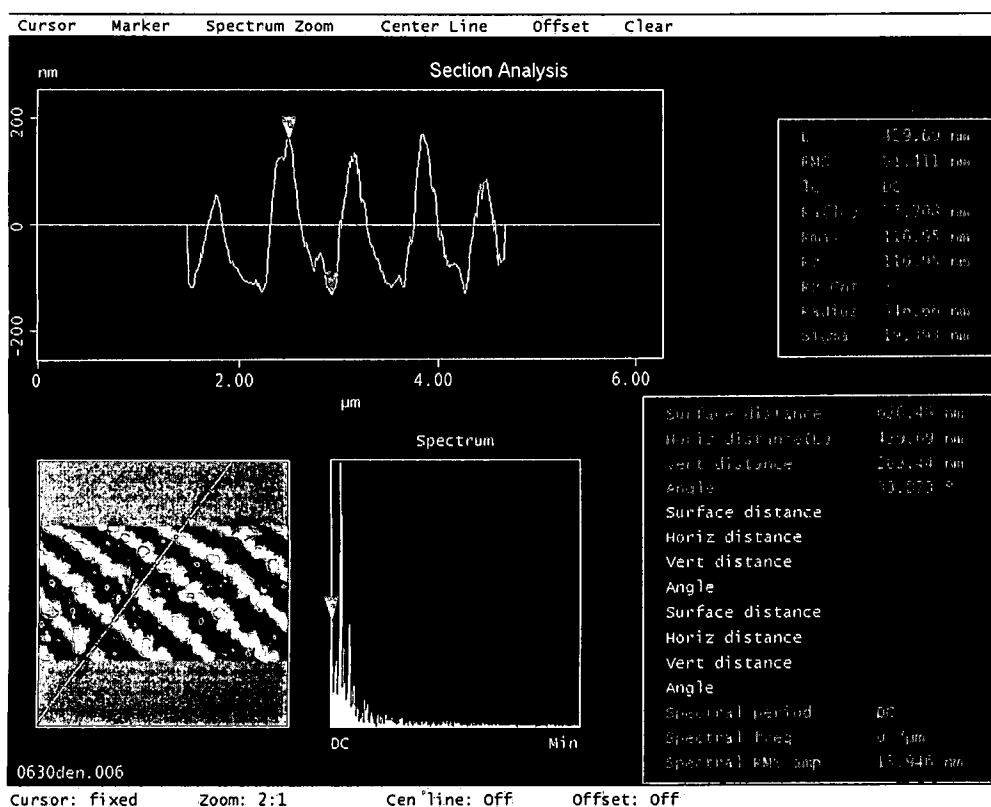


Figure 3.14 - Tapping Mode AFM of lithium niobate with ICP. The depth is 228 nm.

### 3.6 Measurement of Waveguide Effective Index

Several methods, such as prism coupling, Cerenkov SHG radiation, m-dark line and x-ray <sup>[34]</sup>, are reported to characterize the waveguide. In this section, we will demonstrate the methods to characterize to waveguide. The Cerenkov radiation method can be used to find the effective refractive indexes of pump in the waveguide. The prism coupling and diffraction method can also be used to determine all the effective refractive indices in the waveguide. A WKB method can be used to accurately find the index profile and the depth in waveguide.



### 3.6.1. Cerenkov Radiation Method

If the refractive index of the substrate region at  $2\omega$  is greater than the effective index of the guided fundamental mode at  $\omega$ , Cerenkov radiation at the second harmonic will be radiated into both the substrate and the air at the angle of  $\alpha$  as required by the phase-matching condition <sup>[35 - 38]</sup>. By using Cerenkov SHG radiation the effective refractive index of mode of fundamental wave can be easily obtained.

According to the dispersion relation,  $n_e = 2.14$  at  $\lambda = 1.064 \mu\text{m}$   $n_e = 2.21$  at  $\lambda = 0.532 \mu\text{m}$ , therefore, the Cerenkov radiation can be readily observed in our samples and it is quite strong. The following typical data was measured from sample 3 and was used in our experiment:

A Nd: YAG laser was used as the pump. For sample No.1, the SHG radiation angle is measured to be  $\alpha = 13.11^\circ$ .  $n(2\omega) = 2.22$  is the substrate index at the second harmonic and can be referenced to the extraordinary index in our TM mode case. The effective index is  $n_{\text{eff}}(\omega) = 2.22 * \cos(\alpha) = 2.16$ . Given an index increase  $\Delta n(\omega) \approx 0.1$  in the waveguide, where the index profile is step like <sup>[13][35]</sup>. The wavelength of Nd: YAG pump laser is  $1.064 \mu\text{m}$ , then for  $n_{\text{eff}}(\omega) = 2.16$  and Snell's law for the air-waveguide interface at the output face,  $n(2\omega)\sin(\alpha) = \sin(\alpha_1)$ , the angle is  $\alpha_1 = \arcsin(n(2\omega)\sin(\alpha))$ . Therefore, the  $\alpha_1$  is  $30.21^\circ$ , which was observed in the Figure 3.15.

Several methods, such as prism coupling, Cerenkov SHG radiation, m-dark line and x-ray, are available to characterize the waveguide modes. In our experiment several methods were used: prism coupling, grating diffraction, WKB method and Cerenkov SHG radiation. They are complementary and the results reinforce one another.

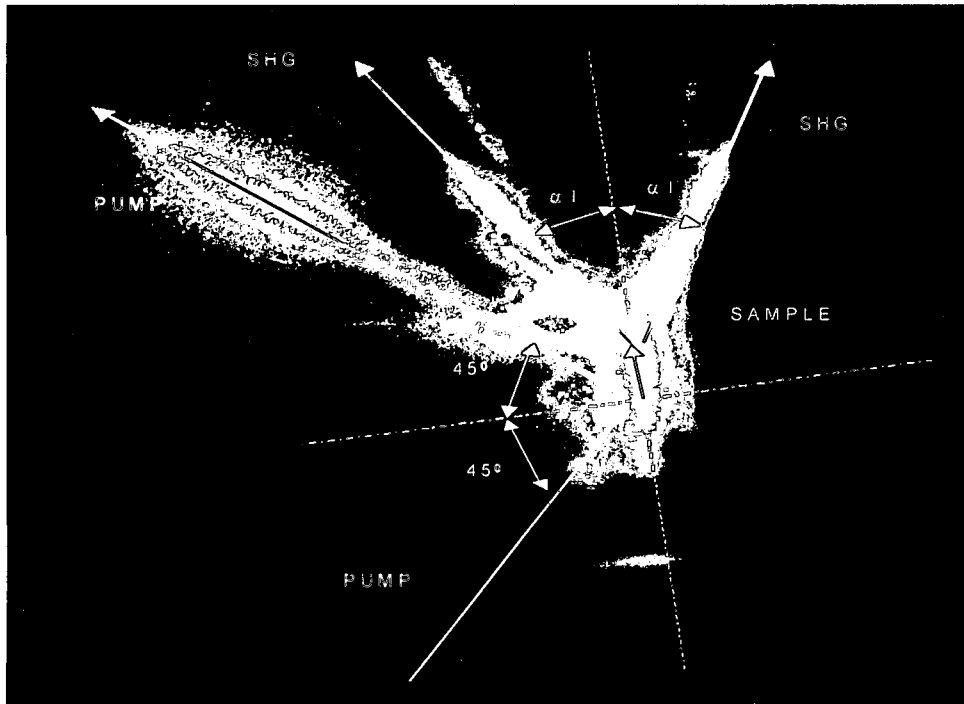


Figure 3.15 a - photos showing sample No.1 is pumped by the YAG and the CSHG output shown in a darkened room, viewed the Y direction in Fig. 2.3.

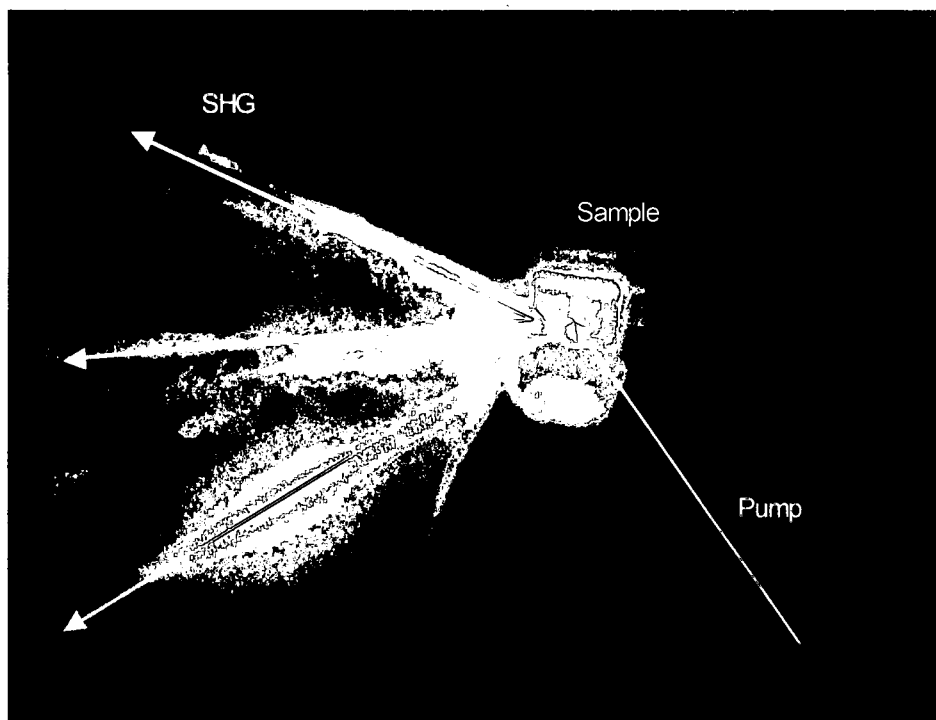


Figure 3.15 b - Real photo of sample No.1, Pump and CSHG can be seen. The first grating can also be seen on the surface of sample.

### *3.6.2 Prism Coupling Method*

The schematic for the prism coupling method is illustrated in Figure 3.16. A He-Ne laser is used and a photograph of the experimental setup is shown in Fig. 3.17. The sample to be measured is brought into contact with the base of a prism by means of a pneumatically operated coupling head, creating a small air gap between the film and the prism. A laser beam strikes the base of the prism and is normally totally reflected at the prism base onto a photodetector. At certain discrete values of the incident angle, called mode angles, photons can tunnel across the air gap into the film and enter into a guided optical propagation mode, causing a drop in the intensity of light at the detector.

The sample in Figure 3.18 was proton exchanged in the benzoic acid at 200° for 30 minutes. Therefore only one TM mode was found at the wavelength of He-Ne laser in this sample. This Figure shows that 20% of the light intensity is coupled into the waveguide. Strong scattering was observed in the waveguide due to the surface damage. To a rough approximation, the angular location of the first mode determines film index, while the angular difference between the modes determines the thickness, allowing the thickness and index to be completely independently measured.

The force between the surface and prism must be very strong so that the shape of sample can be changed a little bit on the order of 0.1  $\mu\text{m}$  adjusting air gap and the curvature of the surface between them, which is essential for coupling light into the waveguide. This force may damage the surface, and therefore leaving a scratch on the waveguide. So it's impossible to make a high quality grating on this sample because of the scratches. The prism coupling method can only be used to approximately determine the formation of waveguide for sample in our experiment. In place of this destructive method, a diffraction method was used in our lab, which does not damage the surface of waveguide.

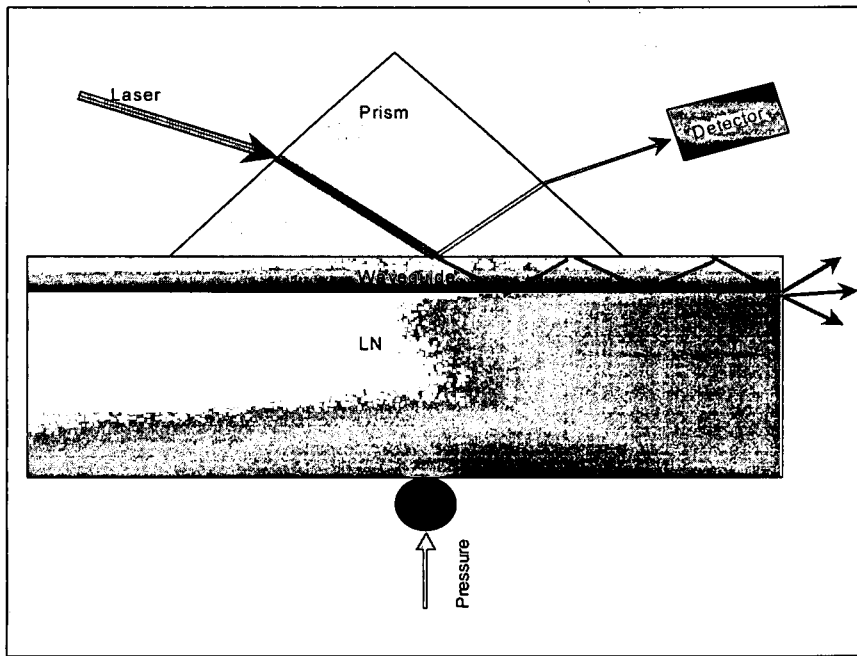


Figure 3.16 - schematic of waveguide mode prism coupling measurement

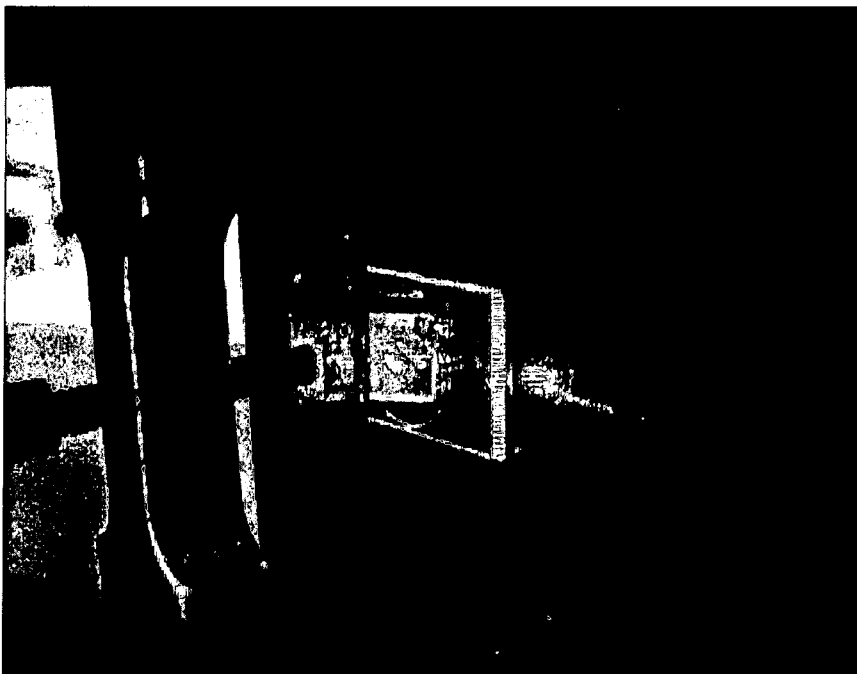


Figure 3.17 - Experimental setup for prism coupling.

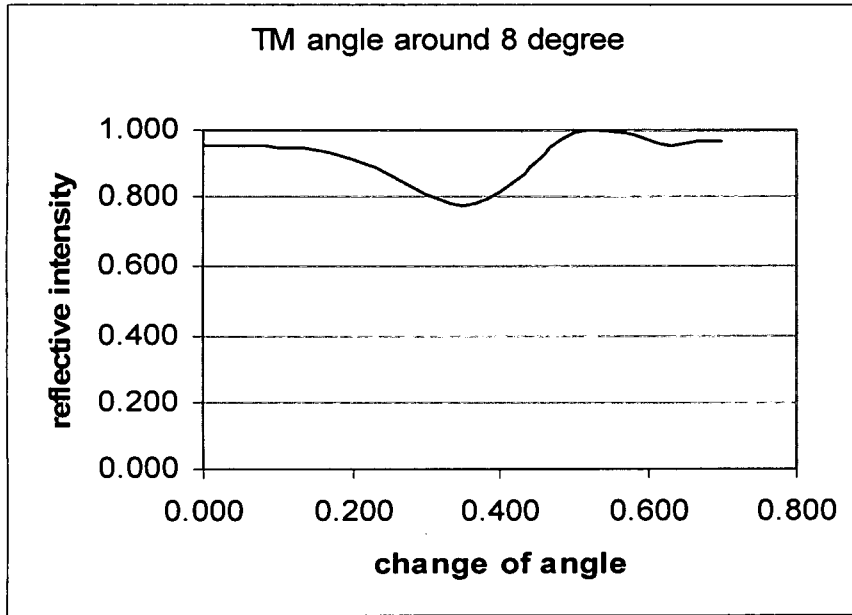


Figure 3.18 - Result of prism coupling. An intensity drop is found at angle of  $8.35^\circ$ , which is the position of 0.39 in the change of angle in this plot

Another method, a modification of the Cerenkov-type SHG method, can also be used in the measurement of  $n_{\text{eff}}$  of fundamental mode in  $\omega$ , the profile and depth can be calculated by using the WKB method. Those methods will be described in the subsequent sections.

### 3.6.3 Determine Waveguide Depth Using the WKB Method

A Cerenkov-type SHG method can also be used in the measurement of  $n_{\text{eff}}$  of fundamental mode in  $\omega$ . The profile and depth can be calculated by using the WKB method [39 - 41]. Getting the waveguide's depth is a difficult part especially when there are very few modes in a waveguide. In order to have more modes in the waveguide, a laser with a shorter wavelength should be used. Also it's known that the waveguide depth is not related to the wavelength of light, so the depth can be accurately determined for all wavelengths by using only one wavelength. In our experiment, there are two modes for the pump with wavelength of  $1.064 \mu\text{m}$ . From the calculation, more

than four modes are expected to be in the waveguide when He-Ne laser in the wavelength of 0.6328  $\mu\text{m}$  is used. Thus a He-Ne laser is used in this method to get the profile of refractive index as well as the depth of waveguide.

First all of the effect refractive indexes in the waveguide should be determined by using the diffractive method. It's proved that <sup>[41]</sup>

$$k_0 n_0 \sin(\theta) = \beta - \kappa = k_0 n_{\text{eff}} - \kappa, \quad (3.7)$$

$$n_{\text{eff}} = \sin(\theta) + \frac{\lambda_0}{\Lambda}. \quad (3.8)$$

So the refractive indexes in the waveguide can be determined by using Equation 3.8 if the wavelength, coupling angle and pitch of grating are known. Then the WKB method can be applied to get the index profile and depth of waveguide by following method. Suppose a waveguide has  $M$  modes. The path length integral for each of the modes has the form <sup>[42]</sup>

$$\int_0^{x_m} [n^2(x) - n_m^2]^{1/2} dx = \frac{4m-1}{8}, m = 1, 2, \dots, M. \quad (3.9)$$

where  $x_m$ , whose unit is the number of wavelength, is defined by  $n(x_m) = n_m$ . We also let  $x_0=0$  and  $n_0=n(0)$ . To determine the values of  $x_m$  from the values of  $n_m$  [and thereby approximate  $n(x)$ ], we proceed by writing Equation 3.9 as a sum of integrals:

$$\sum_{k=1}^m \int_{x_{k-1}}^{x_k} [n^2(x) - n_m^2]^{1/2} dx = \frac{4m-1}{8} \quad (3.10)$$

Next we assume that  $n(x)$  is a piecewise linear function connecting the measured values of  $n_m$ ; i. e.

$$n(x) \approx n_k + \frac{(n_{k-1} - n_k)}{(x_k - x_{k-1})}(x_k - x) \quad \text{for } x_{k-1} \leq x \leq x_k \quad (3.11)$$

If we let  $n(x) + n_m$  be replaced by a midpoint value of  $[(n_{k-1} + n_k)/2] + n_m$  for  $x_{k-1} \leq x \leq x_k$ , the solution for  $x_m$  is

$$x_m = x_{m-1} + \left[ \left( \frac{3}{2} \right) \left( \frac{n_{m-1} + 3n_m}{2} \right)^{-1/2} (n_{m-1} - n_m)^{-1/2} \right] \\ \times \left\{ \left( \frac{4m-1}{8} \right) - \frac{2}{3} \sum_{k=1}^{m-1} \left( \frac{n_{k-1} + n_k}{2} + n_m \right)^{1/2} \left( \frac{x_k - x_{k-1}}{n_{k-1} - n_k} \right) [(n_{k-1} - n_m)^{3/2} - (n_k - n_m)^{3/2}] \right\},$$

(3.12)

and

$$x_1 = \frac{9}{16} \left( \frac{n_0 - 3n_1}{2} \right)^{-1/2} (n_0 - n_1)^{-1/2}. \quad (3.13)$$

Therefore, we have a simple algorithm for calculating  $x_m$  based only on previously determined value starting with  $x_1$ , and  $n(x)$  is determined as approximated in Equation 3.11. Usually, we measure only the guide indices  $n_1, n_2, \dots, n_M$ , and the surface index  $n_0$  is unknown.

Two samples were measured using this method: sample No.2, which was proton exchange processes at 215° for 1 hour and sample No.3 was processes at 215° for 2 hours. Let's discuss sample No.1 first. Three modes were found in this waveguide by using the diffraction method and Equation 3.7 and 3.8. The refractive indexes for those modes are 2.316 2.272 and 2.2096 respectively. The initial index is calculated to be 2.34. Thus the index matrix should be:

$$n = [2.34 \ 2.316 \ 2.272 \ 2.2096].$$

Put those data in the Equations 3.9 – 3.13. An index profile can be reached as shown in Figure 3.19.

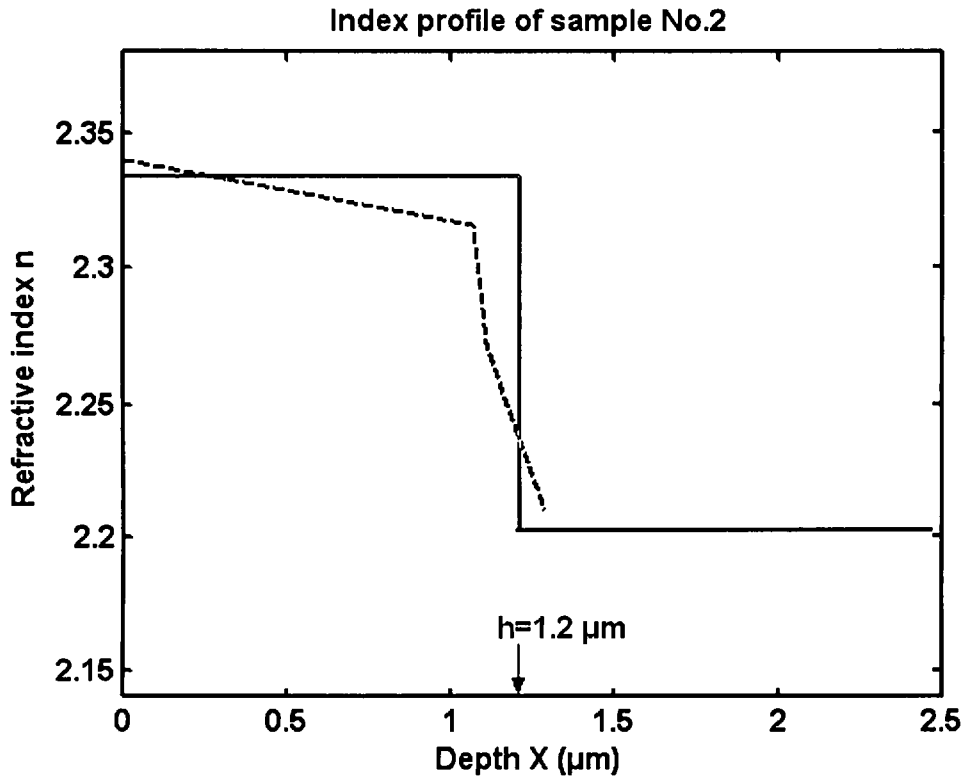


Figure 3.19 - The profile of the refractive index in the waveguide of sample No.2. The dashed line is the WKB result and the solid line represent the step-like fit

In the Figure 3.19, the curved line is drawn from the index and position points found using the WKB method. The step shape line is a fit from the approximation of step profile index. The depth of this waveguide should be  $1.20 \mu\text{m}$ . Therefore for  $\lambda = 0.6328 \mu\text{m}$ ,  $n_c = 1$ ,  $n_f = 2.325$ ,  $n_s = 2.2$  and  $h = 1.20 \mu\text{m}$ .

Doing the same for sample No.3, four modes were found. One more than sample No. 1 because of the longer proton exchange time. The index matrix is given by

$$n = [2.343 \ 2.3329 \ 2.30619 \ 2.27903 \ 2.24182] .$$

Therefore, for  $\lambda = 0.6328 \mu\text{m}$ ,  $n_c = 1$ ,  $n_f = 2.325$ ,  $n_s = 2.2$  and  $h = 1.75 \mu\text{m}$ . An index profile can be drawn from the WKB results as shown in Figure 3.20.



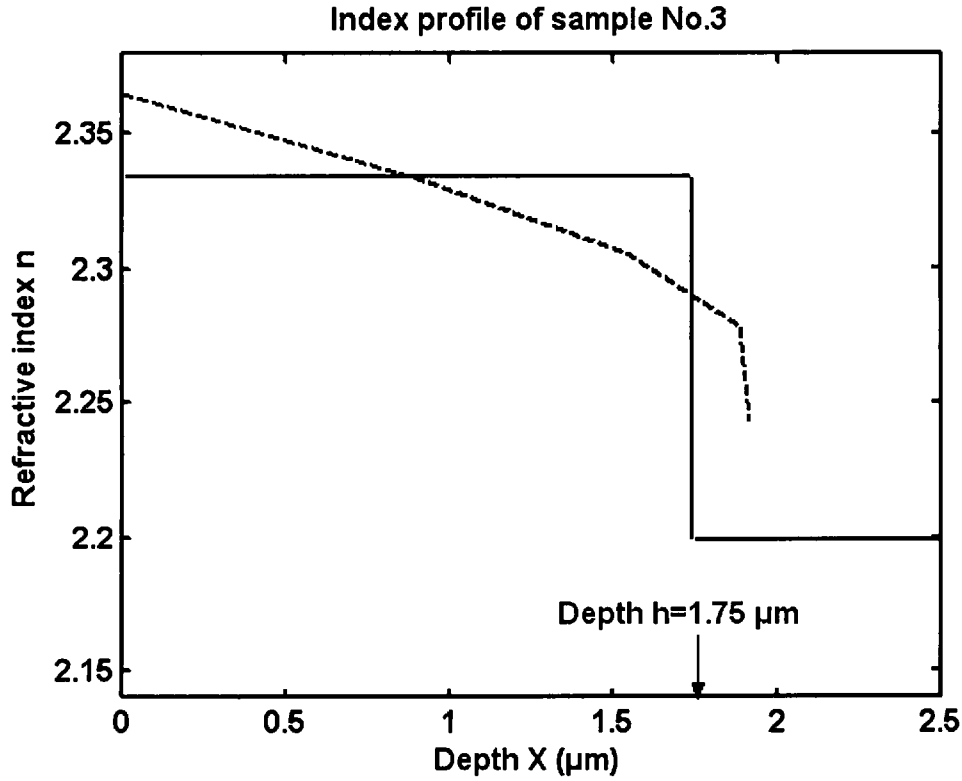


Figure 3.20 - The profile of refractive index in the waveguide No.3. The dashed line is the WKB result and the solid line represent the step-like fit

A Quadratic fitting of the refractive indexes for both samples No.2 and No.3 are shown in Figures 3.21 and 3.22 as a reference in my experiment.

For sample No.2, quadratic fitted equation is:

$$n = -0.088084x^2 + 0.0055027x + 2.3644 \quad (3.14)$$

where  $n$  is the refractive index and  $x$  is the position in the waveguide with a unit of  $\mu\text{m}$ . For sample No.3, quadratic fit equation is:

$$n = -0.02777x^2 - 0.0004357x + 2.3635 \quad (3.15)$$

The depth of waveguide for sample No.1 is measured to be  $h=1.5 \mu\text{m}$ .

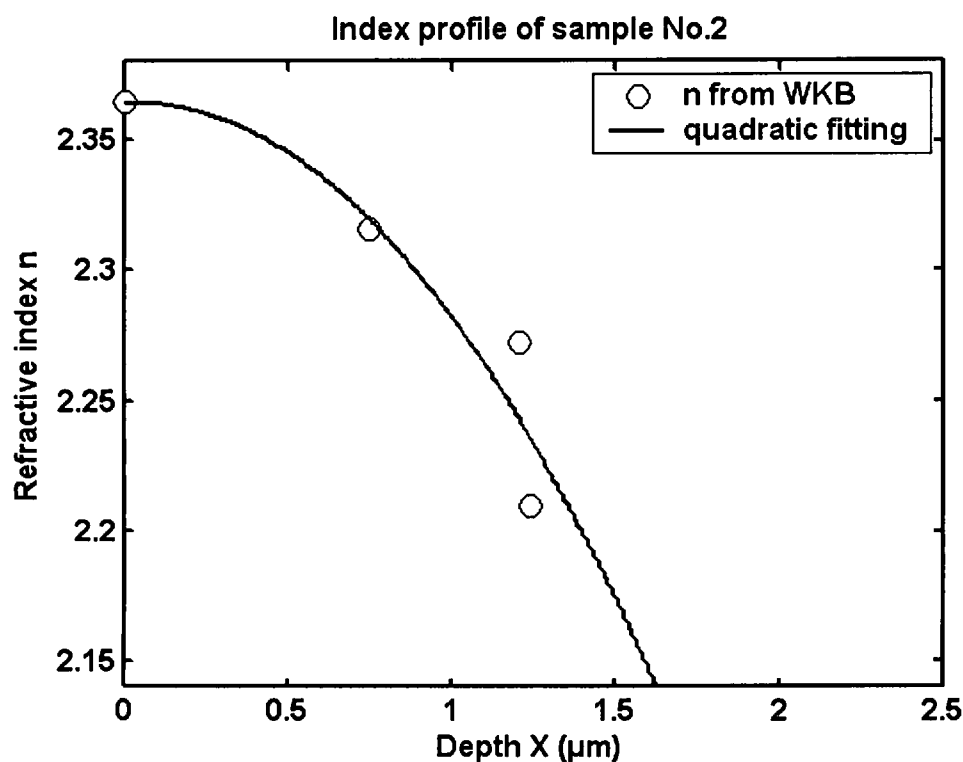


Figure 3.21 - Quadratic fit of the refractive indices for sample No.2.

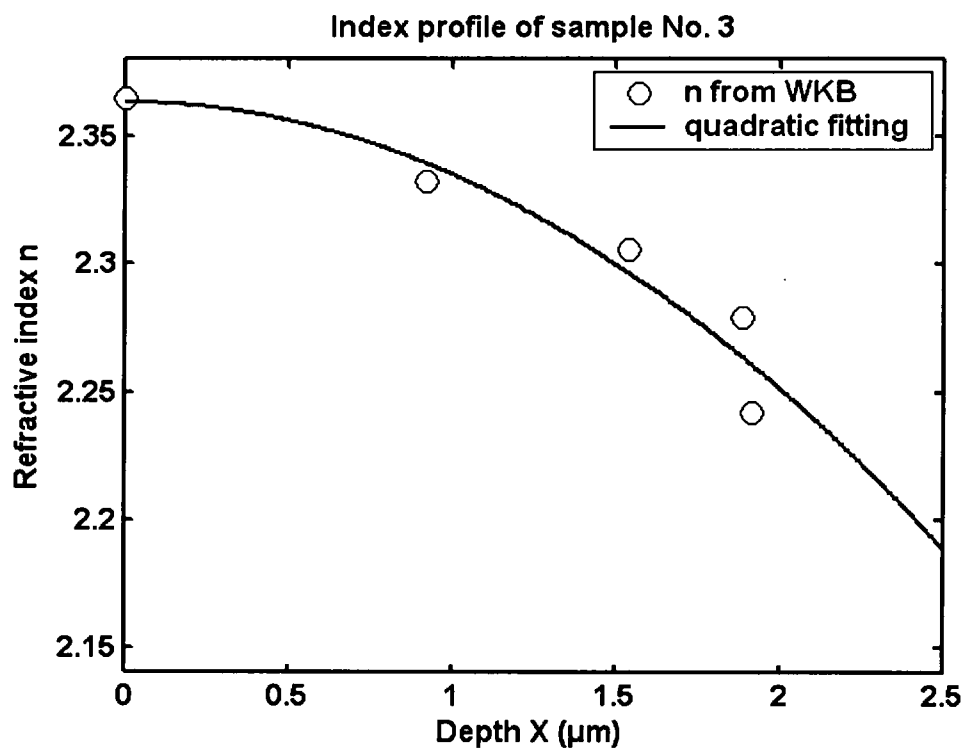


Figure 3.22 - Quadratic fit of the refractive indices for sample No. 3.

### 3.7 Method of Getting Right PBG Pitch on the Waveguide Surface

The process of making a waveguide is not very stable. The effective indices of modes depend on so many variables or details in the fabrication process. Also the pump light may change the effective indices for pump and SHG because it causes temperature changes. It's noted that there is considerable index variations between different materials even when the waveguides were made under the same conditions. The PBG pitches need to be different from each other for different effective refractive indices in different waveguides. So it is very important to determine the pitch for each sample separately. The Bragg condition is used to calculate the pitches by the following well-known formula:

$$\Lambda = m\lambda / (2n_{\text{eff}}) . \quad (3.16)$$

where  $m$  is the order under the Bragg condition.  $n_{\text{eff}}$  must be the effective index of pump in the waveguide, which is not easily controlled.  $\Lambda$  is the pitch of PBG so that the resonance of pump light can be reached around this pitch.

In our lithographic system the accuracy of the pitch can be controlled to under  $\pm 1\text{nm}$ . The pitch must be very accurate according to the PBG theory. For example, the bandwidth of Nd: YAG laser is  $\Delta\lambda=0.4\text{ nm}$  for  $m=1$ , using sample No.1 when  $\lambda=1.064\text{ }\mu\text{m}$ , the effective index for the pump is  $n_{\text{pump\_eff}} \cong 2.1611$ . The required PBG grating pitch is  $\Lambda=246.2\text{ nm}$ . Given the bandwidth of the laser, the spread of the grating pitch corresponds to:  $\Delta\Lambda=\Delta\lambda / (2n_{\text{eff}})$  in other words  $\Delta\Lambda_{\text{pump}} \cong 0.093\text{ nm}$ . To gain further tuning accuracy, the grating is made slightly smaller than the desired length and then the pitch is fine turned by angle turning the beam with respect to the grating normal. This can be done to better than  $0.1\text{ nm}$ .

It is very difficult to reach this accuracy by using our lithographic system. In order to get PBG, the sample was rotated as shown in Figure. 3.23. The incidence angle

of the pump on the grating changes the grating from its normal incidence pitch,  $\Lambda_1$ , to the effectively longer pitch  $\Lambda_2$ .

$\gamma$  is the angle between the pump and the vertical line of PBG grating with pitch of  $\Lambda_1$  the new pitch of the grating is:  $\Lambda_2 = \Lambda_1 / \cos(\gamma)$ . The change of pitch between the two is

$$\Delta\Lambda = \Lambda_2 - \Lambda_1 = \Lambda_1 \left( \frac{1}{\cos(\gamma)} - 1 \right). \quad (3.17)$$

For instance if  $\gamma = 5^\circ$ , using Equation 3.17,  $\Delta\Lambda = 0.9404$  nm which corresponds to a change of  $\Lambda$  around 0.3 %. Now this method can modify the accuracy of the lithography method by changing the angle within  $5^\circ$ .

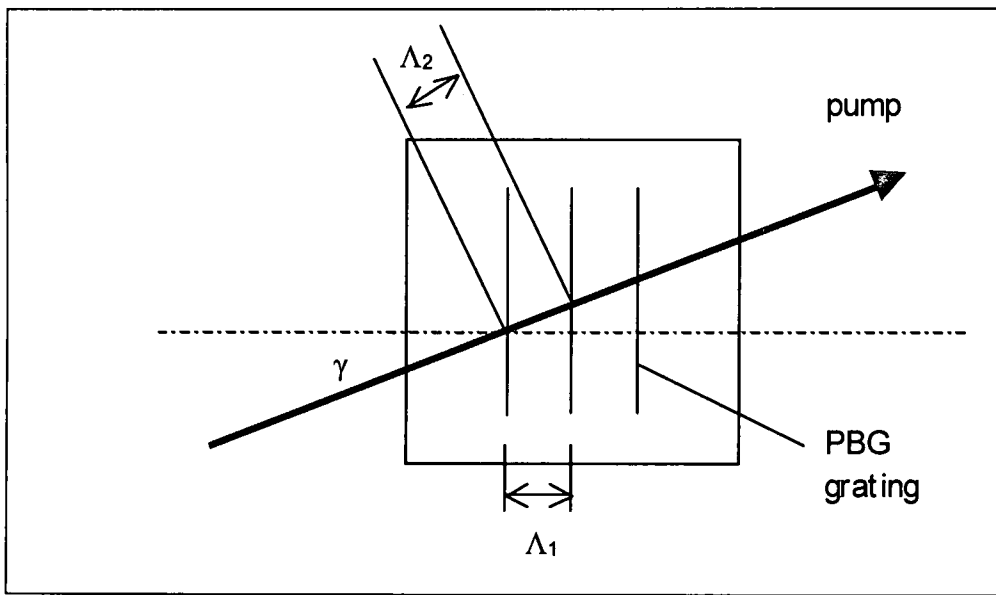


Figure 3.23 – Method changing the grating pitch seen by the pump beam by rotating sample, viewed in – X direction in Figure 3.1.

The last problem is how to get the PBG to within an accuracy of  $\pm 1$  nm. First of all, the photoresist on sample should not be baked so that it can be removed easily. The grating is removed by irradiating the masked photoresist under a UV lamp for two

minutes and then placing the sample in the developer for 30 min. The photoresist can be totally removed. Then the next application of the photoresist grating will be readied. By using this repeatable process, the right pitch can be reached with the accuracy of  $\pm 1\text{nm}$ . The following four methods were used to reach this accuracy.

#### *Method One: Coupling Method*

In Figure 3.24, the incident pump laser beam (ray A) was used to check the pitch and the modes inside the waveguide. The laser can be coupled into the waveguide through the first grating by adjusting the angle of incidence  $\theta$ ; the ray B

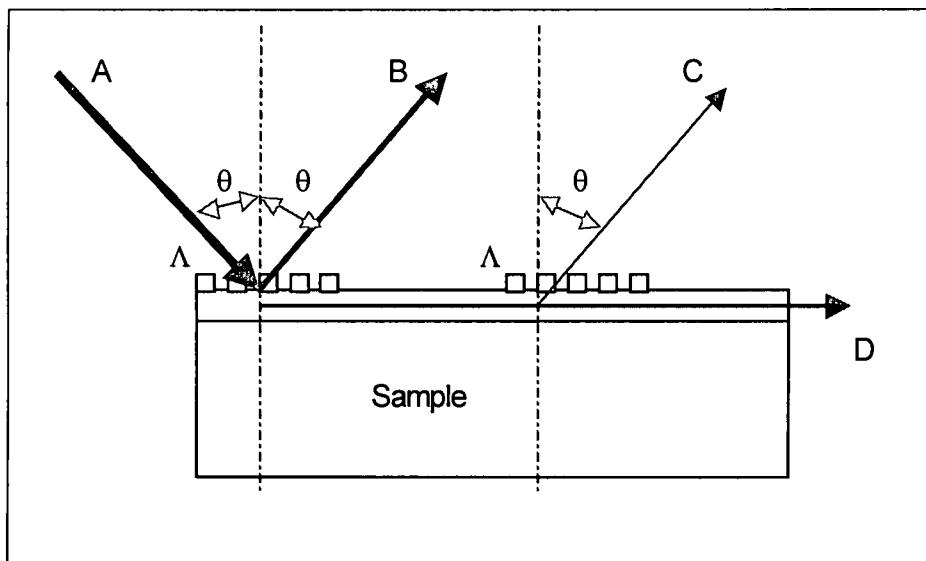


Figure 3.24 - The coupling method for finding modes as well as effective indexes in the waveguide.

was the reflective ray from surface. Ray D is the ray with modes in the waveguide and ray C is the diffracted from the second grating. Since the pitches of two gratings are the same size, the diffractive angle is the same as the coupling angle, which is also the same as the reflective angle  $\theta$ . In the experiment, if the two rays B and C can be observed at the same times on the screen, or by using a detector, it's certain that ray A

was coupled into the waveguide. There is more than one mode inside the waveguide if there are several angles  $\theta$ , and the angle of  $\theta$  can also be used to calculate the pitch. The formula is:

$$\Lambda = \lambda / (n_{eff} \sin(\theta)).$$

#### *Method Two: Diffraction Method*

There are several rays diffracted out from the surface of grating if the incident light irradiates the grating in an angle  $\theta$ . The principle is shown in Figure 3.25. And the formula used to calculate the diffraction is as follows

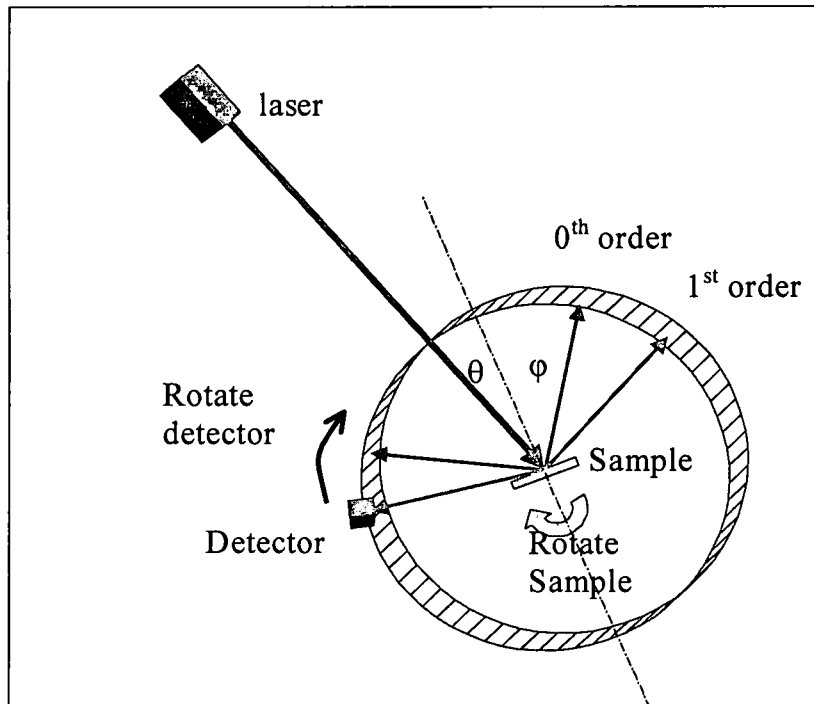


Figure 3.25 - Setup of diffractive method. The pitch was calibrated by both AFM and SEM.

$$k_{out} = k_{in} \pm qK, \quad (3.18)$$

$$K = \frac{2\pi}{\Lambda}, \quad (3.19)$$

$$k_{in} = k_0 n_0 \sin(\theta), \quad (3.20)$$

$$k_{out} = k_0 n_0 \sin(\varphi), \quad (3.21)$$

$$q = 0, \pm 1, \pm 2, \pm 3, \dots \quad (3.22)$$

where  $q$  is the order of diffraction,  $k_0$  is the wave vector in the air,  $n_0$  is the refractive index of air, and  $\Lambda$  is the pitch of grating. By using Equations 3.18 – 3.22,  $\Lambda$  can be determined if the incident and refractive angles  $\theta$  and  $\varphi$  are known.

#### *Method Three: Cerenkov SHG Method*

The principle was introduced in section 3.5.1 before. The effective index can be calculated by using

$$n_{eff}(\omega) = n(2\omega) \cos(\alpha), \quad (3.23)$$

$$n(2\omega) = 2.21. \quad (3.24)$$

$\alpha$  can be easily measured with high accuracy. Using  $\Lambda = \lambda / (2n_{eff})$ . The right pitch for PBG can be made. It must be noted that the  $n_{eff}$  must be the effective index of mode of pump in the waveguide. If the index of waveguide or the substrate for pump was used instead of the effective index, the PBG pitch will be wrong.

#### *Method Four: Second Order Bragg Diffraction Method*

The pump light is used as shown in Figure 3.26. The ray A incidents on the grating vertically. D is the transparent ray. If the pitch

$$\Lambda = m\lambda / (2n_{eff}), \quad (3.25)$$

where  $m=2$ ,  $n_{eff}$  can be got by Cerenkov method, the rays B and C can be seen inside the waveguide. The Cerenkov SHG can also be seen on both side of the waveguide. Then the PBG pitch can be half of that in second order, which is  $\Lambda/2$ . This method can

be used to get the exact pitch used in the PBG for different sample with different mode and effective index.

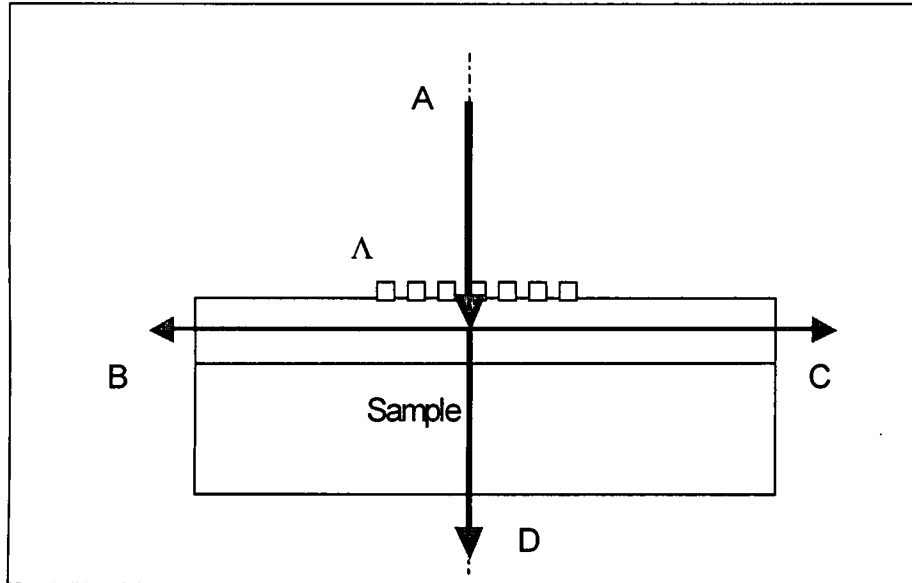


Figure 3.26 - Pump vertically incidents on the second order Bragg grating, resulting two diffractive beams B and C in the waveguide.

Those methods give us the following information: the number of modes in samples, the effective indices of those modes, and The PBG Pitches for all modes. We are only interested in the  $1.5\ \mu\text{m}$  deep waveguide with two modes in the pump wavelength. Finally the right PBG can be fabricated by repeating these four methods many times. When etching is the final step; the ICP etching method was used on the sample with photoresist. The grating can be etched in the waveguide with the depth of some 200 nm. Thus both waveguide and grating can be effectively controlled in our experiment.



## **Chapter 4**

### **Numerical Modeling**

#### *4.1 Introduction*

Many affects in the experiment need to be considered to make a model. It is essentially impossible to make a single model for all the different samples in different experimental environments. Many effects that change the parameters of the samples have been discussed in the previous chapters. Another important issue, the temperature, for example, is also always a key in our experiment.

There are many temperature requirements in all of the experimental process. Those can be the temperature  $215^{\circ}$  in the proton exchange processing. The annealing temperature in the oven is around  $300^{\circ}$ . The environment temperature  $20^{\circ}$  will be maintained stable during all processing, such as the spinning, exposure, developing and the final experiment with all kinds of laser pumps. In the final experiment, the pump will increase the temperature of samples. The temperature changes on the sample including the photoresist grating on the top of sample, the waveguide as well as the substrate should be as small as  $1^{\circ}$ . This is the other reason that the refractive indices are changed all the time. Moreover, the nonlinearity is also related to the temperature. Any change of temperature in any steps may cause a big change in the final result of the CSHG. Only some typical temperatures will be discussed in my model.

Table 1. The typical data of sample No.1 used for the numerical modeling

Parameters	Data	Explanation
The side of Waveguide and photoresist on lithium niobate	+Z	Cutting method
Indices $n_e$ , $n_f$ and $n_s$	$n_f > n_s > n_e$	
Nonlinearity	$d_{22} \cong 2.1 \text{ pm/V}$ $d_{31} \cong -4.35 \text{ pm/V}$ $d_{33} \cong -27.2 \text{ pm/V}$	$d_{33}$ is affected by different waveguide processing techniques in our experiment. This is the only one used in the experiment.
Wavelength of pump	1.064 $\mu\text{m}$	Nd: YAG laser CW and Mode locked 100 ps, The pulse repetition rate 78 MHz
Waveguide index for pump	$n_f=2.23$	Prism coupling, diffraction, WKB and Cerenkov radiation Methods
Substrate index for pump	$n_s=2.1437$	Eq.3.4 and experimental result
Change of index under the proton exchange	$\Delta n = 2.23 - 2.1437 = 0.0863$	
Substrate index for SHG	$n_s=2.2189$	Eq. 3.4 and experiment
Waveguide thickness	$h=1.5 \mu\text{m}$	Prism coupling, diffraction coupling, WKB
Grating depth	$T=0.1 \mu\text{m}$	
Length of coupling grating	$L1=3 \text{ mm}$	Determined by spot size of laser
Length of PBG grating	$L2=6.7 \text{ mm}$	Determined by the coupling efficiency
Refractive indices in the waveguide for pump	Mode= 1          2 $n_{\text{eff}} = 2.2147 \quad 2.1611$	Two modes
Confinements inside the waveguide	$\text{Conf}_1 = 0.9368 \quad 0.7671$	Two modes
The confinement inside substrate	$\text{Conf}_2 = 0.0618 \quad 0.2290$	Two modes
The confinement inside grating with depth of 100 nm	$\text{Conf}_3 = 0.0007 \quad 0.0027$	Calculated from the profile of field in the grating with depth of 100 nm and square shape
Cerenkov angles $\alpha$ from the left edge of sample in Fig. 3	$3.53^\circ \quad 13.11^\circ$	Two modes
$\alpha_1$ caused by Cerenkov angles from the left edge of sample in Fig. 3	$7.84^\circ \quad 30.21^\circ$	Two modes
Pitches for PBG	240.2 nm    246.2 nm	Two modes
Coupling efficiency for pump in the waveguide and grating	$\kappa = 3.4687 \text{ (1/cm)}$ and $14.8002 \text{ (1/cm)}$	Two modes
Enhancement of CSHG with PBG	50 times	For second mode with $\kappa=14.8002 \text{ (1/cm)}$
Standard of clean room	Class 1000	
Environment temperature	$20^\circ$	
Proton exchange time	$215^\circ \quad 2 \text{ hours}$	
Annealing time	0	

However, it's realistic to make a typical model that can be used as a reference so that the data can be analyzed in the experiment. Typical experimental conditions and data on sample No.1 are listed in Table 1. Moreover, the methods to get those parameters will be listed as well, and those will be discussed in the following sections.

#### 4.2 Calculation of Mode Profiles

In our experiment only TM mode is excited inside the waveguide. For an asymmetric waveguide the evanescent transverse wave vector in the cladding is <sup>[41]</sup>

$$\gamma_i = \sqrt{\beta^2 - k_0^2 n_i^2}, \quad (4.1)$$

where  $n_i$  is the cover ( $i=c$ ) or substrate ( $i=s$ ) index. The transverse wave vector in the waveguide is

$$\kappa_f = \sqrt{k_0^2 n_f^2 - \beta^2}.$$

The transverse portions of the electric field amplitudes in the three regions are

$$E_y(x) = Ae^{-\gamma_c x}, \quad 0 < x \quad (4.2)$$

$$E_y(x) = B \cos(\kappa_f x) + C \sin(\kappa_f x), \quad -h < x < 0 \quad (4.3)$$

$$E_y(x) = De^{-\gamma_s(x+h)}, \quad x < -h \quad (4.4)$$

where A, B, C and D are amplitude coefficients to be determined from the boundary conditions,  $\gamma_c$  and  $\gamma_s$  to the coefficients in the cover and substrate, respectively. For the TM case the eigenvalue equation to determine the effective index is

$$\tan(h\kappa_f) = \frac{\kappa_f \left[ \frac{n_f^2}{n_s^2} \gamma_s + \frac{n_f^2}{n_c^2} \gamma_c \right]}{\kappa_f^2 - \frac{n_f^4}{n_c^2 n_s^2} \gamma_c \gamma_s}. \quad (4.5)$$

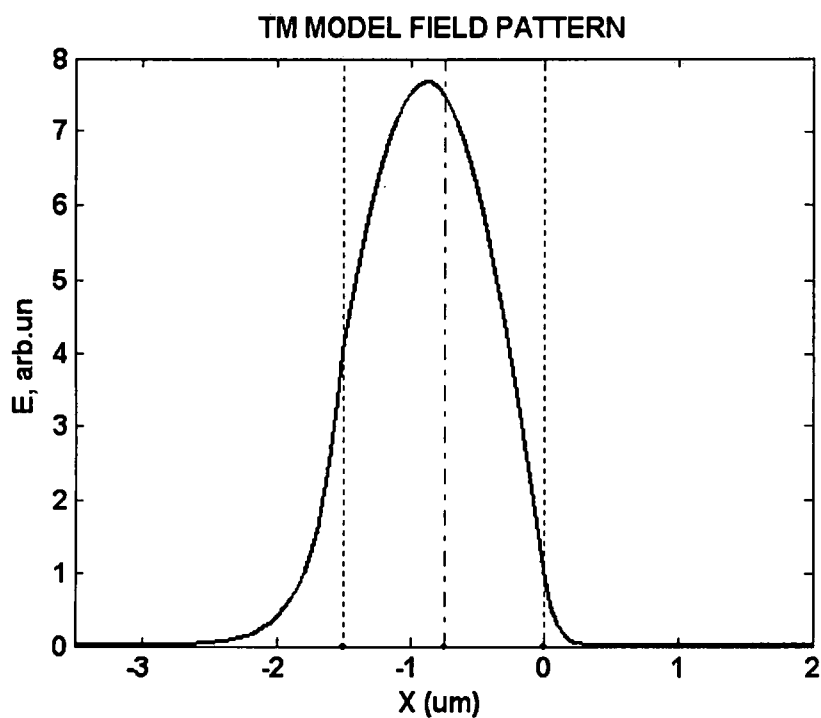


Figure 4.1 - The profile of the first TM modes of pump in waveguide in sample No.1. The area between the dash lines is waveguide. The air is in the right side

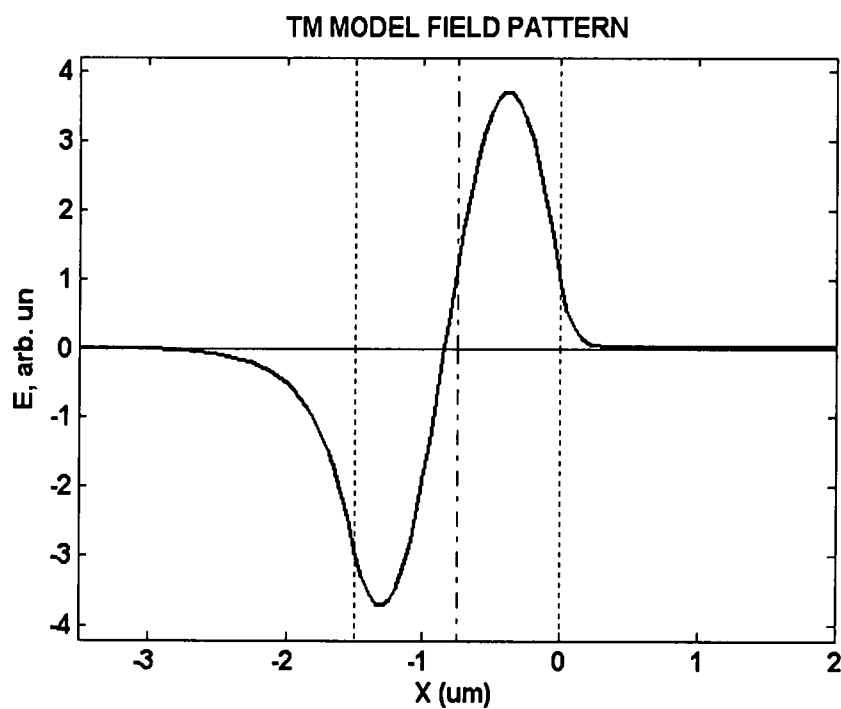


Figure 4.2 - The profile of the second TM modes of pump in waveguide in sample No.1. The area between the dash lines is waveguide. The air is in the right side

It's desirable to have a high confinement inside the waveguide so that there is a stronger pump inside the waveguide and it is not as susceptible to perturbations that can scatter the mode. Figures 4.1 and 4.2 show our calculations of the waveguide modes based on the characterization studies we made.

How much of the mode does energy reside inside the core, and how much energy is carried in the evanescent tail? Power in the guiding layer is found by integrating the Poynting vector over the area of the waveguide structure. The fraction of the power contained the core is give by the expression

$$conf_1 = \frac{P_{core}}{P_{total}} = \frac{\int_{-h}^0 E_y(x) H_x^*(x) dx}{\int_{-\infty}^{\infty} E_y(x) H_x^*(x) dx}, \quad (4.6)$$

where  $h$  is the thickness of the waveguide and the top of the waveguide is assumed to be at  $x=0$ .

In general, higher-order modes are less confined than their lower-order counterparts, and are therefore, more susceptible to bending loss and evanescent coupling. On the other hand the second mode extends further into the substrate, where the nonlinear coefficient is unaffected by the proton exchange process.

The confinement in the grating region is given by a similar integral; if the height of the grating is  $d$  the confinement in the grating is

$$conf_3 = \frac{P_{grating}}{P_{total}} = \frac{\int_0^d E_y(x) H_x^*(x) dx}{\int_{-\infty}^{\infty} E_y(x) H_x^*(x) dx}. \quad (4.7)$$

If the linear coupling coefficient between the counter-propagating modes in the waveguide is larger, there will be a stronger resonance in side the waveguide.

There are three confinements in our experiment, which determine the efficiency of SHG in the waveguide, the coupling constant, and the extension of the mode in the substrate to couple with the CSHG process.

### 4.3. Calculation of Coupling Constant $\kappa$ <sup>[43]</sup>

Consider a periodic dielectric waveguide in which the periodicity is due to a corrugation of one of the interfaces, such periodic waveguides are used for the photonic band gap structure. The corrugation is described by  $\Delta\epsilon(x, y, z) = \epsilon_0 \Delta n^2(x, y, z)$  since  $\Delta n^2(x, y, z)$  is a scalar, it follows that

$$\langle \kappa | \Delta\epsilon | m \rangle = \int E_k^* \bullet \Delta\epsilon E_m dx dy. \quad (4.8)$$

The corrugation couples only TE to TE modes and TM to TM, but not TE to TM

$$\frac{d}{dz} A_k(z) = -\frac{i\omega}{4} \frac{\beta_k}{|\beta_k|} \sum_m \langle \kappa | \Delta\epsilon | m \rangle A_m(z) e^{i(\beta_k - \beta_m)z}, \quad (4.9)$$

According to the above formula, we may consider the right side as a source term driving the  $k^{\text{th}}$  mode. The slowly varying amplitude of the field should not vary appreciably over a distance  $z \gg \Lambda$ , so that it does not average out to zero. For perfect phase matching the condition is

$$\beta_k - \beta_m = l \left( \frac{2\pi}{\Lambda} \right). \quad (4.10)$$

For mode  $m$  with propagation constant  $\beta_m$  and some integer  $l$ , when this condition is satisfied, the  $k^{\text{th}}$  mode and the  $m^{\text{th}}$  mode are resonantly coupled via the  $l$  the Fourier component of the periodic perturbation  $\Delta\epsilon(x, y, z)$ .

To be specific, let us assume that the period  $\Lambda$  of the perturbation  $\Delta n^2(x, z)$  is so chosen that  $l(\pi/\Lambda) \approx \beta_s$  for some integer  $l$ . The phase matching condition as Equation 4.10 can thus be satisfied by the coupling between the mode  $\beta_s$  and its reflected mode, which has a propagation constant of  $-\beta_s$ , since  $\beta_s - (-\beta_s) = 2\beta_s \approx l(2\pi/\Lambda)$ . To calculate the mode amplitudes from the coupled mode equations (6.4-33), we need to expand the perturbation  $\Delta\epsilon(x, z)$  as a Fourier series. Let us consider the specific "square wave" corrugation illustrated in Fig. 23. In this case, the dielectric perturbation  $\Delta\epsilon(x, z)$  can be written

$$\Delta\epsilon(x, z) = \Delta\epsilon(x) \frac{f(z) + 1}{2}, \quad (4.11)$$

where

$$\Delta\epsilon(x) = \epsilon_0(n_1^2 - n_2^2), \quad 0 \leq x \leq d, \quad (4.12)$$

$$= 0 \quad \text{otherwise;}$$

and  $f(z)$  is the square-wave function defined by

$$\begin{aligned} f(z) &= 1, & 0 < z < \frac{1}{2}\Lambda \\ &= -1, & \frac{1}{2}\Lambda < z < \Lambda \end{aligned} \quad (4.13)$$

By using the Fourier series

$$f(z) = \sum_{m \neq 0} \frac{i(1 - \cos m\pi)}{m\pi} \exp\left[-im\left(\frac{2\pi}{\Lambda}\right)z\right]. \quad (4.14)$$

The dielectric perturbation  $\Delta\epsilon(x, z)$  Equation 4.11 becomes

$$\Delta\epsilon(x, z) = \Delta\epsilon(x) \left\{ \frac{1}{2} + \sum_{l \neq 0} \frac{i(1 - \cos(l\pi))}{2l\pi} \exp\left[-il\left(\frac{2\pi}{\Lambda}\right)z\right] \right\}, \quad (4.15)$$

$$= \sum_l \varepsilon_l(x) \exp \left[ -il \left( \frac{2\pi}{\lambda} \right) z \right]. \quad (4.16)$$

Here, Equation 4.16 is a more general form of expansion. For the square-wave corrugation, the  $l^{\text{th}}$  Fourier component  $\varepsilon_l(x)$  is given by

$$\varepsilon_l(x) = \frac{i\Delta\varepsilon(x)}{l\pi} \quad l = \pm 1, \pm 3, \pm 5, \dots, \quad (4.17)$$

$$= \frac{1}{2} \Delta\varepsilon(x) \quad l = 0$$

$$= 0 \quad l = \pm 2, \pm 4, \dots,$$

The coupling between the forward mode ( $\beta_s$ ) and the reflected mode ( $-\beta_s$ ) is described by the contra-directional coupled mode equations

$$\frac{d}{dz} A_1 = -i\kappa A_2 e^{i\Delta\beta z}, \quad (4.18)$$

$$\frac{d}{dz} A_2 = -i\kappa A_1 e^{i\Delta\beta z}, \quad (4.19)$$

which now take the form

$$\frac{d}{dz} A_s = -i\kappa B_s e^{i\Delta\beta z}, \quad (4.20)$$

$$\frac{d}{dz} B_s = -i\kappa^* A_s e^{i\Delta\beta z}, \quad (4.21)$$

Where  $B_s$  is the amplitude of the reflected mode ( $-\beta_s$ ) and  $\Delta\beta$  and  $\kappa$  are given by

$$\Delta\beta = \beta_s - (-\beta_s) - l \left( \frac{2\pi}{\Lambda} \right), \quad (4.22)$$

and

$$\kappa = \frac{\omega}{\pi} \int_{-\infty}^{\infty} \varepsilon_l(x) |E_s(x)|^2 dx, \quad (4.23)$$

We note that the total power carried by both modes is conserved, since



$$\frac{d}{dz} \left[ |A_s|^2 - |B_s|^2 \right] = 0. \quad (4.24)$$

By using Equation 4.13 and 4.17, the coupling constant  $\kappa$  for odd  $l$  can be written

$$\kappa = \frac{i\omega\epsilon_0(n_1^2 - n_2^2)}{4l\pi} \int_0^d |E_s(x)|^2 dx, \quad l = 1, 3, 5, \dots \quad (4.25)$$

$$l = 1$$

In practice the period  $\Lambda$  is chosen so that, for some particular  $l$ ,  $\Delta\beta \approx 0$ . We note that for  $\Delta\beta = 0$

$$\Lambda = l \frac{\lambda_0^{(s)}}{2}.$$

Where  $\lambda_0^s = 2\pi/\beta_s$  is the guide wavelength of the  $s^{th}$  mode.

Let  $l=1$

$$\kappa = \frac{i\omega\epsilon_0(n_1^2 - n_2^2)}{4\pi} \int_0^d |E_s(x)|^2 dx, \quad (4.26)$$

The modes are mutually orthogonal and satisfy the following orthonormality condition:

$$\int_{-\infty}^{\infty} E_i(x) E_j(x) dx = \frac{2\omega\epsilon_0}{\beta_i} \delta_{ij},$$

where  $E_i$  and  $E_j$  are two modes that couples to each other.  $\delta_{ij}$  is the pulse function.

In this case,  $E_i(x) = E_j(x)$  because the profiles of two modes are the same and  $\delta_{ij} = 1$

$$\int_{-\infty}^{\infty} E_y^2(x) dx = \frac{2\omega\epsilon_0}{\beta} = A. \quad (4.27)$$

From Equations 4.26 and 4.27 we have.

$$\kappa = \frac{i\omega\epsilon_0(n_1^2 - n_2^2)}{4\pi} \frac{\int_0^d |E_y(x)|^2 dx}{\int_{-\infty}^{\infty} |E_y(x)|^2 dx} A.$$

As shown in Table 1, the confinement in the grating is defined as

$$conf_3 = \frac{\int_0^d |E_y(x)|^2 dx}{\int_{-\infty}^{\infty} |E_y(x)|^2 dx}. \quad (4.28)$$

$$\begin{aligned} \kappa &= \frac{i\omega\epsilon_0(n_1^2 - n_2^2)}{4\pi} conf_3 \frac{2\omega\epsilon_0}{\beta} \\ &= \frac{i\omega(\epsilon_0\mu_0)2\omega(n_1^2 - n_2^2)}{4\pi\beta} conf_3 \\ &= \frac{i\omega^2(n_1^2 - n_2^2)}{2\pi C^2\beta} conf_3 \\ &= \frac{i\omega(n_1^2 - n_2^2)}{2\pi C n_{eff}} conf_3 \\ &= \frac{i(n_1^2 - n_2^2)}{\lambda_0 n_{eff}} conf_3 \\ \kappa &= \frac{i(n_1^2 - n_2^2)}{\lambda_0 n_{eff}} conf_3. \end{aligned} \quad (4.29)$$

Equation 4.29 will be used to get the Coupling Constant  $\kappa$ . As known, for sample No.1, The depth of grating is 0.1  $\mu\text{m}$ , so there are two modes for pump in Nd: YAG laser. Then the coupling constant for those modes are  $\kappa = 3.4687$  (1/cm) and 14.8002 (1/cm) respectively by using Equation 4.29 and Equations in section 4.2. This is the reason those values were listed in Table 1.

#### 4.4. Calculation of CSHG Efficiency

The scheme of the waveguide is presented in Figure 3.1 in which a Z-cut  $\text{LiNbO}_3$  substrate is configuration that we study is shown in Figure 3.2. The refractive-index profile is given by

$$n^2(x, y, z) = \varepsilon_r + \Delta\varepsilon_r = \varepsilon_r(y, z) + \Delta\varepsilon_r(x, y, z).$$

Thus the Maxwell's equations in perturbed structures (Figs. 3.2 and 4.3) become

$$\Delta \times E = i\omega\mu H, \quad \Delta \times H = -i\omega\varepsilon_0(\varepsilon_r + \Delta\varepsilon_r)E, \quad (4.30)$$

where E and H are the electric and the magnetic field vectors respectively. In recent paper <sup>[6-9]</sup>, we derived the following steady state scalar system of nondepleted-coupled equations.

$$\frac{dA^+}{dz} = iK_L(z)A^- \exp(-i2\beta_{FF}z), \quad (4.31 a)$$

$$\frac{dA^-}{dz} = -iK_L(z)A^+ \exp(i2\beta_{FF}z), \quad (4.31 b)$$

$$B^+ = d_0 A^+ \exp(i\alpha^+), \quad (4.32 a)$$

$$B^- = d_0 A^- \exp(i\alpha^-), \quad (4.32 b)$$

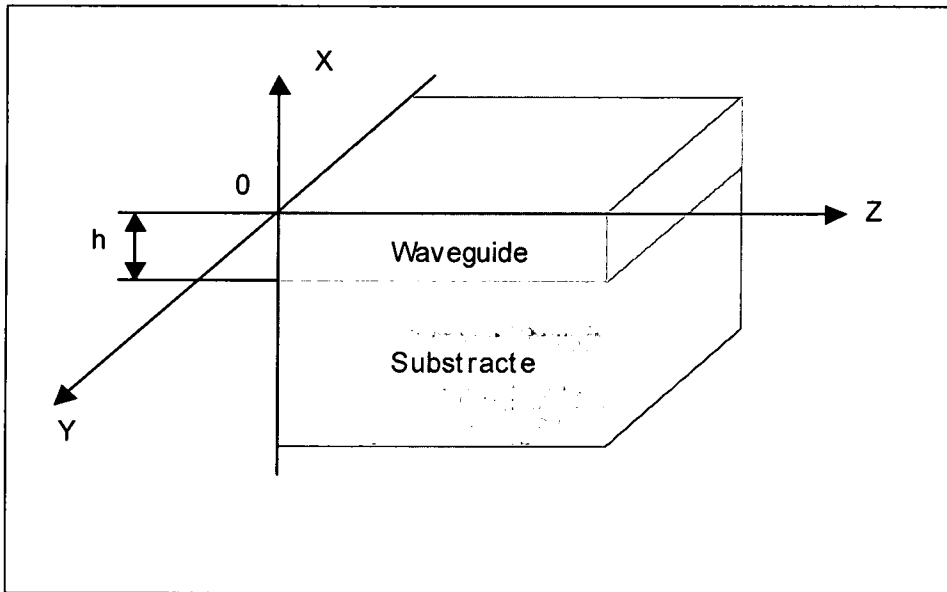


Figure 4.3 Simplified model of sample.

where  $A^+$  is the electrical field of mode of pump in the +x direction,  $A^-$  is the electrical field of mode of pump in the -x direction,  $\beta_{FF}$  is the propagation coefficient of the guided mode of pump inside the waveguide in the +X direction.  $B^+$  is the electrical field of mode of SHG in the +x direction,  $B^-$  is the electrical field of mode of SHG in the -x direction,  $\alpha^+$  is the phase change between pump and SHG in the nonlinear process in the  $x^+$  direction,  $\alpha^-$  is the phase change between pump and SHG in the nonlinear process in the  $x^-$  direction.

$d_0$  is defined as a scaling constant from Cerenkov, which shows the nonlinear efficiency at position of X. This value describes the linear coupling and nonlinear processes of the waveguide mode at the same time. The plus (minus) sign stands for propagation along the positive (negative) x direction. For the Cerenkov emission scheme in our experiment, the  $d_0$  will always be a constant.

Under the Cerenkov radiation condition, the only second-harmonic modes that can be phase-matched are considered. The solution of the coupled-mode Equations 4.31 and 4.32 are carried out analytically in the non-depleted-pump approximation. Introducing the following substitutions

$$A^+(z) = a^+(z) \exp(i\delta_1 z), \quad (4.33 \text{ a})$$

$$A^-(z) = a^-(z) \exp(-i\delta_1 z), \quad (4.33 \text{ b})$$

$$B^+(z) = b^+(z) \exp(-i\delta_2 z), \quad (4.34 \text{ a})$$

$$B^-(z) = b^-(z) \exp(i\delta_2 z), \quad (4.34 \text{ b})$$

where the phases are

$$2\delta_1 = \frac{2\pi}{\Lambda_L} - 2\beta_{FF}. \quad (4.35)$$

The coupling constant is  $K_L$ .

We rewrite Equation 4.31 and 4.32 under the rotating-wave approximation as

$$\frac{da^+}{dz} + i\delta_1 a^+ = iK_L a^-, \quad (4.36 \text{ a})$$

$$\frac{da^-}{dz} - i\delta_1 a^- = iK_L a^+. \quad (4.36 \text{ b})$$

$$b^+(z) = D(a^+)^2, \quad (4.37)$$

$$b^-(z) = D(a^-)^2, \quad (4.38)$$

where  $D$ , related with constant  $d$ , is a scaling constant in our experiment. The solutions of Equations 4.36, 4.37 and 4.38 are

$$a^+(z) = C_1 \cos(\Delta_1 z) + C_2 \sin(\Delta_1 z), \quad (4.39 \text{ a})$$

$$a^-(x) = \left( C_2 \frac{\Delta_1}{iK_L} + C_1 \frac{\delta_1}{K_L} \right) \cos(\Delta_1 x) + \left( C_2 \frac{\delta_1}{K_L} - C_1 \frac{\Delta_1}{iK_L} \right) \sin(\Delta_1 x), \quad (4.39 \text{ b})$$

$$\Delta_1 = \sqrt{\delta_1^2 - K_L^2}. \quad (4.40)$$

The normalized boundary conditions are:

$$a^+(0) = 1, \quad (4.41 \text{ a})$$

$$a^-(L) = 0, \quad (4.41 \text{ b})$$

$$b^+(0) = 0, \quad (4.42 \text{ a})$$

$$b^-(L) = 0; \quad (4.42 \text{ b})$$

where  $L$  is the length of grating. Substitute Equations 4.42 into Equation 4.41 we get:

$$C_1 = 1, \quad (4.43a)$$

$$C_2 = \frac{\Delta_1 \sin(\Delta_1 L) - i\delta_1 \cos(\Delta_1 L)}{\Delta_1 \cos(\Delta_1 L) + i\delta_1 \sin(\Delta_1 L)}. \quad (4.43 b)$$

Then the solutions are

$$a^+(z) = \cos(\Delta_1 z) + \frac{\Delta_1 \sin(\Delta_1 L) - i\delta_1 \cos(\Delta_1 L)}{\Delta_1 \cos(\Delta_1 L) + i\delta_1 \sin(\Delta_1 L)} \sin(\Delta_1 z), \quad (4.44a)$$

$$a^-(z) = \left( C_2 \frac{\Delta_1}{iK_L} + \frac{\delta_1}{K_L} \right) \cos(\Delta_1 z) + \left( C_2 \frac{\delta_1}{K_L} - \frac{\Delta_1}{iK_L} \right) \sin(\Delta_1 z). \quad (4.44b)$$

Substitute Equations 4.44 into Equations 4.37 and 4.38, we get

$$b^+(z) = D(a^+(z))^2, \quad (4.45 a)$$

$$b^-(z) = D(a^-(z))^2. \quad (4.45 b)$$

The total intensity of CSHG in +x direction is

$$I_b^+ = \int_0^L (b^+(z))^2 dz, \quad (4.46 a)$$

$$I_b^- = \int_0^L (b^-(z))^2 dz. \quad (4.46 b)$$

The normalized conversion efficiency can be expressed by the following expressions:

$$\eta_{rel}^+ = \frac{I_{bK}^+}{I_{bo}^+}, \quad (4.47 a)$$

$$\eta_{rel}^- = \frac{I_{bK}^-}{I_{bo}^+}, \quad (4.47 b)$$

where  $I_{bK}^+$  and  $I_{bo}^+$  are intensity of CSHG in +z direction, with grating and without

grating ( $K = 0$ ). As known, for sample No.1, The depth of grating is 0.1  $\mu\text{m}$ . There are two modes for pump in Nd: YAG laser. Then the coupling constant for those modes are  $\kappa = 3.4687$  (1/cm) and 14.8002 (1/cm) respectively by using Equation 4.29. We are only interested in the second mode with are  $\kappa = 14.8002$  (1/cm). The normalized conversion efficiency, therefore, is plotted in Figure 4.4, showing that a small change of  $\kappa$  from 14.6 1/cm to 16.6 1/cm can only slightly change the shape and the position of band. Also the efficiency increases as the coupling constant increases. It does not affect the shape of two plots too much, meaning a small change of grating, such as the shape and depth, will not affect the PBG so much. We also can see from this figure that the relative efficiency is around 50 times when the wavelength is tuned to the left first band edge.

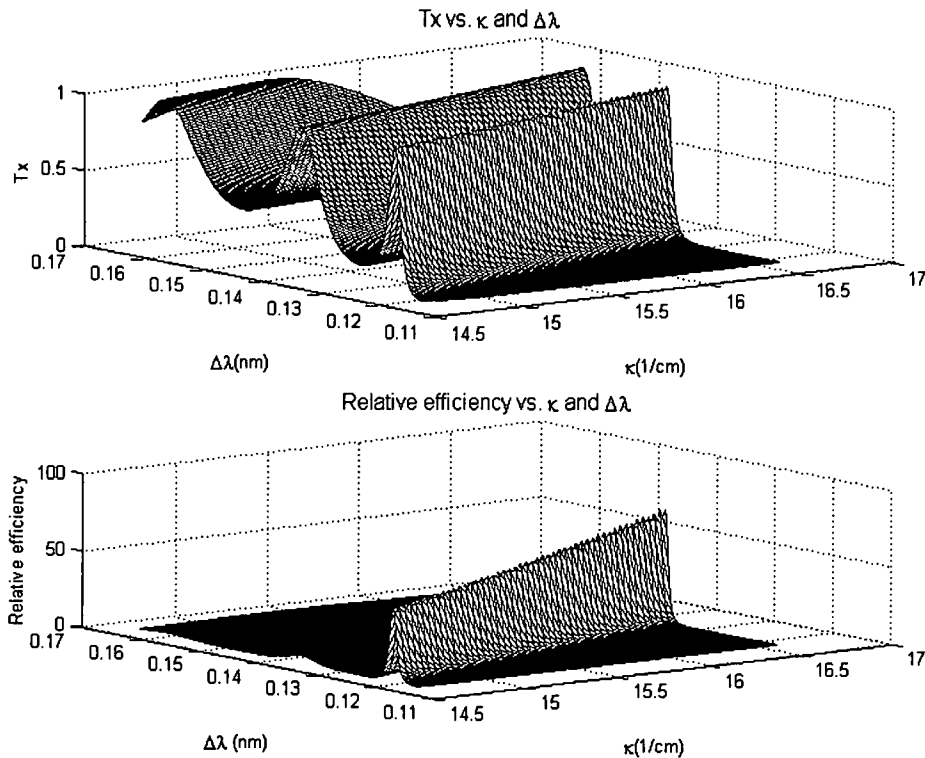


Figure 4.4 - The transmission and relative efficiency with detuning in nm units for direct comparison in the experiment.

Further characters can found in Figure 4.5 too. It's calculated that  $\kappa=14.8002$  (1/cm), which fits model of the second mode in sample No.1. The top relative efficiency is 50 times, bandwidth is about 0.005 at the band edge. Two peaks are at 0.12278 nm and 0.13861 nm. For  $\Delta\lambda=0.12278$  nm the relative efficiency is 48.0836 times and the transmission of the fundamental field is  $T = 1.0000$ . Those results will be compared with the experimental result for sample No.1, and will be proved in the following section right.

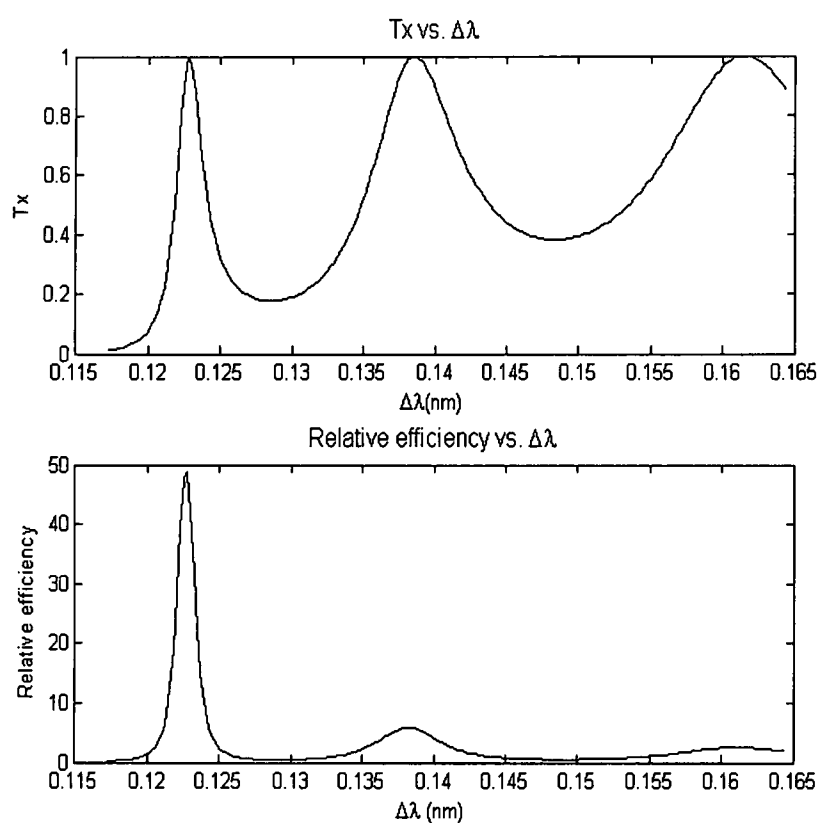


Figure 4.5 - The transmission spectra, on right side of band, with detuning in nm units for direct comparison with experiment. b. The relative efficiency with detuning in nm units for direct comparison with experiment.



#### *4.5 Intensity of Pump in Waveguide with PBG Enhancement*

To figure out the intensity of pump inside the waveguide, three typical turning positions are studied at different wavelengths. The central wavelength from Bragg condition is  $1.064\ \mu\text{m}$ . The turning position for this sample in the change of wavelength is  $\Delta\lambda=0.12278\ \text{nm}$ , calculated and seen in Fig. 28. The second position is  $\Delta\lambda=0.13861\ \text{nm}$ . A spectral position half way between them was also chosen as  $\Delta\lambda=(0.12278+0.13861)/2\ \text{nm}=0.1307\ \text{nm}$ .

The intensities are normalized with respect to the input forward intensity. Figure 4.6 shows a transmission spectrum of a one-dimensional PBG  $\Delta\lambda=0.12278\ \text{nm}$ . The transmission  $T=1$ , the resonance will appear and the efficiency can be calculated by using Equation 4.47 a, and the result is the relative efficiency is  $\eta = 48.0836$  times. As shown in Figure 4.6, the forward intensities of pump is almost 120 times that of the input forward intensity at the middle point of material if we tune the  $\Delta\lambda=0.12278\ \text{nm}$  away from the central wavelength of  $1.064\ \mu\text{m}$ . This figure clearly shows the effect of enhanced DOM on the longitudinal field's profile of the fundamental field tuned at the band-edge transmission resonance. This results in the efficiency of 48.0836 because enhanced pump can produce an enhanced CSHG in the nonlinear optics, which also matches the result in my experiment with the enhancement of 50.

The peak intensities in waveguide, as shown in Figures 4.7 and 4.8 are smaller than those in Figure 4.6. 29 because their  $\Delta\lambda$  are  $-0.0158$ , and  $-0.0079$  respectively, which are the shifts of wavelength from the band-edge. Figure 4.8 shows that the intensities in the material are not enhanced at all, showing the lack of penetration of light into the PBG. In our experiment, we will tune to get the intensity enhancement as high as possible by finding the first transmission maximum, i.e. Figure 4.5. We also note that phase matching is another consideration, which affects the SHG efficiency.

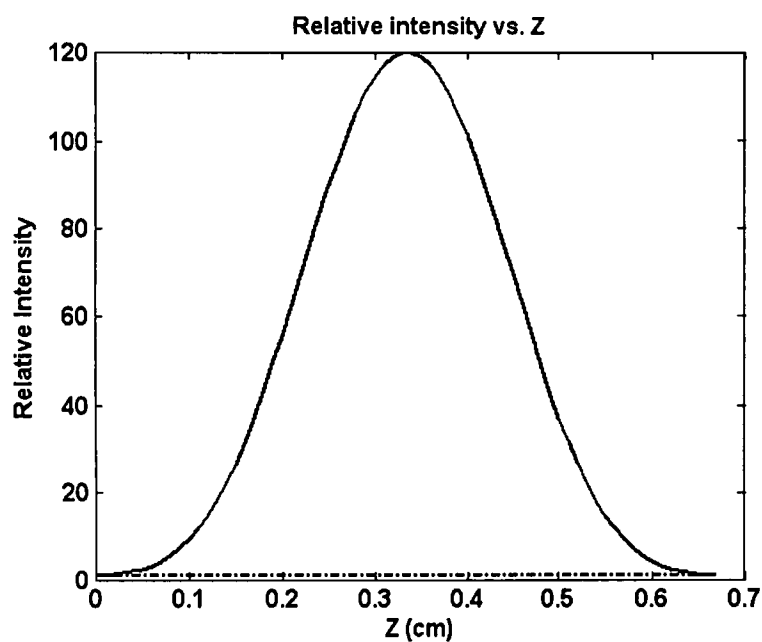


Figure 4.6 - The relative field of pump inside the waveguide at different positions. When  $\Delta\lambda=0.12278$  nm; relative intensity is  $\eta = 48.0836$ ,  $T=1$ . the solid line shows the intensity inside the waveguide with grating the dot line shows the intensity inside the waveguide without grating for sample No.1.

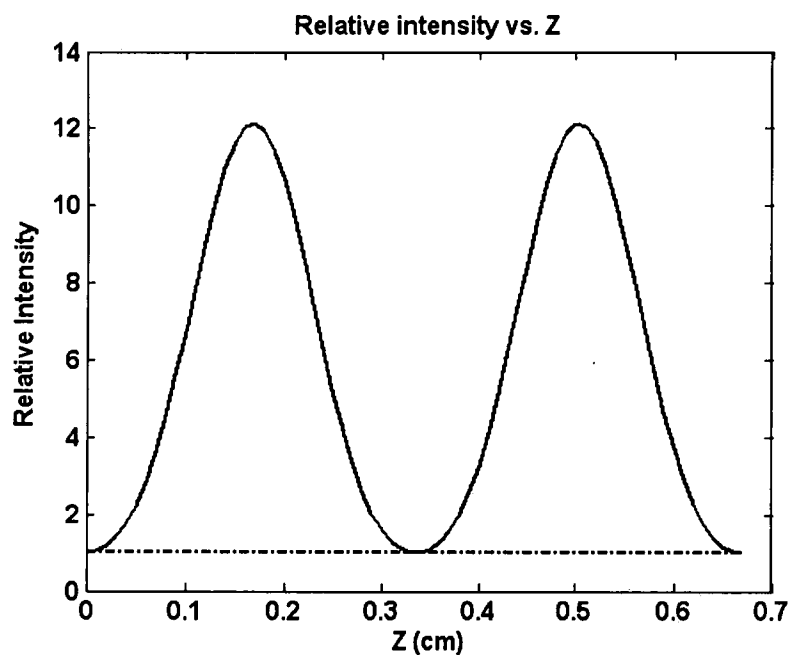


Figure 4.7 - The relative field of pump inside the waveguide at different positions. When  $\Delta\lambda = 0.13861$  nm for sample No.1.

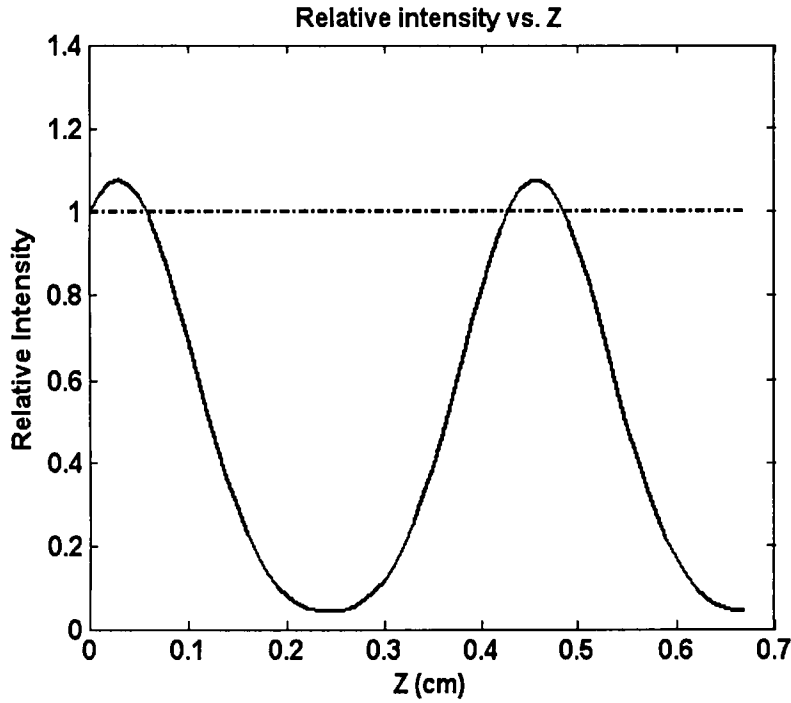


Figure 4.8 - the relative field of pump inside the waveguide at different positions when  $\Delta\lambda = 0.1307$  nm. For sample No.1.

In Figure 4.7,  $\Delta\lambda = 0.13861$  nm,  $T=1$ , relative peak intensities of pump in the waveguide is 12, and relative efficiency is  $\eta = 5.7908$ . Above figures show the relative field of pump inside the waveguide at different positions. When  $\Delta\lambda = 0.12278 + (0.13861 - 0.12278)/2 = 0.1307$  nm;  $T=0.2057$ , the relative efficiency is  $\eta = 0.2057$ . This means that this wavelength shifts make the SHG efficiency worse. The relative intensity is very small, even smaller than the pump without grating at most of the position in the waveguide. Therefore, this situation should not be applied in our experiment.

#### 4.6 Chapter Summary

A typical sample No.1 was analyzed as a data source for modeling. The environments of experiment are discussed. Cerenkov method is used to get refractive

index of the pump in the waveguide and two mode profiles were calculated. The second mode is used in the modeling. The CSHG efficiency and the coupling constant were calculated to be  $\eta = 48.0836$  and  $\kappa = 14.800$  1/cm from this sample and its model. Therefore, a successful model is constructed that can be applied to all the samples in our experiments. Moreover, this model can be used as a database used to compare all the experimental results in the future.

## Chapter 5

### SHG Experiment and Results

#### 5.1 Setup

Sample No.1 is mainly used in this experiment to compare against our theory.

All the data related to this sample have already listed in the Table 1 in section 3.1.

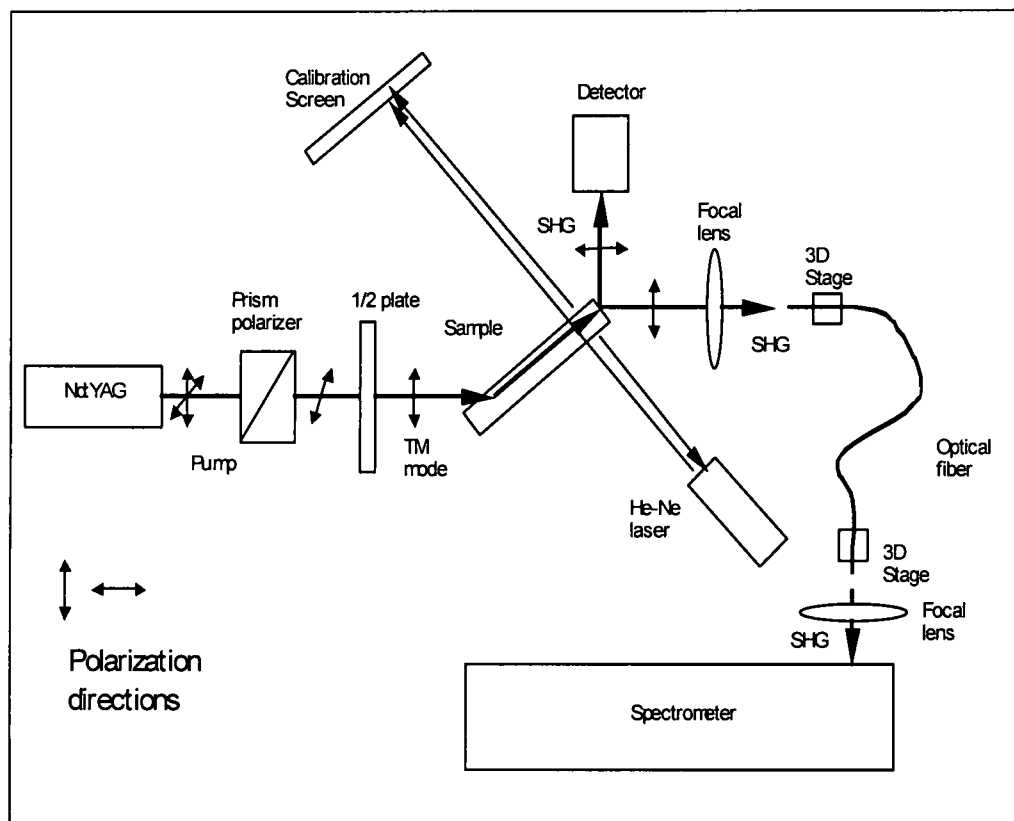


Figure 5.1 - Schematic of the CSHG experiment.

Figure 5.1 shows the experimental setup for PBG enhancement in CSHG. A Nd:YAG laser is mode locked with a pulse duration of 150 ps, repetition rate of 78 MHz. The pulses are linearly polarized using a prism polarizer element. There are only TM modes in the sample No.1 waveguide after the proton exchange processing. In order to get TM coupling a half wavelength plate is applied to rotate the direction of polarization until a TM mode is reached.

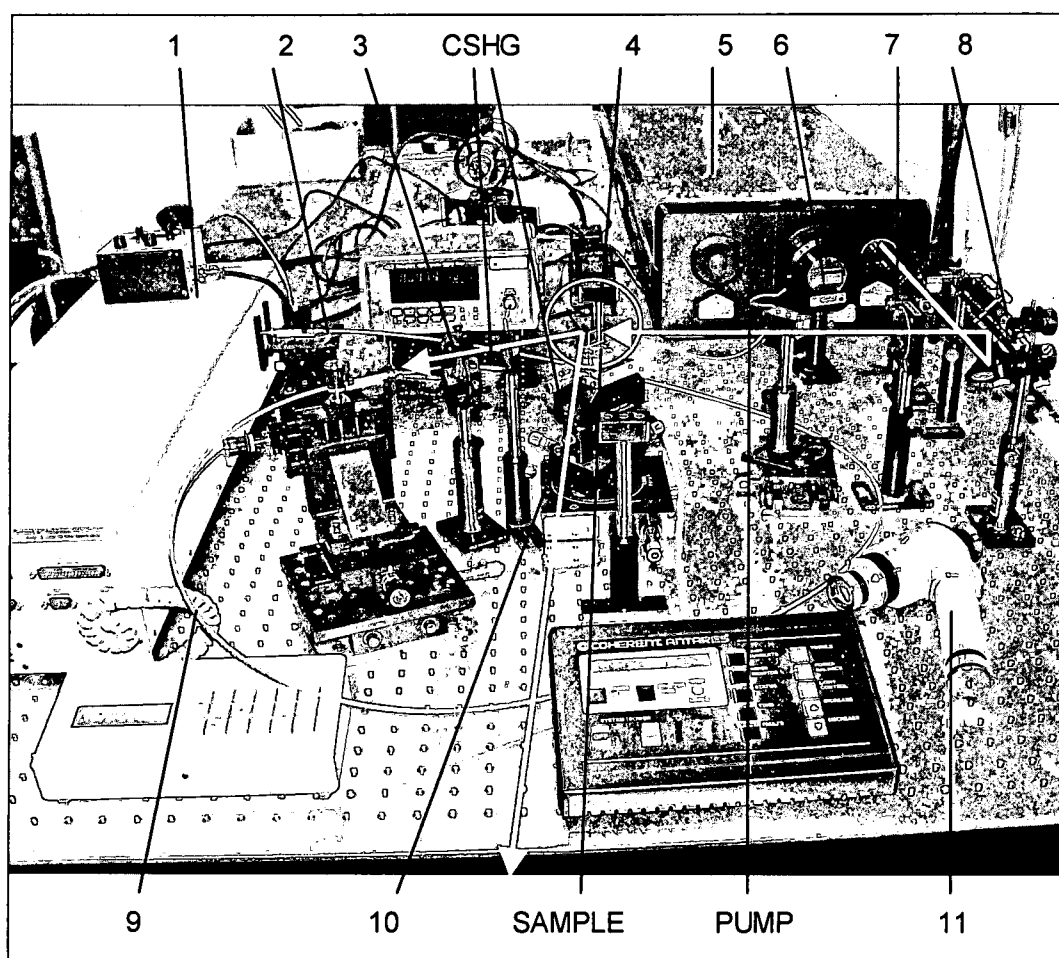


Figure 5.2 – Real setup of the CSHG experiment.

1-spectrometer 2-dimensional stages 3-focucal lens 4-dump 5-Nd:YAG laser 6-power detector 7-half plate 8-mirrors 9-fiber 10-3 dimensional stage with rotation and tilt 11-IR scope

Figs. 5.1 and 5.2 show a mode locked Nd: YAG pump laser is coupled into the waveguide and the SHG emission is collected by a fiber optical cable with diameter of 1 mm that is imaged onto the input slit of a spectrometer. A vertical emission from the PBG grating is also observed. Its angle is very close to vertical and we verify this by calibration of the surface normal using a He-Ne laser for accurate pointing.

The pump is then TM coupled into the waveguide around  $45^\circ$  in X-Z plane through a grating with the pitch of 710 nm, seen in Fig. 2 and 3. In sample No.1, the depth of waveguide is 1.5  $\mu\text{m}$ , so that two modes can be excited in waveguide. Those two modes can be seen separately by changing the coupling angle around  $45^\circ$ . The SHG efficiency caused by the second mode is found to be much higher than the first mode. Thus the second mode is chosen to be studied first in this section. The SHG efficiency for the first mode will be discussed in a later section.

The second PBG grating with pitch of 246.2 nm is made for the second mode in sample No.1. The condition for this pitch is also very close to the first order Bragg condition in the wavelength of 1.064  $\mu\text{m}$ . The reason is that the Bragg condition for pump is

$$\Lambda_{pump} = \frac{\lambda_{pump}}{2n_{eff}}, \quad (5.1)$$

where  $\Lambda_{pump}$  is the pitch for pump using the first-order Bragg condition. The same pitch applies to the SHG signal, as well, i.e.  $\Lambda_{SHG} = \Lambda_{pump}$ , since  $\lambda_{pump} = 2\lambda_{SHG}$  the Bragg condition for the SHG radiation is

$$\Lambda_{SHG} = \frac{2\lambda_{SHG}}{2n_{eff}} = 2 \frac{\lambda_{SHG}}{2n_{eff}} \quad (5.2)$$

Therefore,  $\Lambda_{SHG}$  is the pitch that satisfies the second-order Bragg condition. The conclusion is that the first-order Bragg condition for pump is exactly the second-

order Bragg condition for SHG. Therefore, there is a diffractive emission vertical to the surface of sample, which can be used to monitor the PBG while turning the angle  $\gamma$  of sample in the X-Y plane as in Figure 3.23 during the adjustment of getting PBG.

A He-Ne laser is applied to calibrate this system by irradiating the sample in Figs. 5.1 and 5.2. One ray reflects back to the exit pupil of this laser, meaning that this laser beam is vertical to the surface of sample. In the meantime, a transmitted beam goes through the sample and combines with the SHG diffraction at the screen, point B. This shows that SHG is vertical to the surface, and the grating has the second-order Bragg condition for SHG in the waveguide. Thus it's certain that the PBG grating in first-order Bragg condition is excited by the pump.

There are two angles labeled  $\theta$  in Figure 5.1, which excite the modes. Two strong pumps can be detected at the right edge of sample. Those pumps in these two modes can produce strong SHG either in the waveguide, or emitted as a Cerenkov radiation SHG, which can be seen in angle  $\alpha_1$  in Figure 3.2 and 5.3 for sample No.1. From Table 1, the waveguide for pump has a depth of 1.5  $\mu\text{m}$ . The refractive indexes for the waveguide and substrate are respectively 2.23 and 2.1437. The effective indexes for pump in this waveguide are 2.2147 and 2.1661 respectively. Those are smaller than 2.2189, the refractive index of SHG in the substrate. This is the condition for Cerenkov radiation mentioned in Section 4.5.1, so a CSGH signal appears. The two angle of  $\alpha_1$  are calculated, using Equation in previous section to be  $7.8430^\circ$  and  $30.2089^\circ$ . The measured angles are  $7.83^\circ$  and  $30.31^\circ$ , which are very close to the theoretical result.

A narrow bandwidth filter is placed at the ray of CSHG1 and in front of the detector to monitor the CSHG. The grating coupling and the position of the PBG can be controlled by using this detector.



After the system is adjusted to a PBG condition, the spectrum can be measured as will be presented below. Two conditions must be met for this measurement. One is the coupling efficiencies must be the same when the pumps shifted in the direction of  $y$  on the surface parallel to the plane of  $X$ - $Z$  in Figure 3.1 and 3.2. At the same time all the CSHG should be collected using a Lens, so that the total SHG intensities can be compared in a high accuracy.

In order to reach this goal, while shifting the pump, a Lens is used to image the beam into a fiber. The beam has a 1 mm diameter. A 3D translation stage with an angular stage on it was used to make sure the emission from the edge can be gathered by the fiber. At the other fiber end a 3D stage is fixed at one position and Len focuses the beam into the spectrometer to make sure the slit width is 20  $\mu\text{m}$ . The bandwidth of the pump is around 0.4 nm and the corresponding bandwidth for the SHG light is 0.2 nm. The best resolution for this spectrometer is 0.05 nm. The resolution of this spectrometer is high enough for our experiment.

### *5.2 Sample Images of CSHG*

In Figure 5.3 and 5.4, the incident angle  $\theta$  is around  $45^\circ$ . CSHG can be seen clearly by naked eye for either first or second mode. By turning the angle in the 3D stage with an angle turning, an even stronger CSHG can be observed if the PBG condition is met. Figures 5.3 and 5.4 are sample No.1 under our experimental conditions, viewed from  $-Z$  direction. Paper is used to display the beams. A digital camera with a silicon CCD array was used to capture the pictures. This CCD camera is not only sensitive to visible wavelengths, but also captures infrared light, such as 1.064  $\mu\text{m}$  in our experiment.

In Figure 3.2, a sample No.1 is used, and a strong scattering is seen because of the defect of waveguide, grating and the mode of pump. A CSHG beam with angle  $\alpha_1$  of  $7.83^\circ$  and  $30.31^\circ$  can be seen in Fig. 33, 34 for first two modes in sample No.1.

Those figure actually only show the second mode with effective refractive index of 2.2189. The angle is actually measured to be  $\alpha_1$  of  $30.31^\circ$ , which is consistent with the data in Table 1. Although, in some cases, a CSHG caused by the first mode can be seen by naked eye, we are more interested in the second mode with higher enhancement.



Figure 5.3 - The sample 3 is pumped by a YAG and the CSHG output is shown in a lighted room, viewed -Z direction in Figure 2.3.

Sometimes we observe that CSHG intensity flashes. The reason could be the change of temperature of sample caused by the pump, and a change of photoresist grating from heating. The stability of the Nd: YAG either in CW or in the mode locked is very important in the experiment. It's proved that it's better to operate the laser at the

power of 12 W because both the mode locked and CW is optimized at this power for our Coherent Antares laser.

Figures 5.3 and 3.15 Show that the sample No.1 as pumped by a mode locked Nd: YAG and the SHG is green light. The white light is the IR pump light. The sample is the bright white line near the center of the picture. Lines have been drawn on the photos indicating the pump and CSHG output. Figure 3.15, 3.16, 5.3, 5.4, 5.5 and APPENDIX B show the CSHG beams to be strongly emitted collimated beams of light. The CSHG output shown on a screen in Figure 5.5 reveals a complex pattern of SHG that is attributed to the spreading of the pump and SHG in the waveguide. The bright spots at the crossing of the lines determine the Cerenkov angle. Note that in this case no spot is observed in the center between the two Cerenkov emission spots. The waveguide SHG is very weak for this sample; this is an indication that phase matching is not achieved in the waveguide or the waveguide nonlinearity may also be weak.

Parallel to X-Y plane placed a vertical screen, a complex pattern can be seen in Fig 5.5, which is caused by the wavelength as well as the angles fitting the Cerenkov condition and scattering of source. The shape of the light pattern on the screen should be studied in the future.

The samples are prepared as shown in Fig.1 and used as shown in Figures 3.2 and 3.3 and 5.2. Second-harmonic generation in a planar waveguide produced in a lithium niobate sample by proton exchange with a grating recorded in a photoresist applied to the sample. Pump radiation is coupled into the waveguide through coupling grating on the right side. The second harmonic is coupled out through the output face of the waveguide and through the resonant grating. The top left quarter of the sample has a homogeneous index and the bottom left quarter's cladding index is periodically modulated.

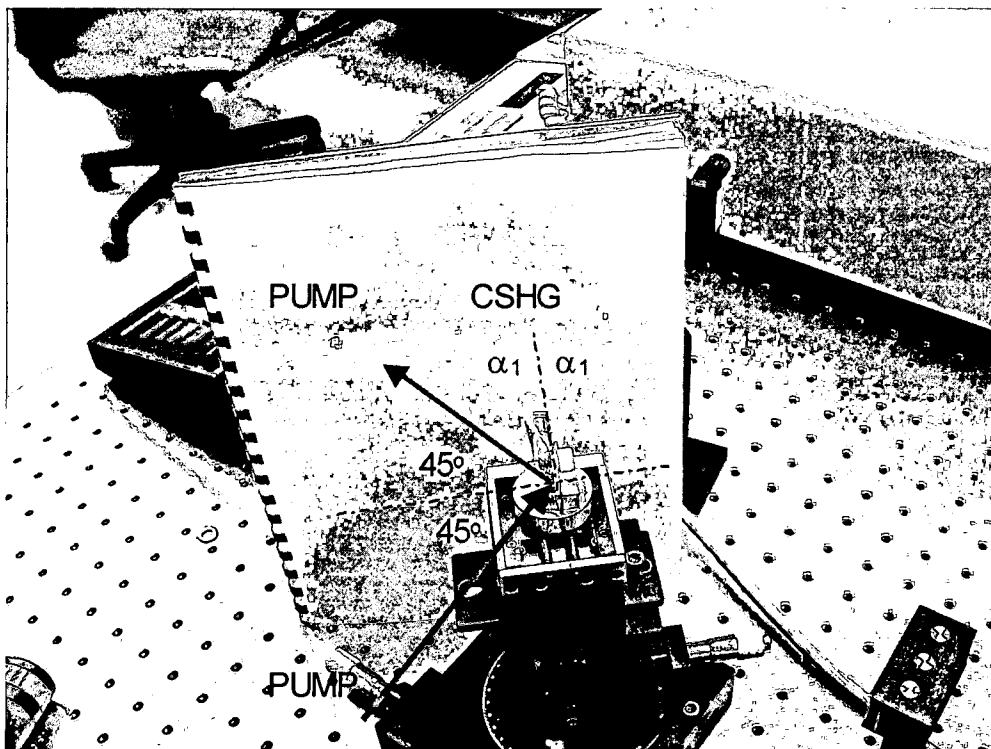


Figure 5.4 - photos showing sample 3 is pumped by the YAG and the CSHG output shown in a darkened room, viewed the -Z direction in Figure 2.3.

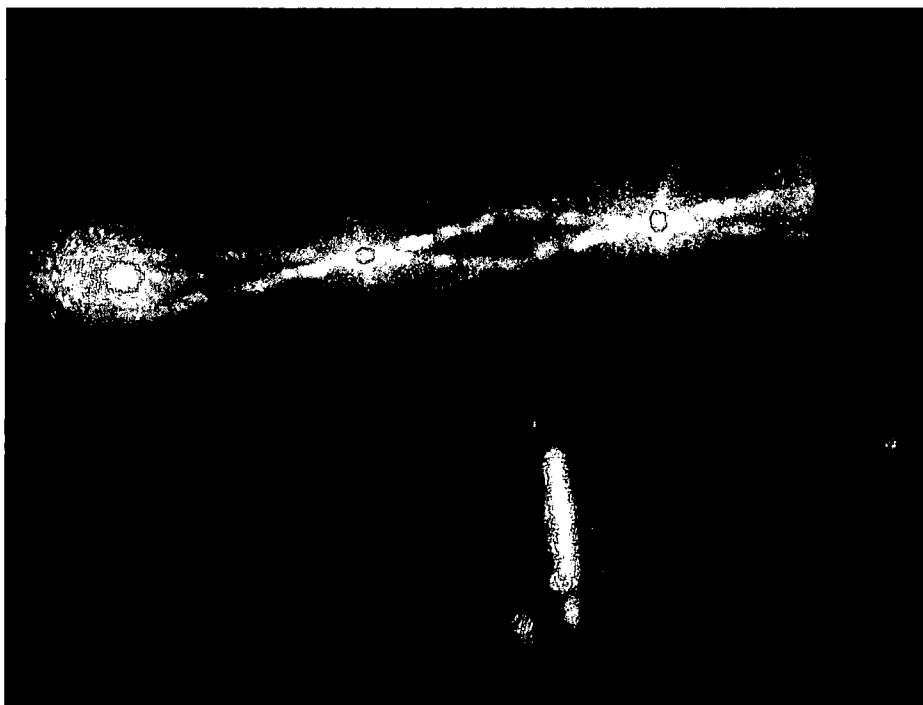


Figure 5.5 - CSHG output of sample No.1 on a screen vertical to the direction of beams, viewed in the -Y direction.

The enhanced forward and backward intensities are sensitive to the frequency tuning and the bandwidth of the laser source should be small enough to remain close to the resonant field condition. In our case this condition is met by a laser with about 3 GHz bandwidth. Phase matching is normally an important consideration for SHG, but in this case CSHG adjusts to the phase matching condition by the emission angle and the SH field is radiated away from the grating and therefore it does not interact with the pump wave. This provides for very efficient SHG that we observe in our experiments.

### 5.3 Spectral Features in CSHG

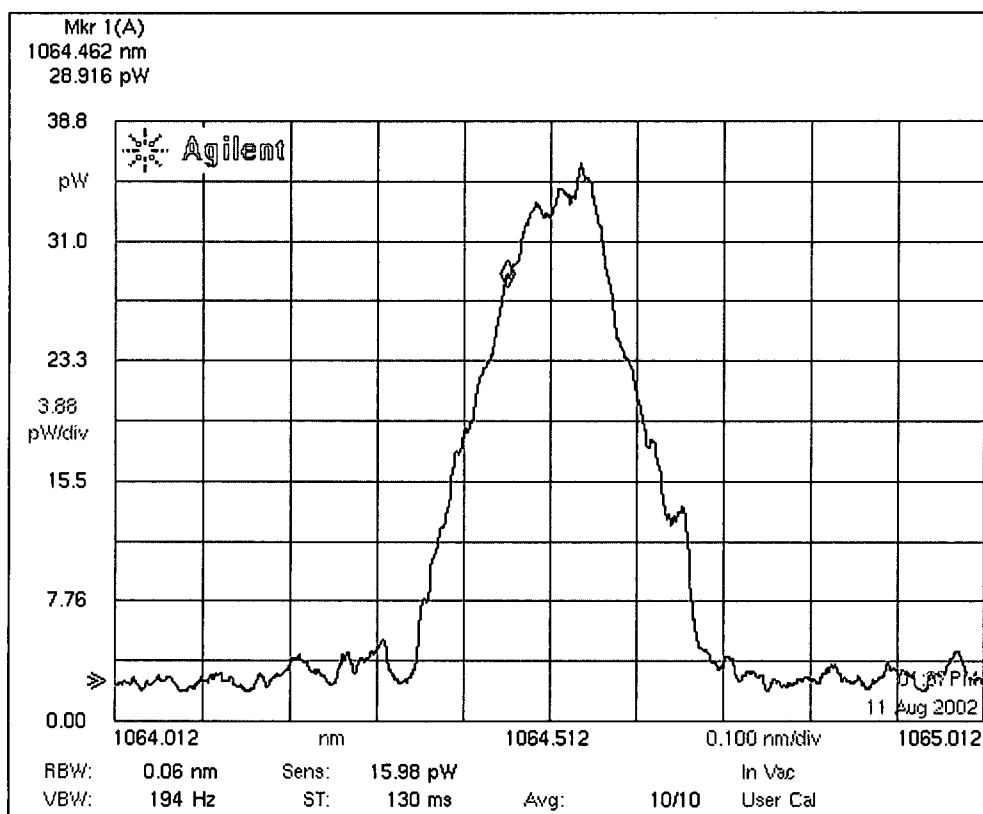


Figure 5.6 - The spectrum of pump, showing the bandwidth of 0.4 nm.

First of all, the spectrum of the pump was measured using the Optical Spectrum Analyzer with a resolution of 0.06 nm. The result is shown in Fig. 36.

In Figure 5.7, the three plots for sample No.1 show the no-grating and grating case and the case where the pump beam is incident on the grating at angle  $\gamma$  of  $5^\circ$  in Fig. 21. The overall enhancement of the CSHG signal is about 50 times for this sample. As the experiment demonstrates detuning the pump from the resonance results in a much reduced SH signal.

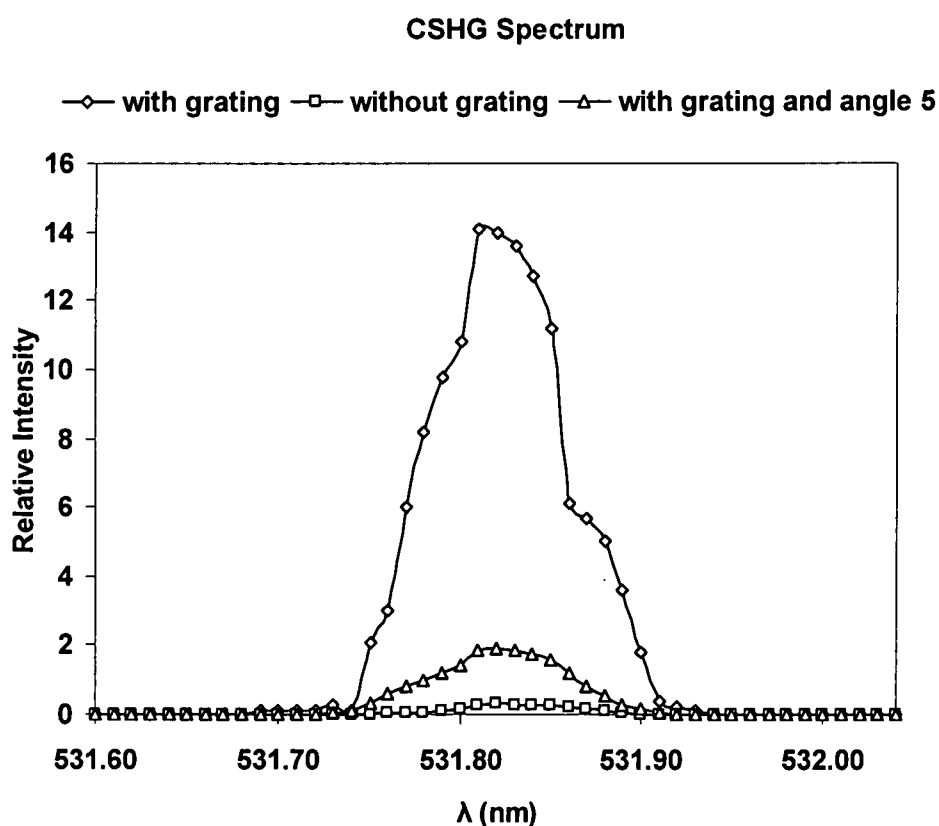


Figure 5.7 a - The CSH emission spectra for sample No.1.

Comparing Figure 5.6, 5.7 a and b, it's found that the shape of pump is similar to that of SHG and the bandwidths of pump is 0.4 nm and it's 0.2 nm for SHG. This

matches the theoretical result about the bandwidth relationship between pump and SHG, which differ by a factor of two.

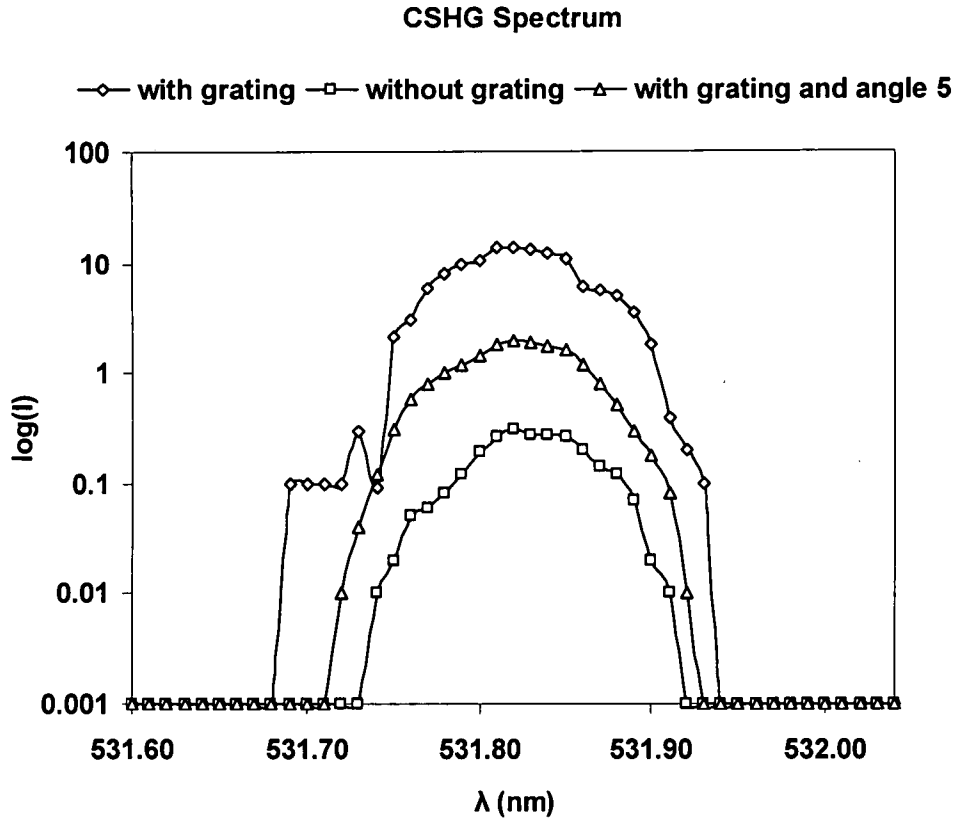


Figure 5.7 b - Log (I) for sample No.1. The Bandwidth is around 0.2 nm.

Actually, we use the first pump mode and last SHG mode with  $\alpha_1=0$  in Figs. 3.1, 3.2 and 3.3. The SHG is found very weak inside the waveguide. So the second mode should be used to get higher SHG. A waveguide with optimized depth of  $1.5\mu\text{m}$  is used for studies after that. The second mode for the pump was chosen because of its larger confinement for the intensity of modes in the substrate. As seen in Table 1, the confinement is  $\text{conf}_2=0.2290$  for the second mode comparing with  $0.0618$  for first mode. Also the nonlinearity  $d_{33}=-27.2\text{ pm/V}$  in the substrate has not been changed after the proton exchange processing. Therefore, we conclude that the larger substrate

confinement and nonlinearity  $d_{33}$  are advantages for the second mode in the Cerenkov radiation case. The real results are shown in Fig. 32-36 for Sample 3. This is the reason that 1.5  $\mu\text{m}$  depth waveguide was chosen and its second mode was used in the previous section with modeling. The enhancement of 50 is just the same as the result in the previous section detailing the numerical model for sample No.1.

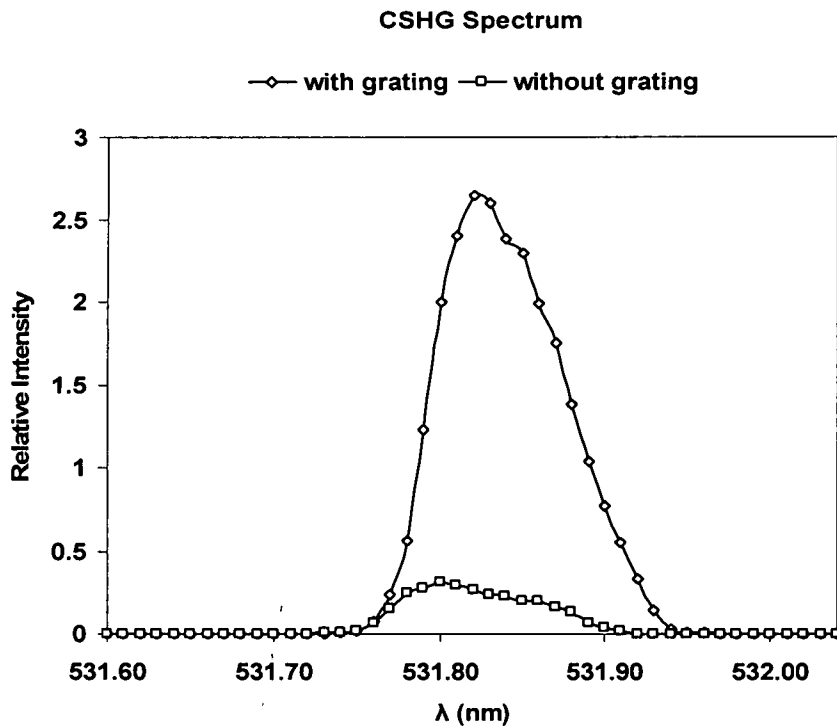


Figure 5.8 - The CSHG emission spectra for sample No.4.

Samples No.4, 5 and 6 are further typical examples with similar waveguides made in similar condition in their making process. All shows significant CSHG signal enhancement in Figures 5.8, 5.9 and 5.10. The CSHG enhancement are all higher than 10 for samples 4, 5 and 6, which proves that PBG did enhance the CSHG.



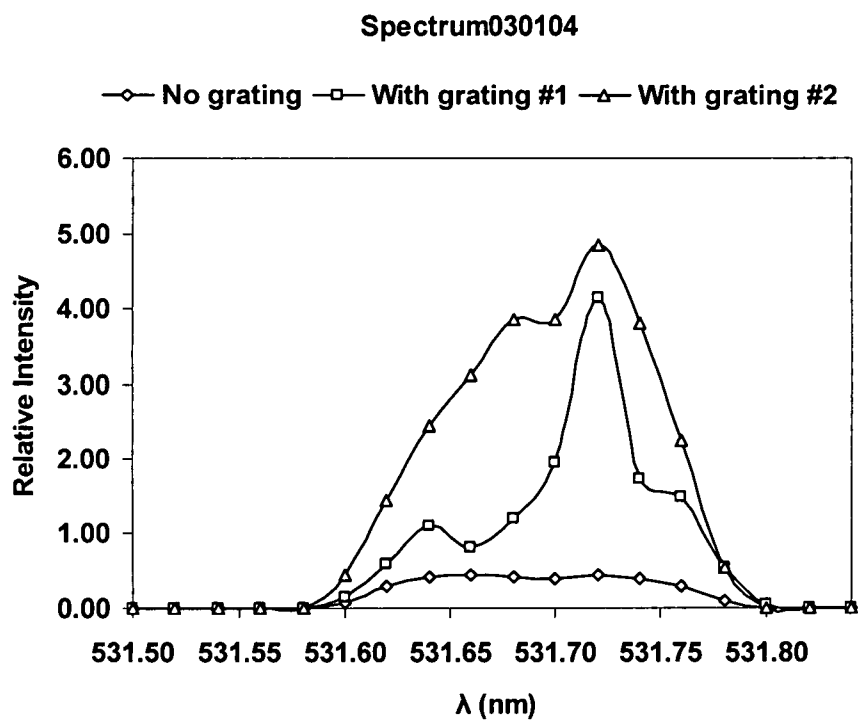


Figure 5.9 - The SH emission spectra for sample No.5.

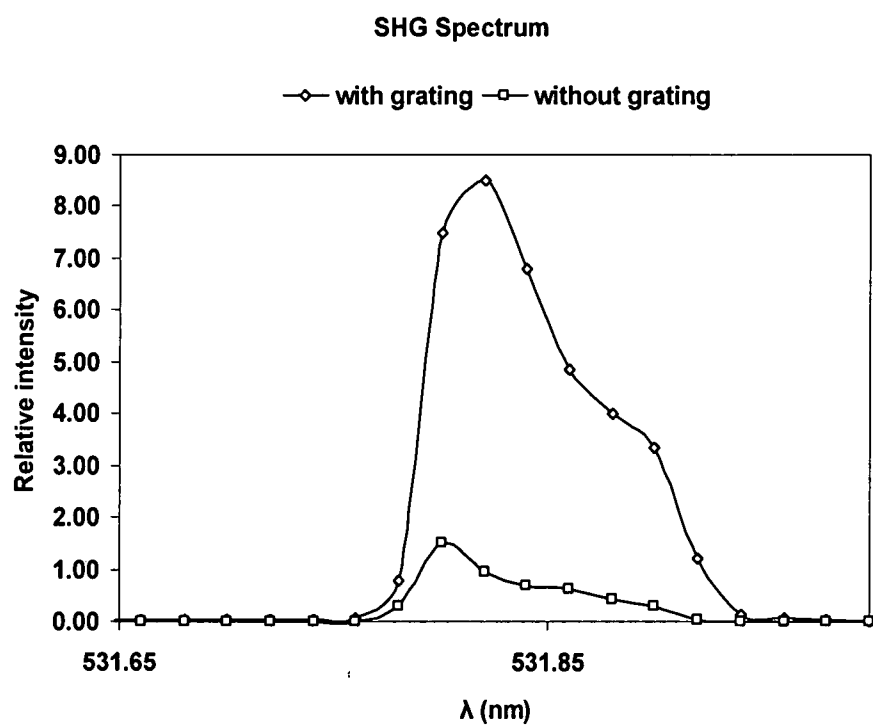


Figure 5.10 - The SH emission spectra for sample No.6.

### 5.4 SHG inside Waveguide

It's experimentally observed that the SHG inside the waveguide is very weak. One reason is that the proton exchange is reported to reduce the nonlinearity of material in the waveguide. An annealing procedure was applied in our lab, but the nonlinearity was apparently not recovered. Another reason for the weak SHG signal in the waveguide is lack of phase matching. The condition for phase matched emission in the waveguide is:

$$n_{\text{eff\_pump}} = n_{\text{eff\_SHG}}, \quad (5.3)$$

where  $n_{\text{eff\_pump}}$  is the effective refractive index of pump as a mode in the waveguide, while  $n_{\text{eff\_SHG}}$  is the effective refractive index of SHG as a mode in the waveguide

From Table 1 we list that  $n_{\text{eff\_pump}} = 2.2147$ , and  $2.1611$  the change of index in the waveguide from the substrate is  $\Delta n = 0.0863$ . The  $n_{\text{eff\_SHG}} = 2.2189$ , which is very close to the  $2.2147$ . It's reasonable to assume the approximate change of refractive index for SHG in inside the waveguide is almost the same as pump, and then the refractive index of SHG in the waveguide is  $2.2189 + \Delta n = 2.3052$ . Therefore,

$$2.2189 < n_{\text{eff\_SHG}} < 2.3052, \quad (5.4)$$

Equation 5.4 can also be seen from Figs. 3.19, 3.20, 3.21 and 3.22, the maxima and minima in those plots are very close to the number in Equation 5.4. This means that it's only possible to have waveguide phase matching for the first mode of the pump and the last mode of the SHG signal inside the waveguide. This is the reason SHG is only observed inside the waveguide for the turning angle corresponding to the first mode in the waveguide. The SHG vertical to the edge of sample can be observed. But it's usually much weaker comparing with the CSHG for the second mode of pump.

Two samples were prepared for the experiment to check the influence of the PBG on SHG efficiency. Two different lasers were used in our experiments. The first

one is Nd: YAG Laser  $\lambda=1.064 \mu\text{m}$ . CW, Nanosecond pulses ( $t=10 \text{ ns}$ ) or Picosecond's pulses ( $t=150 \text{ ps}$ ) were used. One spectrum result is shown in the Figure 5.11. Another one is Cr: forsterite laser ( $\lambda=1.3 \mu\text{m}$ ,  $t=30 \text{ fs}$ ) and the result is shown in Figure 5.12. These experiments were done in Vladimir Yakovlev's laboratory at the University of Wisconsin at Madison. From Figures 5.11 and 5.12, it's found that the band of SHG is narrower and the peak of SHG with grating is bigger than those without grating. But the enhancement is not very high because we used only a photoresist grating, only about 20% enhancement was observed. This problem was addressed during my project.

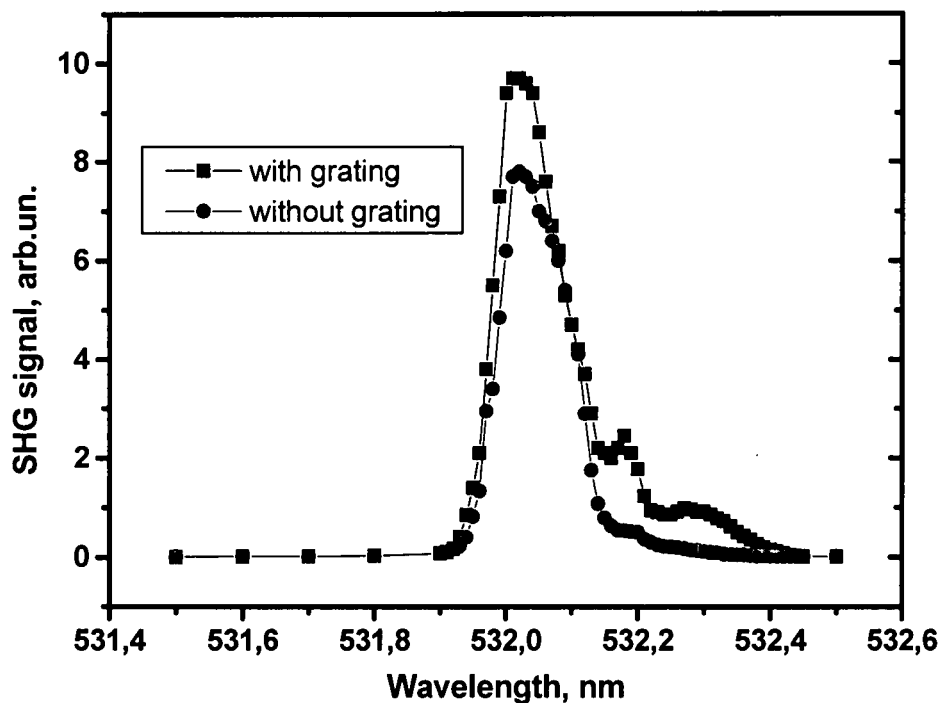


Figure 5.11- Spectra of the second harmonic for sample No. 7 produced by 150-pulses of Nd: YAG. Laser radiation in the area where the refractive index is periodically perturbed due to the diffraction grating (squares) and in the region with a homogeneous cladding index (circles).

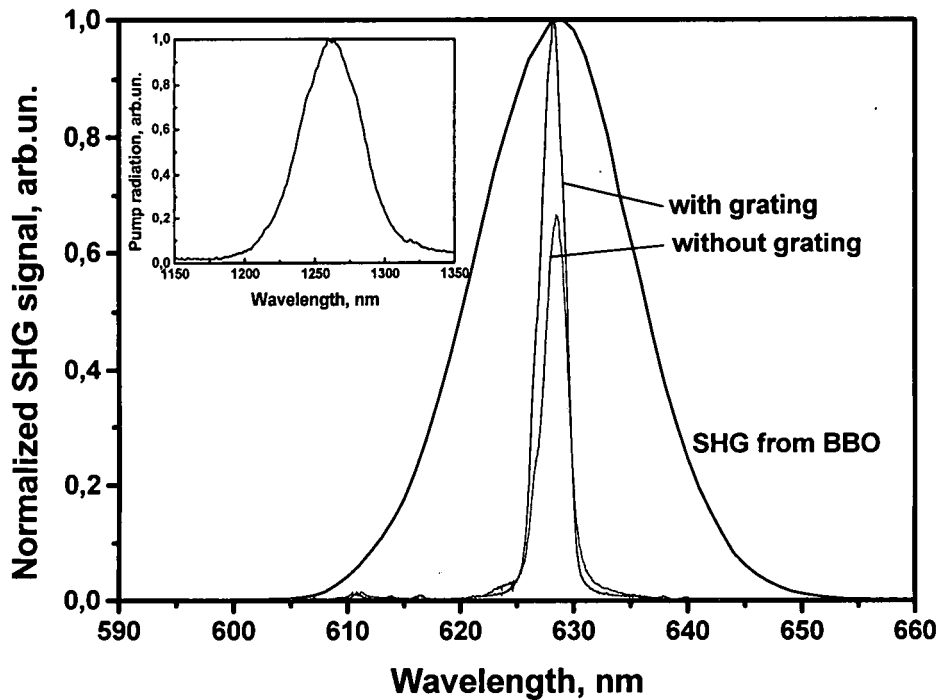


Figure 5.12 - Spectra of the second harmonic for sample No.8 produced by unamplified 30-fs pulses of Cr: forsterite laser radiation in the area where the refractive index is periodically perturbed due to the diffraction grating and in the homogenous region of the cladding index. The spectrum of the second-harmonic signal produced in BBO crystal is shown for comparison. The inset shows the spectrum of the pump pulse.

There is another possibility to get phase matching by carefully making a well-controlled grating with exact designed shape, exact pitch, and exact refractive index of mode. Then, we can modify the refractive indexes of both pump and SHG to meet the phase matching condition in Equation 5.3. Furthermore, the nonlinearity inside the waveguide may be reduced by 50% <sup>[20-22]</sup>. The temperature can also very easily change the conditions of Equation 5.3.

## Chapter 6

### Conclusion and Future Directions

#### *6.1 Conclusion*

In this dissertation I reported the design, fabrication, and demonstration of several novel PBG nonlinear optical devices in a lithium niobate. In creating these devices, I identified, addressed and overcame many of the problems that typically limit the usefulness of our systems. The project required making good, low-loss waveguides, which were made using proton exchange processing, the fabrication of gratings to create the band-edge resonant enhancement effect, and finally the sample was designed and made to explore the enhanced SHG effect.

In Chapter 2, I presented a brief review of nonlinear optics, and basic theory of the PBG enhancement was given. The resonance frequency for the PBG structure is normalized and the transmission spectrum was plotted as well. The theory gave important information on the position and width of the band gap and the expected enhancement of the local field in the waveguide. For instance, the normalized band-edge frequency is identified in Figure 2.2. With the frequency tuned to the first transmission maximum at the low-frequency band edge the corresponding forward and backward intensities plotted in Fig. 2.3 indicate an expected enhancement of more than seven times at the midpoint of material above the input forward intensity. This demonstrated that I can achieve higher pump intensity in the waveguide so that

enhanced SHG can be achieved. This is a type of resonator confinement of the field inside the waveguide volume.

In Chapter 3 I reported the design of my sample as well as the fabrication of samples. A 1.5  $\mu\text{m}$  deep waveguide was made using proton exchange processing. The details of this processing were clearly explained as well. The dispersion of sample was analyzed by several techniques, including a new Cerenkov method that I developed during the dissertation. I found that proton exchange processing may reduce the  $d_{33}$  nonlinearity and annealing was proved not effective for the recovering of nonlinearity of sample. Evidence for this lies in the weak SHG signal that was always found in the waveguide and the fact that the second guided mode, which has a lower confinement in the waveguide, gives the strongest CSHG signal. I worked out the best recipes for heating and annealing cycles to optimize the waveguide design.

A UV laser lithographic technique was used to make the PBG grating. Several wet and dry etch techniques were tried to imprint the grating into the waveguide for stronger coupling. Finally I found that ICP proved to be the best method for etching lithium niobate waveguide and it should be further explored in the future. AFM and SEM techniques were successfully applied to analyze the samples.

Several measurement methods were invented to guarantee the quality of samples. For instance, as mentioned above the Cerenkov radiation method is used to find the effective indices of waveguide. The diffraction method can find the effective indices in the waveguide. The standard prism coupling method was also used to find the waveguide modes. The WKB method can be applied to analyze and determine the waveguide index profile and then determine the depth of waveguide, which can also determine the number of modes using numerical methods once the depth and profile is known. Four methods were introduced to make accurate PBG gratings using our

lithography setup. Finally, high quality samples were made; this includes waveguide fabrication and uniform gratings with well controlled processing techniques.

In Chapter 4, I demonstrated the method of building a numerical model. It's explained that many effects in the fabrication may cause the result different. But those can be controlled in a limited range so that we can make a reasonable and typical model as a data base for further analyzing all samples. I chose sample No.1 as the typical sample. All the experimental data characterizing sample No. 1 are listed in Table 1. Based on the data the profile of each of the two modes in the sample was examined; the confinement and coupling constants were calculated as well. The definition of efficiency of CSHG is given for the calculations.

In Chapter 5, we demonstrated the experimental setup first. A photograph of the experimental setup was shown too. It's observed in all samples that SHG in the waveguide is very weak compared with SHG radiation under the Cerenkov condition. The reasons were thoroughly discussed as well. The CSHG spectra were measured under comparable conditions with and without the PBG grating. The relative intensity of those two SHG signals was used to determine the relative efficiency. A significant enhancement was found to be up to 50 times in Fig. 5.7 for sample No.1. Those results are consistent with our numerical model. Similar SHG signal enhancement was also observed from the other seven samples.

## *6.2 Future Directions*

There are many directions that can be explored for future SHG experiments and further enhancements can be expected. First, the waveguide and waveguide fabrication processing can be improved so that a better-controlled sample can be obtained. The modelocked laser may be required to get a high peak power without damaging or

heating the crystal. The temperature needs to be controlled because its drift will change a narrow resonance.

A spectrometer with higher resolution of 0.005 nm should be used to get the accurate transmission spectrum of pump so that we can classify the PBG band edge in it. The laser diode can be used to be a pump in the device so that a compact blue coherent light device can be made. There are other ways of improving the efficiency achieved here. First, the grating could be etched into the waveguide to give a stronger coupling to the guided wave, i.e. an effective increase in the coupling coefficient. Secondly, a two-dimensional PBG can also be designed to achieve even higher efficiency of SHG by using the interference of off-axis and on-axis interference and diffraction in the confined structure.



## Reference

1. Physics Today, p. 17, July, 2003.
2. J. Webjorn, D. Nam, S. Siala, and R. Waarts, "Nonlinear waveguides on the way to the marketplace." Opt. Photon. News, pp. 16-20, Apr., 1997.
3. J. A. Armstrong, N. Bloembergen, J. Ducuing, and P. S. Pershan, "Interactions between light waves in nonlinear dielectric," Phys. Rev. **127**, 1918-1939 (1962).
4. J. Webjorn, F. Laurell, and G. Arvidsson, "Blue light generated by frequency doubling of laser diode light in a lithium niobate waveguide," IEEE Photon, Technol. Lett., **1**, 316-318 (1989).
5. E. J. Lim, M. M. Feier, and R. L. Byer, "Second harmonic generation of green light in periodically poled lithium niobate waveguide," Electron. Lett. **25**, 174-175 (1989).
6. R. Viswanathan, "Enhanced frequency conversion in periodic structures," Ph.D. Dissertation, Dept. of Physics, Rensselaer Polytechnic Institute, May 1999.
7. J. W. Haus, R. Viswanathan, M. Scalora, A. G. Kalocsai, J. D. Cole, and J. Theimer, "Enhanced second-harmonic generation in media with a weak periodicity," Phy. Rev. A **57**, 2120-2128 (1998).
8. D. Pezzetta, C. Sibilila, M. Bertolotti, R. Ramponi, R. Osellame, M. Marangoni, J. W. Haus, M. Scalora, M. J. Bloemer and C. M. Bowden, "Enhanced Cerenkov second-harmonic generation in a planar nonlinear waveguide that reproduces a one-dimensional photonic bandgap structure", J. Opt. Soc. Am. B **19**, 2102-2110, (2002).
9. D. Pezzetta, C. Sibilila, M. Bertolotti, J. W. Haus, M. Scalora, M. J. Bloemer, C. M. Bowden, "Photonic band-gap structures in planar waveguides: application to second-harmonic generation," Yuri N J. Opt. Soc. Am. B **18**, 1326-1333 (2001).
10. G. D'Aguanno, M. Centini, J.W. Haus et al., "Photonic band edge effects in finite structures and applications to  $\chi^{(2)}$  interactions," Physical Rev. E **64**, 016609 (2001).
11. Y. Dumeige, P. Vidakovic, S. Sauvagnes, "Enhancement of second -harmonic generation in a one-dimensional semiconductor band gap," Appl. Phys Lett. **78**, 3021-3023 (2001).

12. A. V. Balakin, V. A. Bushuev, N. I. Koroteev, B. I. Mantaszyov and A. P. Shkurinov, "Enhancement of second-harmonic generation with femtosecond laser pulses near the photonic band edge for different polarizations of incident light," *Opt. Lett.*, **24**, 793-795 (1999).
13. V. Foglietti, E. Cianci, D. Pezzetta, C. Sibilia, M. Marangoni, R. Osellame, R. Ramponi, "Fabrication of band-gap structures in planar nonlinear waveguides for second harmonic generation," *Microelectronic Engineering* **67-68**, 742-748 (2003).
14. J. Torres, D. Coquillat et al. "Giant second-harmonic generation in a one-dimensional GaN photonic crystal," *Physical Review B* **69**, 08505 (2004).
15. G. Blau, E. Popov et al. "Grating-assisted phase-matched second-harmonic generation from a polymer waveguide," *Opt. Lett.* **20** (1995).
16. R. W. Boyd, *Nonlinear Optics*, Academic Press, Inc., 1992.
17. M. Quillec, *Materials for Optoelectronics*, Kluwer Academic Publishers, USA, 1996.
18. G. I. Stegeman and C. T. Seaton, "Nonlinear integrated optics," *J. Appl. Phys.* **58**, R57-R78, 1985.
19. E. Glavas, J. M. Cabrera, and P. D. Townsend, "A comparison of optical damage in different types of LiNbO<sub>3</sub> waveguides," *J. Phys. D: Appl. Phys.* **22**, 611-616 (1989).
20. F. Laurell, M. G. Roelofs and H. Hsiung, "Loss of optical nonlinearity in proton-exchanged LiNbO<sub>3</sub> waveguides," *Appl. Phys. Lett.* **60**, 301-303 (1992).
21. W-Y. Hsu, C. S. Willand, V. Gopalan and M. C. Gupta., "Effect of proton exchange on the nonlinear optical properties of LiNbO<sub>3</sub> and LiTaO<sub>3</sub>," *Appl. Phys. Lett.* **61**, 2263-2265 (1992).
22. M. L. Bortz, L. A. Eyres, and M. M. Fejer, "Depth profiling of the d<sub>33</sub> nonlinear coefficient in annealed proton exchanged LiNbO<sub>3</sub> waveguides," *Appl. Phys. Lett.* **62**, 2012-2014 (1993).
23. N. Goto and G. L. Yip, "Characterization of proton-exchange and annealed LiNbO<sub>3</sub> waveguides with pyrophosphoric acid," *Appl. Opt.* **28**, 60-65 (1989).
24. C. Ziling, L. Pokrovskii, et al., "Optical and structural properties of annealed PE: LiNbO<sub>3</sub> waveguides formed with pyrophosphoric and benzoic acids," *J. Appl. Phys.* **73**, 3125-3132 (1993).
25. J. Rams and J. M. Cabrera, "Preparation of proton-exchange LiNbO<sub>3</sub> waveguides in benzoic acid vapor," *J. Opt. Soc. Am. B* **16**, 401-406 (1999).
26. A. Di Lallo, A. Cino, C. Conti and G. Assanto, "Second Harmonic generation in reverse proton exchanged Lithium Niobate waveguides," *Optics Express* **8**, 232-237 (2001).

27. Y. N. Korkishko, V. A. Fedorov, T. M. Morozova, F. Caccavale, F. Gonella, and F. Segato, "Reverse proton exchange for buried waveguides in  $\text{LiNbO}_3$ ," J. Opt. Soc. Am. A **15**, 1838-1842 (1998).
28. S. Nonogaki, *Microlithography Fundamentals in Semiconductor Devices and Fabrication Technology*, Marcel Dekker, Inc., USA (1998).
29. D. A. Darbyshire, "Ion and Plasma Assisted Etching of Holographic Gratings", Vacuum. **36**, 55-60, (1985).
30. R. S. Cheng, "Wet-Etched Ridge Waveguides in Y-Cut Lithium Niobate", J. of Lightwave Technology **15**, 1880-1887, (1997).
31. F. Laurell, "Wet Etching of Proton-Exchanged Lithium Niobate—A Novel Processing Technique", J. of Lightwave Tech. **10**, 1606-1609 (1992).
32. R. S. Cheng, "Mach-Zehnder Modulators with Lithium Niobate Ridge Waveguides Fabricated by Proton-Exchange Wet Etch and Nickel Indiffusion", IEEE Photonics Tech. Lett. **7**, 1282-1284, (1995).
33. A. J. Boyland, "Latency Effects and Periodic Structures in Light-induced Frustrated Etching of Fe: doped  $\text{LiNbO}_3$ ", Appl. Phys. Lett., **77**, 2792-2794 (2000).
34. Y. N. Korkishko, V. A. Fedorov, S. M. Kostitskii, "Optical and X-ray characterization of  $\text{HxLi}_{1-x}\text{NbO}_3$  phases generated in proton exchanged  $\text{LiNbO}_3$  optical waveguides," J. Appl. Phys. **84**, 2411-2419 (1998).
35. N. A. Sanford and W.C. Robinson, "Direct measurement of effective indices of guided modes in  $\text{LiNbO}_3$  waveguides using Cerenkov second harmonic," Opt. lett. **12**, 445-447 (1987).
36. R. Ramponi, R. Osellame, M. Maragoni, and V. Russo, "Near-infrared refractometry of liquids by means of waveguides Cerenkov second-harmonic generation," Appl. Opt. **37**, 1-6 (1998).
37. P. K. Tien, R. Ulrich and R. J. Maetin, "Optical second harmonic generation in form of coherent Cerenkov radiation from a thin-film waveguide," Appl. Phys. Lett. **17**, 447-450 (1970).
38. M. J. Li, M. De Micheli, Q. He, and D. B. Ostrowsky. "Cerenkov configuration second harmonic generation in proton-exchanged Lithium Niobate guides," IEEE J. Quant. Electron. **26**, 1384-1393 (1990).
39. Y. N. Korkishko, V. A. Fedorov and S. M. Kostitskii, "Optical and X-ray characterization of  $\text{HxLi}_{1-x}\text{NbO}_3$  phases generated in proton exchanged  $\text{LiNbO}_3$  optical waveguides," J. Appl. Phys. **84**, 2411-2419 (1998).
40. K. S. Chiang, "Construction of refractive-index profiles of planar dielectric waveguides from the distribution of effective indexes," J. Lightwave Tech., **LT-3**, 385-391 (1985).

41. C. R. Pollock, *Fundamental of Optoelectronics*, Richard D. Irwin, Inc., 1995.
42. J. M. White and P. F. Heidrich, "Optical waveguide refractive index profiles determined from measurement of mode indices: a simple analysis," *Appl. Opt.***15**, 151-155 (1976).
43. S. Martellucci, *Advances in Integrated Optics*, Plenum Press, USA, 1994.

# APPENDIX A

## Matlab Programs

### Program 1

#### Dispersion of extra-ordinary wave

```
%Dispersion of extra-ordinary
clear;
% x1 wavelength of pump, x2 SHG
x1=1.064;
x2=x1/2;
x = linspace(x2,x1,1000);
ne=4.54528+0.091649./(x.^2-0.046079)-0.0303*x.^2;
ne=sqrt(ne);
plot(x,ne);
xlabel('wavelength(um)');
ylabel('ne');
```

### Program 2

#### PBG method transmission

```
%PBG method transmission
clear all;
de=5e-4;
n=1.00025;
w=linspace(0.999,1.0005,1000);
d1=w.*n^2-1;
k=de./w/2;
L=pi*1e+4;
D1=sqrt(d1.^2-k.^2);
af1=D1./(D1.*cos(D1.*L)+i*d1.*sin(D1.*L));
y=(abs(af1)).^2;
plot(w,y);
xlabel('\omega')
ylabel('Transmission')
title('Transmission vs \omega')
axis([0.999 1.0005 0 1.3])
```

### Program 3

#### Intensity of light around PBG

```
%Intensity of light around PBG
%Intensity_1
%intensity of pump in side the waveguide at different
% positions
clear all;
de=5e-4;
n=1.00025;
L=pi*1e+4;
w=0.99925;
```

```

d1=w.*n^2-1;
k=de./w/2;
D1=sqrt(d1.^2-k.^2);
z=linspace(0,L,1000);
af10=1;
ab10=i*k.*sin(D1.*L)/(D1.*cos(D1.*L)+i*d1.*sin(D1.*L));
af1=(cos(D1.*z)-i*d1.*sin(D1.*z)/D1).*af10+i*k.*sin(D1.*z).*ab10./D1;
ab1=(cos(D1.*z)+i*d1.*sin(D1.*z)/D1).*ab10-i*k.*sin(D1.*z).*af10./D1;
If=(abs(af1)).^2;
Ib=(abs(ab1)).^2;
plot(z,If,z,Ib,'-.');
xlim([0 L]);
xlabel('z')
ylabel('Intensity')
title(' Intensity vs.Position z at \omega=0.99925 ')
legend('Forward field','Backward field')
axis([0 L 0 1.5])

```

## Program 4

### WBK method

%Program to calculate index profile using WBK method

```

clear;
% a is wavelength in um
a=0.6328;
% sample No. 2
n = [2.365 2.3329 2.30619 2.27903 2.2418];
% sample No. 3
% n = [2.34 2.3329 2.30619 2.27903 2.2418];
len=length(n);
z(1)=0;
z(2)=(9/16)*(sqrt((n(1)+3*n(2))/2)*sqrt(n(1)-n(2)))^-1;
for m=3:len;
    sum=0;
    for k = 2:m-1
        sum=sum+((n(k-1)+n(k))/2+n(m))^.5*((z(k)-z(k-1))/(n(k-1)-n(k)))*((n(k-1)-n(m))^1.5-(n(k)-n(m))^1.5));
    end
    sum=(4*m-5)/8-2*sum/3;
    z(m)=z(m-1)+(3/2*((n(m-1)+3*n(m))/2)^-.5*(n(m-1)-n(m))^-0.5)*sum;
end
z
plot(z*a,n,'o');
xlim([0 2.5])
ylim([2.14 2.38])

```

## Program 5

### Modes profile and kappa for sample No.1

```
% Modes profile and kappa for sample No.1
% Program to calculate the propagation constants for slab waveguide
% TM case, neff and confinement, Kapa
clear;
% indices nc, nf and ns. assumes ns>nc.
%nc=input('Index of cover (superstrate) medium: ')
%nf=input('Index of film medium: ')
%ns=input('Index of substrate medium: ')
%h=input('thickness of the slab (cm): ')
%lambda=input('wavelength (cm): ')
%nc=1;nf=2.35;ns=2.2;lambda=.0001064;
%lambda=.00006328;
nc=1;nf=2.35;ns=2.2;lambda=.0001064;
%Confined area is from d11 to d12 um, depth of grating is dep um
h=.00015;
d11=-h*1e+4;
d12=0;
dep=0.1;

k0=2*pi/lambda;k02=k0*k0;
nf2=nf*nf;nf4=nf*nf2;nc2=nc*nc;ns2=ns*ns;
% number of points in plot
M=200;
% plot the two elements of the transcendental equation
% Use kappa as the variable only in the region where the gamma's and
beta are real
kappa=k0*sqrt(nf2-ns2)*(0:M-1)/M;
beta=sqrt(k02*nf2-kappa.*kappa);
gammac=sqrt(beta.*beta-k02*nc2);
gammass=sqrt(beta.*beta-k02*ns2);
for i=1:M;
    x=kappa(i)*h;
    yt(i)=tan(x);
    if(yt(i) >20.)
        yt(i)=20.;
    end;
    if(yt(i)<-20.)
        yt(i)=-20.;
    end;
    % Transcendental equation for teh TM case
    ss(i)=(kappa(i)*kappa(i)-nf4*gammac(i)*gammass(i)/nc2/ns2);
    rr(i)=nf2*kappa(i)*(gammass(i)/ns2+gammac(i)/nc2)/ss(i);
    if(imag(rr(i))~=0.)
        rr(i)=0.;
    end
    if(rr(i) >20.)
        rr(i)=20.;
    end;
    if(rr(i)<-20.)
        rr(i)=-20.;
    end;
end
end
figure
%plot(kappa,yt,'b-');
```

```

plot(kappa,yt,'b-',kappa,rr,'r-');
xlabel(['\kappa']);ylabel(['tan,poly']);
pause
% find the exact eigenvalue 'kappa', then determine beta.
% find the estimates
k=0;
for i=1:M-1;
    if((rr(i)-yt(i))/(rr(i+1)-yt(i+1)) < 0.)
        k=k+1; II(k)=i; kall(k)=kappa(i);rall(k)=rr(i);
        % counts all chnages of values
    end
end
hold on;
plot(kall,rall,'g. ');
pause
% refine the solutions
kk=0;kl=0;
for j=1:k;
    if (abs(yt(II(j)+1)-yt(II(j))) < 5.)
        kk=kk+1; IINT(kk)=II(j); kint(kk)=kall(j); rint(kk)=rall(j);
        % counts only small changes of values
    end
end
% Further refinement
for l=1:kk;
    if(abs(rr(IINT(l)+1)-rr(IINT(l)))<2.)
        kl=kl+1; IFIN(kl)=IINT(l); kfin(kl)=kint(l); rfin(kl)=rint(l);
    end
end
deng_kappa=kfin;
deng_beta=sqrt(k02*nf2-deng_kappa.*deng_kappa);

plot(kfin,rfin,'m. ');
% Now home in on the precise solutions.

% deng modified follows
pause
% calculate the field profiles
for i=1:kl;
    % Define parameters for the function subroutine
    kappal=kfin(i);gammacl=gammac(IFIN(i));gammacl=gammac(IFIN(i));
    ix=0;
    % d is in microns
    for d=-5:.05:3;
        ix=ix+1;
        % distance in centimeters
        xx(ix)=.0001*d;
        % Electric field for the slab waveguide. The three regions are
        divided.
        if (xx(ix)>0)
            ey(ix) = exp(-gammacl*xx(ix));
        elseif (xx(ix)<=0)
            ey(ix)=(cos(kappal*h)+gammacl*sin(kappal*h)/kappal)*exp(gammacl*(xx(ix)
            +h));
        else
            ey(ix)=cos(kappal*xx(ix))-gammacl*sin(kappal*xx(ix))/kappal;
        end
    end
end
end

```



```

xx=xx.*1e+4;
figure;
plot(xx,ey,'r');
title('TM MODEL FIELD PATTERN')
    xlabel('X (um)')
    ylabel('E')

ey_max=1.2*max(ey);
ey_min=1.2*min(ey);

hold on;
    stem(0,ey_max,'b.',':');
    stem(0,ey_min,'b.',':');
    stem(-h/2.*1e+4,ey_max,'g.','-.');
    stem(-h/2.*1e+4,ey_min,'g.','-.');
    stem(-h.*1e+4,ey_max,'b.',':');
    stem(-h.*1e+4,ey_min,'b.',':');
    %legend('E(x)')
    hold off;

Z(i) = trapz(xx,ey.^2);

% confinement for grating field dep um

ixl=0;
    for d1=d12:.0005:dep;
        %for d1=-dep:.0005:d12;
        ixl=ixl+1;
        % distance in centimeters
        xx1(ixl)=.0001*d1;
        % Electric field for the slab waveguide. The three regions are
        divided.

        if (xx1(ixl)>0)
            eyl(ixl) = exp(-gammacl*xx1(ixl));
        elseif (xx1(ixl)<-h)
            eyl(ixl)=(cos(kappal*h)+gammacl*sin(kappal*h)/kappal)*exp(gammasl*(xx1
            (ixl)+h));
        else
            eyl(ixl)=cos(kappal*xx1(ixl))-gammacl*sin(kappal*xx1(ixl))/kappal;
        end
    end
Z1(i) = trapz(xx1,eyl.^2);
    Mode=i;

end
conf=Z1./Z;
%Kapa is the coupling efficiency 1/cm; e0 is Farad/cm;c is in cm/s
% u0=p*4e-9 Henry/cm; C_2 is the squart of the normalizing C
e0=8.8542e-14;
c=3e+10;
%dn_2=1.5^2-1;
dn_2=1.5^2-1;
omiga=2*pi*c/lambda;
u0=pi*4e-9;
A=2*omiga*u0./deng_beta;

neff=deng_beta/k0
conf
%Kapa=omiga*e0*dn_2*A.*conf/4/3.14159

```

```
Kappa=dn_2*conf./neff./lambda
```

## Program 6

### Determine the efficiency vs. K for sample No.1

```
% Determine the efficiency vs. K for sample No.1

clear;
L=0.67;% cm
ZZ=L;
% kappa is for second mode in sample No.1
Kappa=14.8002;% 1/cm
for ii=1:200;
    del=Kappa+3*ii*1e-2+.0000001;
    %x(ii)=1.0640e-004+del*7.9082e-010;
    %x(ii)'s unit is nm
    x(ii)=del*7.9082e-3;
    for jj=1:20;
        K=Kappa+0.001*jj*1e-1;
        %K=1;
        y(jj)=K;
        delta1=sqrt(del^2-K^2);
        C1=delta1*cos(delta1*L)+i*del*sin(delta1*L);
        C2=(delta1*sin(delta1*L)-i*del*cos(delta1*L))/C1;
        %delta1=sqrt(abs(del^2-K^2));
        Z=0:0.01:ZZ;
        b=(cos(delta1*Z)+C2*sin(delta1*Z)).^2;
        B=trapz(Z,abs(b).^2);
        % b is with grating while b0 is without grating K=0
        C10=del*cos(del*L)+i*del*sin(del*L);
        C20=(del*sin(del*L)-i*del*cos(del*L))/C10;
        b0=(cos(del*Z)+C20*sin(del*Z)).^2;
        B0=trapz(Z,abs(b0).^2);

        z(ii,jj)=B/B0;
        ap=cos(delta1*ZZ)+C2*sin(delta1*ZZ);
        T=abs(ap)^2;
        zz(ii,jj)=T;
    end
end

%figure(1)
subplot(2,1,1);
mesh(y,x,zz,'EdgeColor','black')
%mesh(zz);
%surf(y,x,zz)
%shading interp
ylabel('\Delta\lambda(nm)')
xlabel('\kappa')
zlabel('Tx')
title('Tx vs. \kappa and \Delta\lambda','FontSize',12)

%figure(2)
subplot(2,1,2);
mesh(y,x,z,'EdgeColor','black')
%mesh(z);
```

```

%surf(y,x,z)
%shading interp
ylabel('\Delta\lambda (nm)')
xlabel('\kappa')
zlabel('Relative efficiency')
title('Relative efficiency vs. \kappa and
\Delta\lambda','FontSize',12)

```

## Program 7

### Determine the band gap and efficiency vs. lab for sample No.1

```

% Determine the band gap and efficiency vs. lab for sample No.1
clear;
L=0.67;% cm
ZZ=L;
Kappa=14.8;% 1/cm
for ii=1:200;
    del=Kappa+3*ii*1e-2+.0000001;
    %x(ii)=1.0640e-004+del*7.9082e-010;
    %x(ii)'s unit is nm
    x(ii)=del*7.9082e-3;
    K=Kappa;
    %K=1;
    delta1=sqrt(del^2-K^2);
    C1=delta1*cos(delta1*L)+i*del*sin(delta1*L);
    C2=(delta1*sin(delta1*L)-i*del*cos(delta1*L))/C1;
    %delta1=sqrt(abs(del^2-K^2));
    Z=0:0.01:ZZ;
    b=(cos(delta1*Z)+C2*sin(delta1*Z)).^2;
    B=trapz(Z,abs(b).^2);
    % b is with grating while b0 is without grating K=0
    C10=del*cos(del*L)+i*del*sin(del*L);
    C20=(del*sin(del*L)-i*del*cos(del*L))/C10;
    b0=(cos(del*Z)+C20*sin(del*Z)).^2;
    B0=trapz(Z,abs(b0).^2);

    y(ii)=B/B0;
    ap=cos(delta1*ZZ)+C2*sin(delta1*ZZ);
    T=abs(ap)^2;
    yy(ii)=T;
end

%figure(1)
subplot(2,1,1);
plot(x,yy)
xlabel('\Delta\lambda (nm)')
ylabel('Tx')
title('Tx vs. \Delta\lambda','FontSize',12)

%figure(2)
subplot(2,1,2);
plot(x,y)
xlabel('\Delta\lambda (nm)')
ylabel('Relative efficiency')
title('Relative efficiency vs. \Delta\lambda','FontSize',12)

```

## Program 8

### Determine the band gap and intensity vs. position for sample No.1

```
% Determine the band gap and intensity vs. position for sample No.1
% Here we only consider the forward field
clear;

L=0.67;% cm
ZZ=L;
Kappa=14.8;% 1/cm
ii=1;
%del=Kappa+3*ii*1e-2+.0000001;
%x(ii)=1.0640e-004+del*7.9082e-010;
%x(ii)'s unit is nm, which is del_lambda
%x(ii)=del*7.9082e-3;
%x(ii)=0.12278;
x(ii)=0.13861;
del=x(ii)/7.9082e-3;
K=Kappa;
%K=1;
deltal=sqrt(del^2-K^2);
C1=deltal*cos(deltal*L)+i*del*sin(deltal*L);
C2=(deltal*sin(deltal*L)-i*del*cos(deltal*L))/C1;
%deltal=sqrt(abs(del^2-K^2));
Z=0:0.01:ZZ;
b=(cos(deltal*Z)+C2*sin(deltal*Z)).^2;
B=trapz(Z,abs(b).^2);
% b is with grating while b0 is without grating K=0
C10=del*cos(del*L)+i*del*sin(del*L);
C20=(del*sin(del*L)-i*del*cos(del*L))/C10;
b0=(cos(del*Z)+C20*sin(del*Z)).^2;
B0=trapz(Z,abs(b0).^2);

y(ii)=B/B0
ap=cos(deltal*ZZ)+C2*sin(deltal*ZZ);
T=abs(ap)^2
yy(ii)=T;

%end

plot(Z,abs(b).^2,Z,abs(b0).^2,'.')
xlabel('Z (cm)')
ylabel('Relative Intensity')
title('Relative intensity vs. Z','FontSize',12)
```

## APPENDIX B

### PHOTOS OF SAMPLE IN EXPERIMENT

Those pictures show more details in CSHG

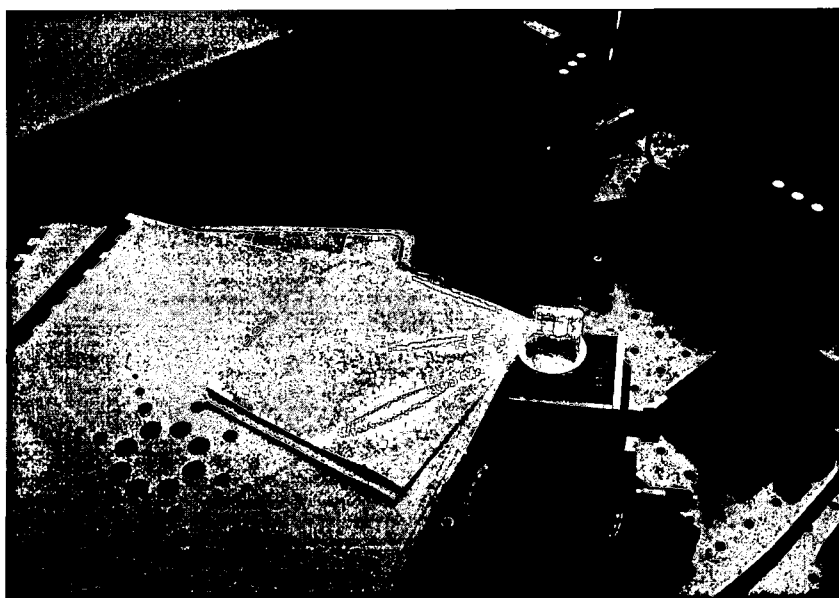


Figure B.1 - SHG experiment of sample No.1 with room lights on.

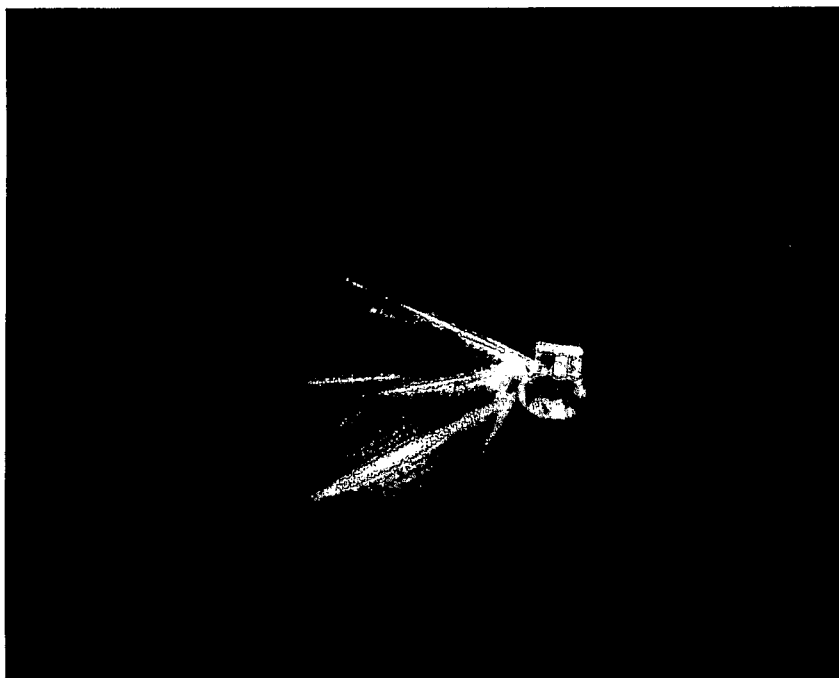


Figure B.2 - SHG experiment of sample No.1 in dark.

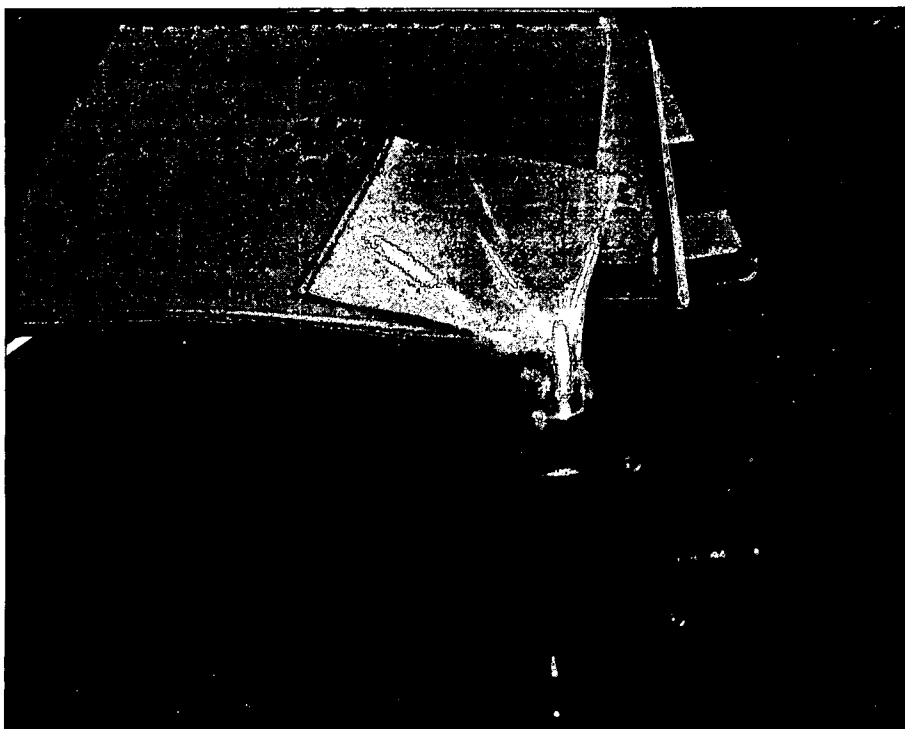


Figure B.3 - SHG experiment of sample No.1 with room lights on.

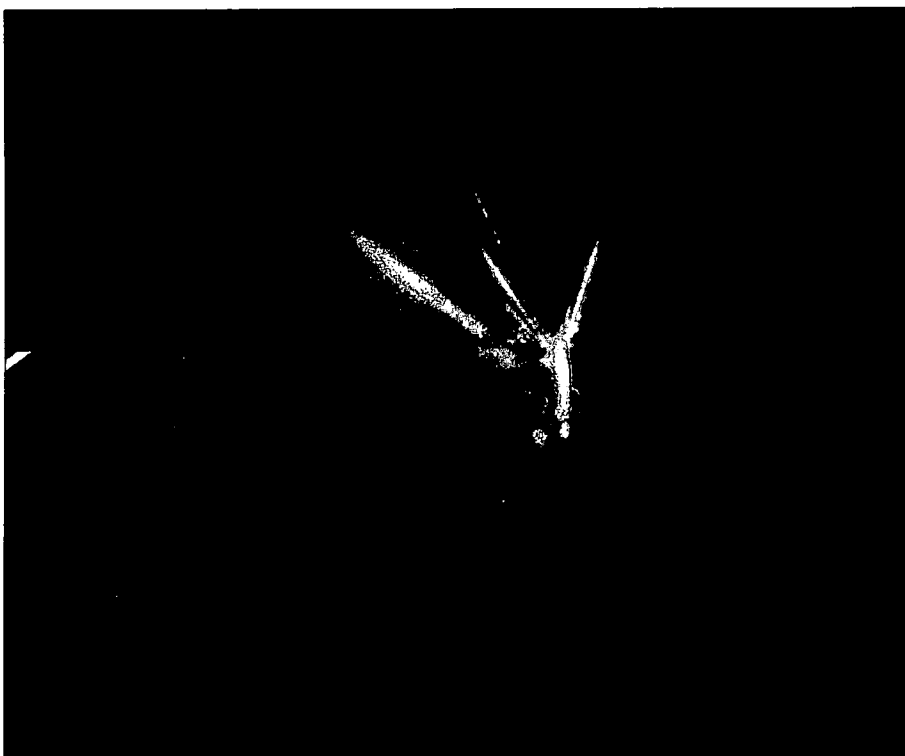


Figure B.4 - SHG experiment of sample No.1 in dark.

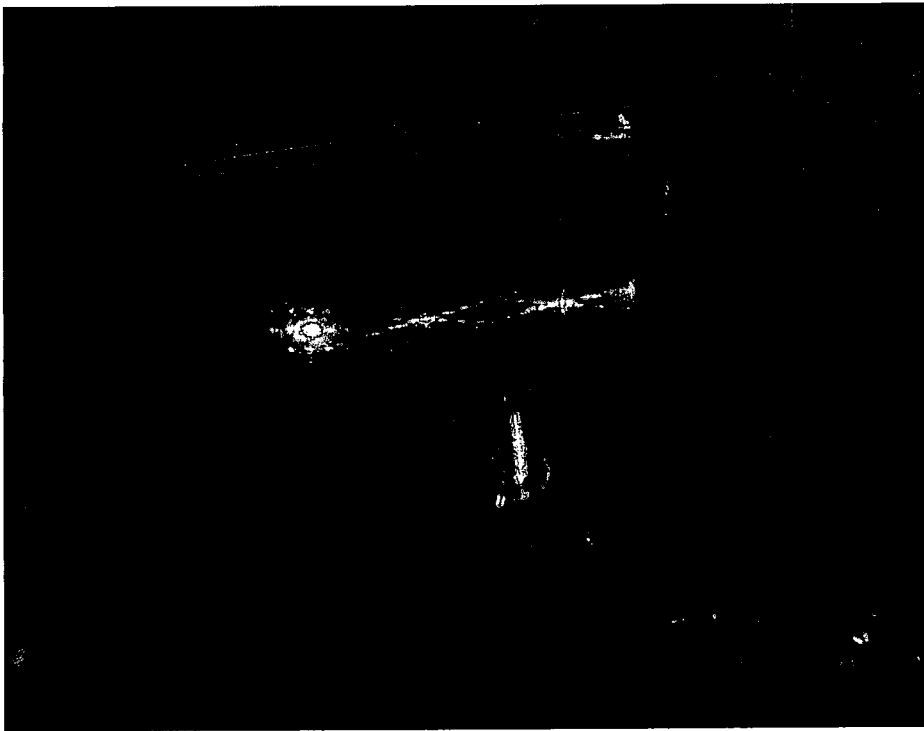


Figure B.5 - SHG experiment of sample No.1 in dark. CSHG can be seen on the screen.

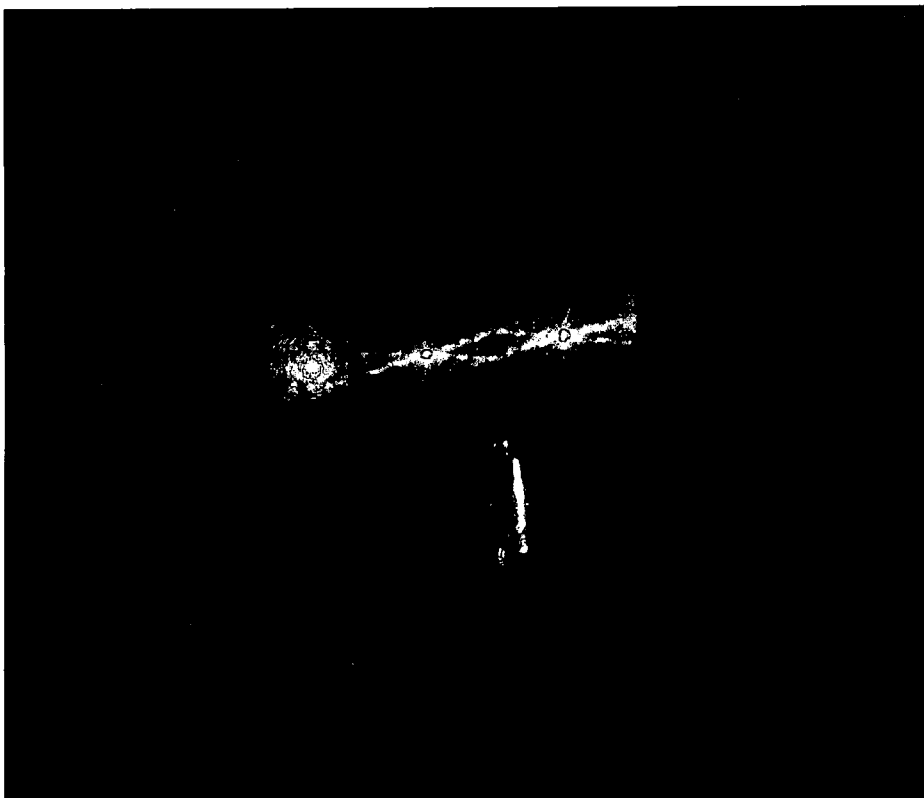


Figure B.6 - SHG experiment of sample No.1 in dark. CSHG can be seen on the screen.

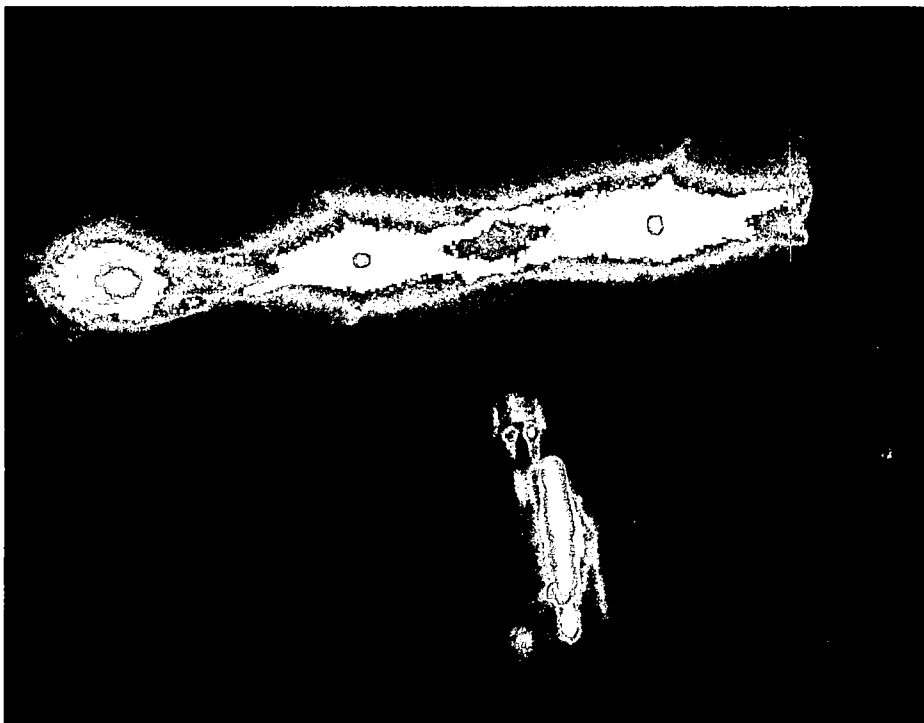


Figure B.7 - SHG experiment of sample No.1 in dark. CSHG can be seen on the screen.

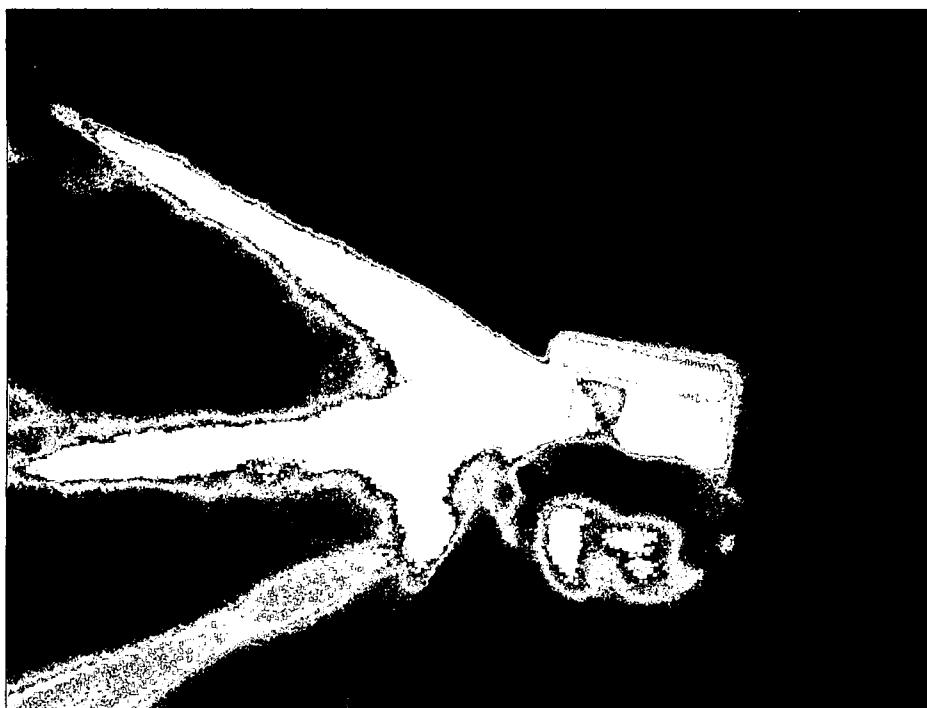


Figure B.8 - SHG experiment sample No.1 in dark.



R702031964